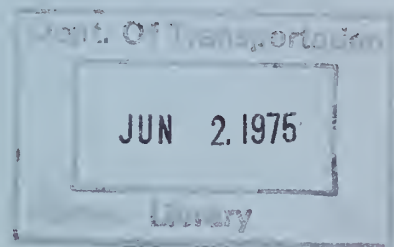


TE  
662  
.A3  
no.  
FHWA-  
RD-  
75-10

Report No. FHWA-RD-75-10

**AN INVESTIGATION OF THE EFFECTIVENESS OF  
EXISTING BRIDGE DESIGN METHODOLOGY IN  
PROVIDING ADEQUATE STRUCTURAL RESISTANCE  
TO SEISMIC DISTURBANCES. Phase III: Analytical  
Investigations of Seismic Response of Short, Single,  
or Multiple-Span Highway Bridges.**

**M. Chen and J. Penzien**



**October 1974  
Final Report**

This document is available to the public  
through the National Technical Information  
Service, Springfield, Virginia 22161

**Prepared for  
FEDERAL HIGHWAY ADMINISTRATION  
Offices of Research & Development  
Washington, D.C. 20590**

#### DISCLAIMER

The contents of this report reflect the views of the authors who are responsible for the facts and the accuracy of the data presented herein. The contents do not necessarily reflect the official views or policy of the Department of Transportation. This report does not constitute a standard, specification or regulation.

JUN 2 1975

Technical Report Documentation Page

1. Report No. FHWA-RD-75-10		2. Government Accession No.		3. Recipient's Catalog No.	
4. Title and Subtitle An Investigation of the Effectiveness of Existing Bridge Design Methodology in Providing Adequate Structural Resistance to Seismic Disturbances. Phase III: Analytical Investigations of Seismic Response of Short, Single, or Multiple-Span Highway Bridges.				5. Report Date October 1974	
				6. Performing Organization Code	
7. Author(s) M. Chen and J. Penzien				8. Performing Organization Report No.	
9. Performing Organization Name and Address University of California Campus Research Office 118 California Hall Berkeley, California 94720				10. Work Unit No. (TRAIS) 35A2-012	
				11. Contract or Grant No. DOT-FH-11-7798	
12. Sponsoring Agency Name and Address Office of Research and Development Federal Highway Administration U. S. Department of Transportation Washington, D. C. 20590				13. Type of Report and Period Covered Phase III - Final Report	
				14. Sponsoring Agency Code 50314	
15. Supplementary Notes FHWA Contract Manager: J. D. Cooper, HRS-11 This report is the third in a series. The others in the series are: Phase I Report, FHWA-RD-73-13, Literature Survey, NTIS PB 226-718 AS Phase II Report, FHWA-RD-74-3, Long Bridges, NTIS PB 233-711 AS					
16. Abstract This report is the third in a series to result from the study, "An Investigation of the Effectiveness of Existing Bridge Design Methodology in Providing Adequate Structural Resistance to Seismic Disturbances," sponsored by the U. S. Department of Transportation, Federal Highway Administration. Descriptions are given to the analytical investigations of the seismic response of short, single or multiple-span highway bridges of the type where soil-structure interaction effects are important. Six different mathematical model elements are incorporated into the computer program which possess the capability of performing linear or non-linear analyses. Finite element modeling is used for the backfill soils. Bridge deck, piers, and abutments are modeled using prismatic beam elements. A frictional element is used to model the discontinuous behavior at the interface of backfill soils and abutments. Discontinuous type expansion joint elements are also included. Linear spring elements provide flexibility at the vertical soil boundaries. The soil foundation flexibilities under columns are established using elastic half-space theory. In the non-linear mathematical model the effects of separation and impact at the interface between abutments and backfills, the yielding at concrete columns and backfill soils and slippage at the expansion joints are taken into consideration. Parameter studies are first carried out considering a rigid wall backfill soil system. A short, stiff, three-span bridge is then investigated with full soil-structure interaction effects included. Finally, based on the analytical results, a general conclusion regarding the analyses capability is deduced.					
17. Key Words Earthquake, Bridge Seismic Analysis, Structural Analysis, Seismic Design Criteria.			18. Distribution Statement No restrictions. This document is available through the National Technical Information Service, Springfield, Virginia 22151		
19. Security Classif. (of this report) Unclassified		20. Security Classif. (of this page) Unclassified		21. No. of Pages 176	
22. Price					





UNITED STATES GOVERNMENT

# Memorandum

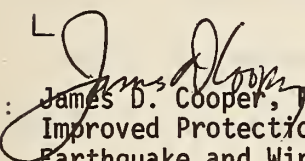
U.S. DEPARTMENT OF TRANSPORTATION  
FEDERAL HIGHWAY ADMINISTRATION

FEB 18 1975

TO : Individual Researchers

DATE:

In reply refer to: HRS-11

FROM :  James D. Cooper, Project Manager, FCP Project 5A,  
Improved Protection Against Natural Hazards of  
Earthquake and WindSUBJECT: Transmittal of Research Report No. FHWA-RD-75-10  
"Effectiveness of Existing Bridge Designs in Resisting Earthquakes,  
Phase III: Short, Single or Multiple-Span Highway Bridges"

Distributed with this memorandum is the subject report intended primarily for research audiences. This report will be of interest to structural researchers concerned with earthquake resistant highway bridges.

This recently issued report is the third in a series to result from research being conducted at the University of California, Berkeley, for the Federal Highway Administration. Analytical investigations of the seismic response of short, single or multiple-span highway bridge structures of the type which suffered heavy damage during the San Fernando earthquake of February 9, 1971, are described in the report.

Additional copies are available from the National Technical Information Service (NTIS), Department of Commerce, 5285 Port Royal Road, Springfield, Virginia 22151. A small charge is imposed for copies provided by NTIS.

Attachment



## PREFACE

The investigation with interpretation as described in this report was sponsored by the U. S. Department of Transportation, Federal Highway Administration, under Contract No. DOT-FH-11-7798 covering the period July 1, 1971 through September 30, 1974.

The general investigation called for in this contract is under the supervision and technical responsibility of Professors R. W. Clough, W. G. Godden, and J. Penzien. Professor Penzien acts as principal investigator.

### ACKNOWLEDGEMENT

The authors wish to express their sincere appreciation to the California State Division of Highways, Department of Public Works, for providing the engineering data of the bridge structures studied in this investigation.

## TABLE OF CONTENTS

### Page

PREFACE . . . . .	iv
ACKNOWLEDGEMENT . . . . .	v
TABLE OF CONTENTS . . . . .	vi
LIST OF TABLES . . . . .	viii
LIST OF FIGURES . . . . .	ix
I. INTRODUCTION	
A. Statement of Problem . . . . .	1
B. Review of Pertinent Investigations . . . . .	1
C. Review of Damages Caused by Earthquakes . . . . .	3
D. Scope of Present Investigation . . . . .	4
II. ELASTIC STIFFNESSES OF MODEL ELEMENTS	
A. Soil Finite Element of a Continuum . . . . .	7
B. Soil Boundary Element . . . . .	14
C. Prismatic Beam Element . . . . .	14
D. Frictional Element . . . . .	17
E. Expansion Joint Element . . . . .	19
F. Equivalent Column for Foundation . . . . .	19
III. MATERIAL PROPERTIES OF SOIL	
A. Stress-Strain Relationship . . . . .	29
B. Mohr's Envelope, p-q Diagram . . . . .	32
C. Active and Passive Stress . . . . .	34
D. Damping . . . . .	36
IV. NON-LINEAR STIFFNESSES OF MODEL ELEMENTS	
A. General Elastic-Perfectly Plastic Stress-Strain Relations . . . . .	49
B. Soil Finite Element . . . . .	52
C. Column Element . . . . .	57
D. Frictional Element . . . . .	61
E. Expansion Joint Element . . . . .	62

# TABLE OF CONTENTS (cont.)

	<u>Page</u>
F. Soil Boundary Element and Equivalent Column of Foundation . . . . .	62
V. DYNAMIC ANALYSIS PROCEDURES	
A. Equation of Motion . . . . .	66
B. Stiffness Matrix . . . . .	67
C. Mass Matrix . . . . .	67
D. Damping Matrix . . . . .	68
E. Step-by-Step Integration Techniques . . . . .	69
F. Time Interval $\Delta t$ . . . . .	74
G. Earthquake Input . . . . .	75
VI. PARAMETER STUDIES	
A. Rigid Wall-Backfill System . . . . .	78
B. Integration-Time-Interval Sensitivity Analysis . . . . .	84
C. Bridge-Soil System . . . . .	85
D. Comparison of Resultant Abutment Backfill Force Obtained by Analysis and the Monobe-Okabe Method . . . . .	89
VII. GENERAL CONCLUSION . . . . .	118
BIBLIOGRAPHY . . . . .	119
APPENDIX COMPUTER PROGRAM LISTINGS . . . . .	130



## LIST OF TABLES

- Table 1 Details of Rigid Wall Systems for Study of Lateral Extent
- Table 2 Comparison of Responses of Rigid Wall System at Different Lateral Extent
- Table 3 Comparison of Responses of Rigid Wall System With Different Length to Height Ratio  $R = a/b$
- Table 4 Comparison of Response of Rigid Wall System with  $R = 2$  for  $x < 2H$  and  $R = 10$  for  $x > 2H$  at Different Time Step
- Table 5 Comparison of Maximum Total Seismic Force on the Bridge With or Without Soil Interaction

## LIST OF FIGURES

- Fig. 1 Bridge Structure and Analytical Model
- Fig. 2 Two Dimensional Isoparametric Element
- Fig. 3 Boundary Element
- Fig. 4 Beam Element Coordinate System
- Fig. 5 Frictional Element, Height = 0, Local Coordinate
- Fig. 6 Expansion Joint Element
- Fig. 7 Displacement Types
- Fig. 8 Pier with Four Columns
- Fig. 9 Hysteretic Stress-Strain Relationships at Different Strain Amplitudes - Secant Modulus
- Fig. 10 Secant Shear Modulus of Sands at Different Void Ratios
- Fig. 11 Typical Reduction of Secant Shear Modulus with Shear Strain for Saturated Clays
- Fig. 12 Variation of Tangent Modulus with Shear Strain for Sand
- Fig. 13 Idealized Stress-Strain Relationship
- Fig. 14 In-Situ Secant Moduli for Saturated Clays
- Fig. 15 Variation of Tangent Modulus with Shear Strain for Clays
- Fig. 16 Mohr's Envelope for Soil Sample
- Fig. 17 Stresses at Maximum Shear Plane
- Fig. 18 p-q Diagram
- Fig. 19 Mohr Circle
- Fig. 20 Stress Paths for Rankine Active and Passive Conditions
- Fig. 21 Stress Conditions at Field
- Fig. 22 Mohr Circle in 3 Planes
- Fig. 23 Active and Passive Failure

LIST OF FIGURES (cont.)

- Fig. 24 Equivalent Viscous Friction vs. Yield
- Fig. 25 Mohr - Coulomb Yield Function
- Fig. 26 Column Interaction Curve
- Fig. 27 Interaction Diagram of Concrete Column
- Fig. 28 Situation at Overshooting
- Fig. 29 Overshooting at Discontinuity
- Fig. 30 Simulated Ground Acceleration Record of the San Fernando Earthquake at the Olive View Hospital Site
- Fig. 31 General Plan of North Connector Undercrossing
- Fig. 32 Abutment and Backfills
- Fig. 33 Rigid Wall System for Studying the Effects of Lateral Extent of Backfills
- Fig. 34 Static and Maximum Dynamical Total Lateral Earthpressure for Different Lateral Extent  $L/H$
- Fig. 35 Maximum Horizontal Displacement at Points 1 to 6 for Different Lateral Extent  $L/H$
- Fig. 36 Maximum Horizontal Accelerations at Points 1 to 6 for Different Lateral Extent  $L/H$
- Fig. 37 Finite Element Model for Studying the Length to Height Ratio  $R$
- Fig. 38 Static and Maximum Dynamical Total Lateral Pressure for Different Element Size  $R = a/b$
- Fig. 39 Maximum Horizontal Displacement at Points 1 to 6 for Different Element size  $R = a/b$
- Fig. 40 Maximum Horizontal Acceleration at Points 1 to 6 for Different Element Size  $R = a/b$
- Fig. 41 Static and Maximum Dynamical Pressure Distribution with Different Number of Layers - Rigid Wall System
- Fig. 42 Total Lateral Earthpressure - Rigid Wall System

LIST OF FIGURES (cont.)

- Fig. 43 Static and Maximum Dynamical Pressure Distribution with Different Soil Properties - Rigid Wall System
- Fig. 44 Model for Studying Frictional Element, Rigid Wall System
- Fig. 45 Effect of Stiffness of Frictional Element on Total Lateral Force - Rigid Wall System
- Fig. 46 Lateral Force and Horizontal Acceleration at Point No. 1 - Rigid Wall System
- Fig. 47 Vertical Acceleration at Point No. 1
- Fig. 48 North Connector Undercrossing, Bridge-Soil Systems
- Fig. 49 Static and Maximum Dynamical Pressure Distribution with Different Boundary Conditions at the Base of Abutment
- Fig. 50 Static and Maximum Dynamical Pressure Distribution of Bridge-Soil System with Different Substructures
- Fig. 51 Static and Dynamic Pressure Distribution of Bridge-Soil System with Different Degrees of Non-linearity
- Fig. 52 Static and Maximum Dynamical Pressure Distribution of Bridge-Soil System with Different Foundation





## I INTRODUCTION

### A. STATEMENT OF PROBLEM

The seismic response of short, single or multiple span, highway bridges are greatly affected by the phenomenon of soil-structure interaction. The dynamic forces exerted by backfills on the abutments often add significantly to the maximum seismic forces developed in the overall structural system. Also, bridges of this type usually have relatively short and stiff columns which interact strongly with their supporting foundations. Neglecting these interaction effects can lead to large errors in predicting design loads. It is therefore the objective of this investigation to establish appropriate mathematical models which will yield realistic seismic response for certain soil-structure systems of this type. Further, computer programs are written to carry out time-history dynamic analyses as an aid to the design process.

### B. REVIEW OF PERTINENT RESEARCH INVESTIGATIONS

Numerous analytical investigations have been carried out in the past to determine dynamic earth pressures acting on retaining walls. One of the earliest was carried out by Okabe and later a similar study was reported by Mononobe and Matsuo [80, 74]\*. In each of these investigations an equivalent static earth pressure was determined as a function of acceleration with its resultant acting on the wall at a

---

\*Numbers in square brackets refer to Bibliography numbers.

position corresponding to that of static fluid pressure, i.e. at a height one-third the distance from the base. Much later, Valera used the finite element method to predict the intensities of seismic earth pressures acting on rigid walls [106]. In this investigation, nonlinear soil behavior was considered. Seed and Whitman summarized 31 investigations carried out from 1926 to 1969 and made valuable suggestions for their application to design [97]. Later, Wood derived analytical expressions for earth pressures acting against rigid and rotating walls using linear soil properties [117]. All of these investigations were concerned with intensities of dynamic pressures but in each case they assumed the pressures to act independently of the dynamic response of the wall itself.

In recent years, the influence of soil conditions on the seismic response of structural systems has received considerable attention. Seed recently published a report covering two main aspects of this problem: (1) changes in seismic ground motions adjacent to buildings as a result of physical interaction effects, and (2) changes in seismic response of buildings as a result of the changes in ground motions due to different soil deposits. This investigation did not, however, include full dynamic soil-structure interaction effects for structures other than buildings [98].

Few analytical investigations have been reported in which dynamic soil-bridge interaction effects were treated rigorously. One such study was reported by Penzien in 1970 [82]. In this particular investigation, the soil foundation was represented by a series of lumped masses interconnected by bilinear hysteretic shear springs having properties which varied with soil depth and also interconnected with

viscous linear dashpots. The bridge deck, supporting piers, and pile foundations were also modelled as lumped mass systems. The three dimensional effects of the foundation soils were determined using the Mindlin Theory of the elastic half-space. Equations of motion were developed which considered all dynamic interaction effects. Recently, Tseng and Penzien reported an investigation on the seismic response of long multiple span bridges in which the mathematical modelling included soil-structure interaction effects at the bases of columns; however, due to the long structural types considered, soil-abutment interaction effects were neglected [105].

As far as experimental results are concerned, most investigations have been carried out on simple wall-soil systems. Important contributions have been made by Matsuo, Ishii and Arai and Tsuchida, Matsuo and Ohara, Tschebotanoff, Ohara, and Niwa [68, 52, 69, 104, 79, 78].

Shepherd and Charleson, and Shepherd and Sidwell have conducted field experiments on an existing bridge in the small loading range [100, 101]. Their results show that the soil around the bridge displayed high energy absorption qualities, i.e. provided considerable damping to the overall soil-structure system. Broms and Ingelson have also conducted field experiments to determine the static earth pressures acting on abutment walls [11].

#### C. REVIEW OF DAMAGES CAUSED BY EARTHQUAKES

Iwasaki, Penzien, and Clough prepared an extensive summary of the damages caused to bridges during earthquakes for the period 1923 to 1971 [53]. Jennings and Wood, and Lew, Legendecker, and Dijkers have



reported on the damages to bridges during the San Fernando earthquake of February 9, 1971 [59, 65]. Duke and Leeds reported similar damages caused by the Chilean earthquake of 1960, while Rose, Seed, and Migliaccio reported on the Alaskan earthquake of 1964 [29, 92]. As indicated in these reports, short bridges have suffered damages ranging from column failures to cracking, tilting, and even overturning of piers, abutments, and wing walls. Clearly, this evidence shows that large dynamic forces are induced in the overall structural system by backfill earth pressures.

#### D. SCOPE OF PRESENT INVESTIGATION

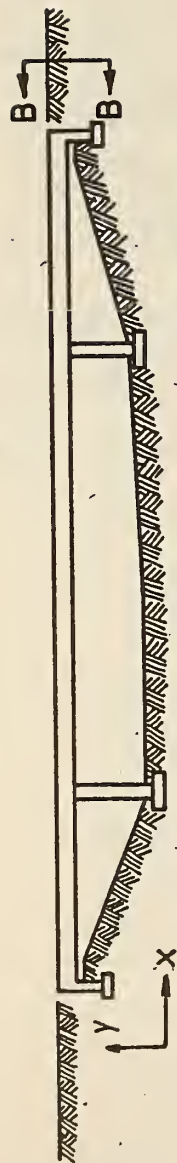
The present investigation is a study of the seismic response of short, single or multiple span, highway bridges having narrow abutment backfills as shown in Fig. 1.

Since the earth pressures acting against the abutments can greatly affect the seismic response of the bridge, the mathematical modelling includes a two-dimensional soil element representation of the abutment backfills. This representation accounts for nonlinear soil properties and allows different vertical boundaries to be present as shown in Figs. 1D, 1E and 1F. The bridge deck, piers (or columns), and abutments are modelled using prismatic beam elements which may be permitted to have hysteretic yielding properties. A frictional element is used to model the nonlinear, discontinuous behavior at the interfaces of backfill soils and abutments and nonlinear, discontinuous type of expansion joint element is included. The soil foundation flexibilities under the columns are represented by equivalent columns. The mathematical model

of the overall soil-structure system permits the study of interaction effects and yields the distribution of forces throughout the system.

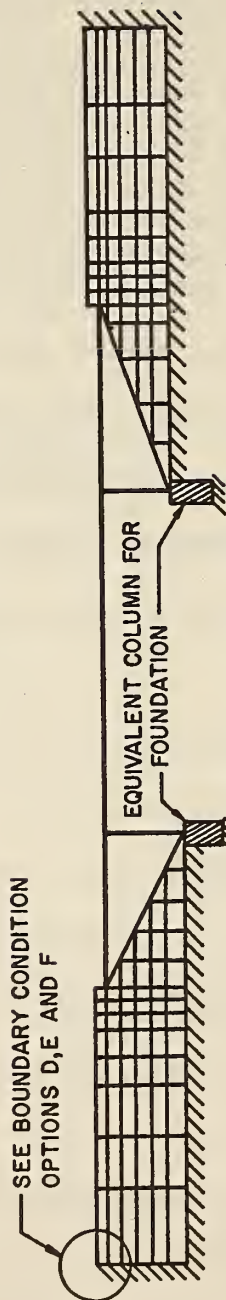
Chapter II of this report describes the different elements used in the mathematical modelling and presents the derivations of elastic stiffnesses used for these elements. Chapter III discusses soil material properties used in the modelling with particular emphasis on nonlinear properties. Chapter IV develops the stiffnesses of nonlinear elements with emphasis on the derivation of the elasto-plastic force-displacement relations for the soil finite elements and the bridge column elements. Chapter V presents the numerical techniques used in the time-history dynamic analysis while Chapter VI presents the results of parameter studies. Chapter VII presents certain conclusions and recommendations. Finally, listings of the computer program are presented in Appendix A.



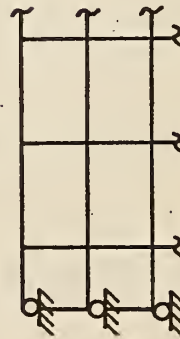


B. SECTION B-B

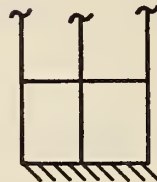
A. ELEVATION



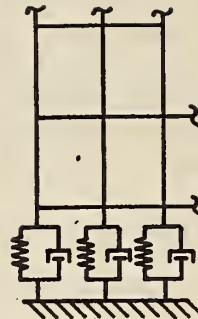
C. ANALYTICAL MODEL



D. ROLLER



E. FIXED END



F. SPRING AND DASHPOT

FIG. 1 BRIDGE STRUCTURE AND ANALYTICAL MODEL

## II ELASTIC STIFFNESSES OF MODEL ELEMENTS

Six basic elements are used in the mathematical modelling of the bridge-soil system (1) soil finite element of a continuum, (2) soil boundary element, (3) frictional element at interface of soil and abutment wall, (4) prismatic beam element, (5) expansion joint element, and (6) equivalent column of foundation. It is the purpose of this chapter to describe these elements and to derive their elastic stiffnesses.

### A. SOIL FINITE ELEMENT OF A CONTINUUM

The bridge-soil system shown in Fig. 1 is subjected to earthquake motions in the vertical direction and in one horizontal direction coinciding with the longitudinal axis of the bridge. Because of the conditions of symmetry, it is assumed that the soils adjacent to the abutments respond to these motions in a two-dimensional manner. This assumption allows these soils to be modelled using two-dimensional finite elements of a continuum interconnected at their nodal points. Material properties are defined individually for each element which may have an arbitrary quadrilateral or triangular shape.

The quadrilateral element used is the isoparametric element for which the geometry and displacements are described in terms of the same parameters of similar order. Using the natural coordinate system and interpolation displacement models, the isoparametric formulation has several advantages over the generalized coordinate method [25]. First,

the nodal displacements provide a more direct visualization of actual structural deformations than do the generalized displacements. Second, it is computationally more efficient since no transformation from one coordinate system to another is required. Finally, the local coordinate system of the isoparametric approach coincides with the global coordinate system; thus, eliminating the need for transformation of loads and stiffnesses from one coordinate frame to the other.

The following derivation of the stiffness matrix for the two-dimensional quadrilateral isoparametric element is similar to that found in certain textbooks [25, 34, 118].

1. Coordinate System - The global Cartesian coordinates  $(x,y)$  and the local (or natural) coordinates  $(s,t)$  as shown in Fig. 2 are related through an interpolation function  $h_i$  by the relations

$$\begin{aligned} x &= \sum_{i=1}^4 h_i x_i \\ y &= \sum_{i=1}^4 h_i y_i \end{aligned} \tag{1}$$

where

$$\begin{aligned} h_1 &= \frac{1}{4} (1-s) (1-t) \\ h_2 &= \frac{1}{4} (1+s) (1-t) \\ h_3 &= \frac{1}{4} (1+s) (1+t) \\ h_4 &= \frac{1}{4} (1-s) (1+t) \end{aligned} \tag{2}$$

2. Strain-Displacement Equations - The displacements are approximated using the same interpolation function which can provide for both

flexible and rigid body modes. In this case, one can state

$$\begin{aligned} u_x(s,t) &= \sum_{i=1}^4 h_i u_{x_i} \\ u_y(s,t) &= \sum_{i=1}^4 h_i u_{y_i} \end{aligned} \quad (3)$$

The two-dimensional strains are obtained by taking derivations of the displacements with respect to x and y in the following manner:

$$\underline{\varepsilon} = \begin{Bmatrix} \varepsilon_{xx} \\ \varepsilon_{yy} \\ \varepsilon_{xy} \end{Bmatrix} = \begin{Bmatrix} \frac{\partial u_x}{\partial x} \\ \frac{\partial u_y}{\partial y} \\ \frac{\partial u_x}{\partial y} + \frac{\partial u_y}{\partial x} \end{Bmatrix} = \begin{Bmatrix} \sum_{i=1}^4 \frac{\partial h_i}{\partial x} u_{x_i} \\ \sum_{i=1}^4 \frac{\partial h_i}{\partial y} u_{y_i} \\ \sum_{i=1}^4 \left( \frac{\partial h_i}{\partial y} u_{x_i} + \frac{\partial h_i}{\partial x} u_{y_i} \right) \end{Bmatrix} \quad (4)$$

Since functions  $h_i$  ( $i=1,2,3,4$ ) are expressed in terms of s and t, the chain rule of derivations can be applied using the equations

$$\begin{aligned} \frac{\partial h_i}{\partial x} &= \frac{\partial h_i}{\partial s} \frac{\partial s}{\partial x} + \frac{\partial h_i}{\partial t} \frac{\partial t}{\partial x} \\ \frac{\partial h_i}{\partial y} &= \frac{\partial h_i}{\partial s} \frac{\partial s}{\partial y} + \frac{\partial h_i}{\partial t} \frac{\partial t}{\partial y} \end{aligned} \quad (5)$$

The chain rule is

$$\begin{Bmatrix} \frac{\partial ( )}{\partial s} \\ \frac{\partial ( )}{\partial t} \end{Bmatrix} = \begin{bmatrix} \frac{\partial x}{\partial s} & \frac{\partial y}{\partial s} \\ \frac{\partial x}{\partial t} & \frac{\partial y}{\partial t} \end{bmatrix} \begin{Bmatrix} \frac{\partial ( )}{\partial x} \\ \frac{\partial ( )}{\partial y} \end{Bmatrix} \quad (6)$$

which in its inverted form becomes

$$\begin{pmatrix} \frac{\partial ( )}{\partial x} \\ \frac{\partial ( )}{\partial y} \end{pmatrix} = \frac{1}{J} \begin{bmatrix} \frac{\partial y}{\partial t} & -\frac{\partial y}{\partial s} \\ -\frac{\partial x}{\partial t} & \frac{\partial x}{\partial s} \end{bmatrix} \begin{pmatrix} \frac{\partial ( )}{\partial s} \\ \frac{\partial ( )}{\partial t} \end{pmatrix} \quad (7)$$

where the Jacobian J is defined by

$$J = \frac{\partial x}{\partial s} \frac{\partial y}{\partial t} - \frac{\partial x}{\partial t} \frac{\partial y}{\partial s} \quad (8)$$

Thus, the required derivatives are given by

$$\begin{bmatrix} \frac{\partial s}{\partial x} & \frac{\partial t}{\partial x} \\ \frac{\partial s}{\partial y} & \frac{\partial t}{\partial y} \end{bmatrix} = \frac{1}{J} \begin{bmatrix} \frac{\partial y}{\partial t} & -\frac{\partial y}{\partial s} \\ -\frac{\partial x}{\partial t} & \frac{\partial x}{\partial s} \end{bmatrix} \quad (9)$$

Taking derivatives of Eqs. (1), one can write

$$\begin{aligned} \frac{\partial x}{\partial s} &= \sum_{i=1}^4 \frac{\partial h_i}{\partial s} x_i \\ \frac{\partial x}{\partial t} &= \sum_{i=1}^4 \frac{\partial h_i}{\partial t} x_i \\ \frac{\partial y}{\partial s} &= \sum_{i=1}^4 \frac{\partial h_i}{\partial s} y_i \\ \frac{\partial y}{\partial t} &= \sum_{i=1}^4 \frac{\partial h_i}{\partial t} y_i \end{aligned} \quad (10)$$

Making use of Eqs. (2) and (10), the Jacobian, as defined by Eq. (8)

becomes



$$\begin{aligned}
J = & \frac{1}{8} [s(x_3 - x_4)(y_1 - y_2) - (x_1 - x_2)(y_3 - y_4) \\
& + t(x_2 - x_3)(y_1 - y_4) - (x_1 - x_4)(y_2 - y_3) \\
& + (x_1 - x_3)(y_2 - y_4) - (x_2 - x_4)(y_1 - y_3)]
\end{aligned} \quad (11)$$

and the strain vector defined by Eq. (4) becomes

$$\underline{\varepsilon} = \begin{bmatrix} \frac{\partial h_1}{\partial x} & 0 & \frac{\partial h_2}{\partial x} & 0 & \frac{\partial h_3}{\partial x} & 0 & \frac{\partial h_4}{\partial x} & 0 \\ 0 & \frac{\partial h_1}{\partial y} & 0 & \frac{\partial h_2}{\partial y} & 0 & \frac{\partial h_3}{\partial y} & 0 & \frac{\partial h_4}{\partial y} \\ \frac{\partial h_1}{\partial y} & \frac{\partial h_1}{\partial x} & \frac{\partial h_2}{\partial y} & \frac{\partial h_2}{\partial x} & \frac{\partial h_3}{\partial y} & \frac{\partial h_3}{\partial x} & \frac{\partial h_4}{\partial y} & \frac{\partial h_4}{\partial x} \end{bmatrix} \begin{Bmatrix} u_{1x} \\ u_{1y} \\ u_{2x} \\ u_{2y} \\ u_{3x} \\ u_{3y} \\ u_{4x} \\ u_{4y} \end{Bmatrix} \quad (12)$$

or in compact form may be expressed as

$$\underline{\varepsilon} = \underline{B} \underline{u} \quad (13)$$

The derivatives in the coefficient matrix of Eq. (12) can now be expressed in their final manipulable form

$$\frac{\partial h_1}{\partial x} = \frac{1}{16J} [y_2(h_1 + h_2) + y_3(h_4 - h_2) - y_4(h_1 + h_4)]$$

$$\frac{\partial h_2}{\partial x} = \frac{1}{16J} [-y_1(h_1 + h_2) + y_3(h_2 + h_3) + y_4(h_1 - h_3)]$$

$$\frac{\partial h_3}{\partial x} = \frac{1}{16J} [y_1(h_2 - h_4) - y_2(h_2 + h_3) + y_4(h_3 + h_4)]$$

$$\frac{\partial h_4}{\partial x} = \frac{1}{16J} [y_1(h_1 + h_4) + y_2(h_3 - h_1) - y_3(h_4 + h_3)]$$

$$\frac{\partial h_1}{\partial y} = \frac{1}{16J} [-x_2(h_1 + h_2) + x_3(h_2 - h_4) + x_4(h_1 + h_4)]$$

$$\begin{aligned}
\frac{\partial h_2}{\partial y} &= \frac{1}{16J} [x_1(h_1 + h_2) - x_3(h_2 + h_3) + x_4(h_3 - h_1)] \\
\frac{\partial h_3}{\partial y} &= \frac{1}{16J} [x_1(h_4 - h_2) + x_2(h_2 + h_3) - x_4(h_3 + h_4)] \\
\frac{\partial h_4}{\partial y} &= \frac{1}{16J} [-x_1(h_1 + h_4) + x_2(h_1 - h_3) + x_3(h_3 + h_4)]
\end{aligned}
\tag{14}$$

Using standard index notation with  $i$  permutating 1 through 4, Eqs. (14) can be written in the two single equations

$$\begin{aligned}
\frac{\partial h_i}{\partial x} &= \frac{1}{16J} [y_{i+1}(h_i + h_{i+1}) + y_{i+2}(h_{i+3} - h_{i+1}) - y_{i+3}(h_i + h_{i+3})] \\
\frac{\partial h_i}{\partial y} &= \frac{1}{16J} [-y_{i+1}(h_i + h_{i+1}) + x_{i+2}(h_{i+1} - h_{i+3}) + x_{i+3}(h_i + h_{i+3})]
\end{aligned}
\tag{15}$$

3. Element Stiffness and Numerical Integration - Considering a thickness  $\omega$  (normal to the plane of element shown in Fig. 2), the element stiffness matrix can be expressed in the form

$$\underline{K} = \int_{\text{vol}} \underline{B}^T \underline{C} \underline{B} \, dv = \int_{\text{area}} \underline{B}^T \underline{C} \underline{B} \, \omega dA \tag{16}$$

where  $\underline{C}$  is the stress-strain matrix with integration being carried out over the entire area of the element. For purposes of numerical integration, Eq. (16) can be written in terms of the  $s$  and  $t$  coordinates giving

$$\underline{K} = \int_{-1}^1 \int_{-1}^1 \underline{B}^T \underline{C} \underline{B} (\det J) \, \omega ds \, dt \tag{17}$$

Upon application of standard one-dimensional numerical integration formulas, Eq. (17) becomes

$$\underline{K} = \sum_j \sum_k \omega_j \omega_k (\det J) \underline{B}^T(s_j, t_k) \underline{C} \underline{B}(s_j, t_k) \omega \quad (18)$$

in which  $s_j$  and  $t_k$  are integration points and  $\omega_j$  and  $\omega_k$  are the appropriate weighting functions. Using the Gauss-Legendre quadrature formula of degree 2, one obtains

$$\left. \begin{array}{l} s_i = \pm 0.577350 \\ t_i = \pm 0.577350 \\ \omega_i = 1 \end{array} \right\} \quad i = 1, 2 \quad (19)$$

For plane stress, matrix  $\underline{C}$  has the form

$$\underline{C} = \frac{E}{1-\nu^2} \begin{bmatrix} 1 & \nu & 0 \\ \nu & 1 & 0 \\ 0 & 0 & \frac{1-\nu}{2} \end{bmatrix} \quad (20)$$

while for plane strain it becomes

$$\underline{C} = \frac{E}{(1+\nu)(1-2\nu)} \begin{bmatrix} 1-\nu & \nu & 0 \\ \nu & 1-\nu & 0 \\ 0 & 0 & \frac{1-2\nu}{2} \end{bmatrix} \quad (21)$$

where  $E$  is Young's Modulus and  $\nu$  is Poisson's ratio.

As shown above, the final form of the element stiffness matrix is a function of geometry, element thickness, and material properties. The overall stiffness matrix of the entire system is assembled by the direct stiffness method [22]. The band width of this matrix depends upon the system of numbering nodal points. Therefore, the nodal points should be numbered in a manner to minimize computer storage requirement

and operating time.

#### B. SOIL BOUNDARY ELEMENT

Boundary elements are used in the mathematical model to account for the elastic action which occurs at the vertical boundaries of the soils being considered. The type of element used for this purpose is a simple elastic spring as shown in Fig. 3. This element has a stiffness matrix  $\underline{k}$  in the local coordinate system of the form

$$\underline{k} = E \begin{bmatrix} 1 & -1 \\ -1 & 1 \end{bmatrix} \quad (22)$$

where E is the equivalent stiffness of the spring, which can be obtained using standard methods [82,89].

#### C. PRISMATIC BEAM ELEMENT

Prismatic beam elements are used to model the bridge deck, piers, abutment walls and equivalent columns for soil foundations. The derivation of the stiffness matrix for a beam element considering axial, shear, and bending deformations can be found in many textbooks [86]. Therefore, only the main features of this matrix will be presented here.

The force components acting on the beam element are axial forces  $s_1$  and  $s_4$ , shearing forces  $s_2$  and  $s_5$ , and bending moments  $s_3$  and  $s_6$  as shown in Fig. 4. The positive directions of these force components (s) and their respective displacement components (u') correspond to those shown in the figure. The stiffness matrix for this element in terms of

the local coordinates is given by the standard form

$$\begin{aligned}
 \underline{k}_{(6 \times 6)} = & \left[ \begin{array}{ccccc}
 \frac{EA}{l} & & & & \\
 0 & \frac{12EI_z}{l^3(1+\phi_y)} & & & \text{SYMMETRICAL} \\
 0 & \frac{6EI_z}{l^2(1+\phi_y)} & \frac{(4+\phi_y)EI_z}{l(1+\phi_y)} & & \\
 -\frac{EA}{l} & 0 & 0 & \frac{EA}{l} & \\
 0 & \frac{-12EI_z}{l^3(1+\phi_y)} & \frac{-6EI_z}{l^2(1+\phi_y)} & 0 & \frac{12EI_z}{l^3(1+\phi_y)} \\
 0 & \frac{6EI_z}{l^2(1+\phi_y)} & \frac{(2-\phi_y)EI_z}{l(1+\phi_y)} & 0 & \frac{-6EI_z}{l^2(1+\phi_y)} \quad \frac{(4+\phi_y)EI_z}{l(1+\phi_y)}
 \end{array} \right]
 \end{aligned}
 \tag{23}$$

where

$$\phi_y = \frac{12EI_z}{G A_{sy} l^2} = 24(1+\nu) \frac{A}{A_{sy}} \left( \frac{\gamma_z}{l} \right)^2
 \tag{24}$$

represents the shear deformation parameter for reinforced concrete elements and where

- $l$  = element length
- $\gamma_z$  = radius of gyration about z axis
- $I_z$  = Moment of inertia about z axis
- $A$  = cross sectional area
- $A_{sy}$  = equivalent shear area in y direction



E = modulus of elasticity

G = modulus of elasticity in shear

v = Poisson's ratio

The matrix equation relating displacements in the local coordinates  $u'$  to displacements in the global coordinates  $u$  is given by

$$\underline{u'} = \underline{\lambda} \underline{u} \quad (25)$$

where  $\lambda$  has the two-dimensional form

$$\underline{\lambda} = \begin{bmatrix} D_x/D_\ell & D_y/D_\ell & 0 & 0 & 0 & 0 \\ -D_y/D_\ell & D_x/D_\ell & 0 & 0 & 0 & 0 \\ 0 & 0 & 1 & 0 & 0 & 0 \\ 0 & 0 & 0 & D_x/D_\ell & D_y/D_\ell & 0 \\ 0 & 0 & 0 & -D_y/D_\ell & D_x/D_\ell & 0 \\ 0 & 0 & 0 & 0 & 0 & 1 \end{bmatrix} \quad (26)$$

and where

$$\begin{aligned} D_x &= x_j - x_i \\ D_y &= y_j - y_i \\ D_\ell &= \sqrt{D_x^2 + D_y^2} \end{aligned} \quad (27)$$

Thus, the stiffness matrix  $\underline{K}$  in global coordinates becomes

$$\underline{K} = \underline{\lambda}^T \underline{k} \underline{\lambda} \quad (28)$$

as indicated above, the stiffness matrix is linearly proportional to the areas and moments of inertia. Therefore, a unit width analysis can be carried out, if desired, by dividing all areas and moments of

inertia by the width of the bridge deck.

#### D. FRICTIONAL ELEMENT

A so called frictional element is used to model the frictional action, separation, and impact which take place at the interfaces of soil backfills and abutment walls. This element has the following characteristics (1) the frictional force per unit area is proportional to the normal interface pressure and a coefficient of friction; thus, slippage occurs when the direction angle of the resultant of pressure and friction exceeds the soil angle of friction, (2) impact occurs at the interface upon closure of any gap which may have earlier developed, and (3) no frictional resistance can develop at the interface when wall and soil surfaces have separated. Discontinuous elements similar to this have been developed by Ghaboussi and Wilson, Scholes and Strover, White and Enderly, and Tseng and Penzien [40, 94, 111, 105]; however, the element developed by Goodman and Taylor has been adopted here [41].

This frictional element is a four nodal element as shown in Fig. 5 having length  $L$  but with a height equal to zero, i.e. nodal points 1 and 4 coincide as do points 2 and 3. It is shown in a local coordinate system with the origin at the center of the element and the  $x$  axis directed along the length of the element.

The relative displacement vector  $\underline{u}$  is expressed in terms of the displacement vector  $\underline{u}_i$  through the linear interpolation function formula

$$\underline{u} = \begin{Bmatrix} (u_x^{\text{top}} - u_x^{\text{bottom}}) \\ (u_y^{\text{top}} - u_y^{\text{bottom}}) \end{Bmatrix}$$

or

$$\underline{u} = \begin{bmatrix} -(1 - \frac{2x}{L}) & 0 & -(1 + \frac{2x}{L}) & 0 & (1 + \frac{2x}{L}) & 0 & (1 - \frac{2x}{L}) & 0 \\ 0 & -(1 - \frac{2x}{L}) & 0 & -(1 + \frac{2x}{L}) & 0 & (1 + \frac{2x}{L}) & 0 & (1 + \frac{2x}{L}) \end{bmatrix} \begin{Bmatrix} u_{1x} \\ u_{1y} \\ u_{2x} \\ u_{2y} \\ u_{3x} \\ u_{3y} \\ u_{4x} \\ u_{4y} \end{Bmatrix} \quad (29)$$

The material property matrix  $\underline{k}$  expressing the stiffness per unit length in the normal and tangential directions is given by

$$\underline{k} = \begin{bmatrix} k_s & 0 \\ 0 & k_n \end{bmatrix} \quad (30)$$

Upon applying the variational principle of solid mechanics, the elastic stiffness matrix in the local coordinate system becomes

$$\underline{K} = \frac{1}{6} \begin{bmatrix} 2k_s & 0 & 1k_s & 0 & -1k_s & 0 & -2k_s & 0 \\ 0 & 2k_n & 0 & 1k_n & 0 & -1k_n & 0 & -2k_n \\ 1k_s & 0 & 2k_s & 0 & -2k_s & 0 & -1k_s & 0 \\ 0 & 1k_n & 0 & 2k_n & 0 & -2k_n & 0 & -1k_n \\ -1k_s & 0 & -2k_s & 0 & 2k_s & 0 & 1k_s & 0 \\ 0 & -1k_n & 0 & -2k_n & 0 & 2k_n & 0 & 1k_n \\ -2k_s & 0 & -1k_s & 0 & 1k_s & 0 & 2k_s & 0 \\ 0 & -2k_n & 0 & -1k_n & 0 & 1k_n & 0 & 2k_n \end{bmatrix} \quad (31)$$

#### E. EXPANSION JOINT ELEMENT

An expansion joint may be present between the bridge deck and an abutment as shown in Fig. 6. This joint can develop horizontal frictional forces which should be modelled properly. For this purpose, the frictional element previously described can be adopted; however, two additional boundary conditions must be imposed, namely, (1) the relative displacement of the upper and lower part of the joint element,  $u_{3x} - u_{2x}$ , cannot cause a gap closure (between deck and abutment) greater than the original gap dimension, and (2) frictional forces can be developed only when the relative displacement,  $u_{1x} - u_{3x}$ , causing a widening of the gap is less than the original "seat" dimension. As soon as the relative displacement ( $u_{1x} - u_{3x}$ ) exceeds the original seat dimension, the bridge deck falls from its support; thus, the computer analysis is stopped at this point.

#### F. EQUIVALENT COLUMN FOR FOUNDATION

Various mathematical models have been used for structural foundations. As reported in the literature, Parmelee, Whitman and Roesset, Dobry, and others [81, 108] used a simple spring dashpot model; Jennings and Bielak and Richart, Hall, and Woods [58, 89] used the elastic half space; Whitman [109] used an equivalent lumped mass model; and, Dans and Butterfield, Finn, Lysmer and Kuhlemeyer, and Wilson [31, 36, 66, 114] used a finite element mesh. Various methods have been reported for estimating the lateral stiffness of foundations employing piles [84, 88].



The replacement of the foundation flexibility with an equivalent column through use of the elastic half space theory and under the assumption of quasi-static behavior has been reported by Penzien, et. al. [8]. This method has been adopted in the present investigations.

The first step in finding the equivalent column for the foundation is to determine the lateral, vertical, and rotational stiffnesses of the foundation at the footing (or pile cap) level. Once these three stiffnesses have been determined, the foundation is replaced by a column of length  $L$ , flexural stiffness  $EI$ , and axial stiffness  $AE$  which when fixed at its base provides the equivalent lateral, vertical, and rotational stiffnesses to the footing. The stiffness matrix for this column is given in the form of Eq. (23) under the assumption of no shear deformation, i.e.  $\phi_y = 0$ .

The foundation stiffnesses can be obtained by either the numerical procedure outlined by Penzien or by a closed form approach reported by Gerrand and Harrison [82, 39].

1. Closed Form Solution for Lateral Stiffness of Circular Footing - The closed form solution for lateral stiffness is available for a circular shaped footing as shown in Fig. 7-c. If the footing is rectangular in shape, an equivalent radius  $r_0$  should be calculated for a circular footing having the same area, then

$$k_x = \frac{8 r_0 G}{2-\nu} \quad (32)$$

where

$k_x$  = lateral stiffness for a single footing

$r_0$  = radius of footing



$G$  = shear modulus of soil

$\nu$  = Poisson's ratio

For a pier of multiple supports, the interactions between footings are estimated by Eq. (33) which describes the lateral displacement at a distance  $r$  from a loaded footing.

$$u = T_h \frac{1}{4\pi r_0 G} \left[ (2-\nu) \cdot \sin^{-1} \frac{1}{r} + \nu \cdot \frac{(r^2-1)^{\frac{1}{2}}}{r^2} \right] \quad (33)$$

where

$u$  = the displacement

$T_h$  = the total applied force at a single footing

$r$  = the distance in terms of radius  $r_0$

By calculating the average displacement of all footings in a pier and dividing the total force by the average displacement, the equivalent stiffness of a pier with multiple footings is then obtained.

## 2. Numerical Solution Using the Mindlin Equation to Calculate

Lateral Stiffness - The Mindlin equation has the following form.

When the  $x$  component of displacement on the surface is to be calculated, as produced by a single concentrated force  $P$  located at the origin  $(0, 0, 0)$  on the surface of an isotropic half space and acting in the  $x$ -direction

$$u_x(x, y, 0) = \frac{P(0, 0, 0)}{16\pi(1-\nu)G} \left\{ \frac{(3-4\nu)}{R} + \frac{1}{R} + \frac{4(1-\nu)(1-2\nu)}{R} + x^2 \left[ \frac{1}{R^3} + \frac{3-4\nu}{R^3} - \frac{4(1-\nu)(1-2\nu)}{R^3} \right] \right\} \quad (34)$$

in which

$$R^2 = x^2 + y^2$$

Under the assumption that the lateral force is uniformly distributed over the area of the footing, the procedure to calculate the lateral stiffness of a single footing is (1) replace the uniform pressure by as many concentrated loads  $P$  as accuracy requires, (2) calculate the lateral displacement of each load point over the footing area due to each concentrated load, (3) sum the resulting displacements at each load point within the footing as caused by the full set of loads, (4) average the load point displacements, and (5) divide the total resultant force by the average of the load point displacements to obtain the lateral stiffness.

Again, if a pier has many footings, the same averaging procedure is applied by assuming a concentrated force at the center of each footing; thus, the lateral stiffness of each pier foundation can be obtained.

3. Comparison of Two Methods for Lateral Stiffness - To compare the two previously described methods for obtaining foundation lateral stiffness, consider the pier shown in Fig. 8 having four footings. Assuming the footing is 8.5 x 8.5 ft and the distance between footings is 26 ft, the individual footing stiffness  $k_x$  and pier stiffness  $k_p$  obtained by the two approaches have the following values in k/ft:

$$k_x = \begin{cases} 32.5 \text{ G} & \text{Numerical method} \\ 25.5 \text{ G} & \text{closed form solution} \end{cases}$$

$$k_p = \begin{cases} 100.6 \text{ G} & \text{Numerical method} \\ 80.0 \text{ G} & \text{closed form solution} \end{cases}$$

Where the unit of  $G$  is in  $k/ft^2$ .

In each case the stiffnesses differ by approximately 20%. In the numerical solution the footing is considered to have 36 concentrated forces applied at equal grid intervals over the area. If the resultant force had been discretized at more than 36 points, the differences in stiffness would have decreased.

4. Vertical Stiffness with Friction Piles - Assuming the friction force per unit length of pile varies in a linear manner from a maximum value at the top to zero at the bottom, and assuming zero vertical displacement at the bottom of the pile, the vertical stiffness of the pile  $k_v$  is

$$k_v = 3AE/L \quad (35)$$

Where  $L$ ,  $A$ , and  $E$  are the length, area, and modulus of elasticity, respectively, of the pile.

5. Vertical Stiffness Without Piles - Assuming uniform vertical displacements as shown in Fig. 7-a, the vertical stiffness of a circular footing without piles is given by

$$k_v = \frac{4 r_0 G}{1-\nu} \quad (36)$$

For other footing shapes, similar stiffness relations have been reported by Lysmer and Duncan [67].

6. Rotational Stiffness Without Piles - Assuming rotational displacements as shown in Fig. 7-b, the rotational stiffness of a circular footing without piles is given by

$$k_{\theta} = \frac{8 r_0^3 G}{3(1-\nu)} \quad (37)$$

The rotational stiffness of a rigid footing with piles can be calculated directly from the vertical stiffness of each pile.

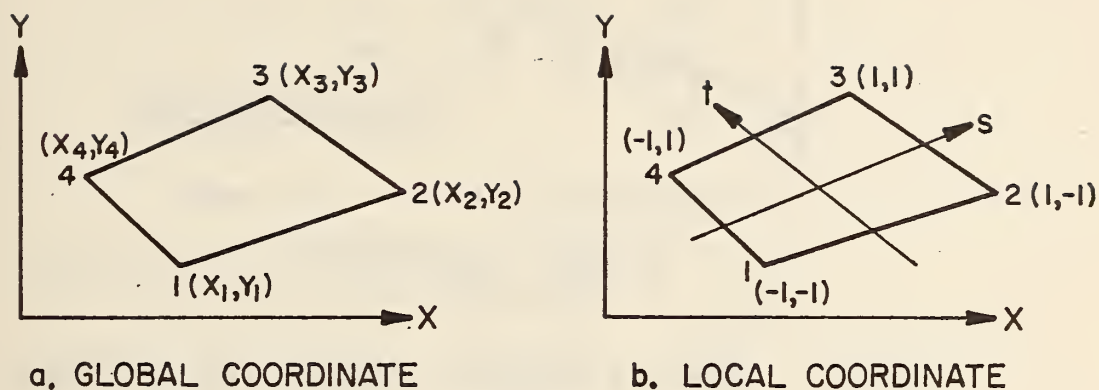


FIG. 2 TWO DIMENSIONAL ISOPARAMETRIC ELEMENT

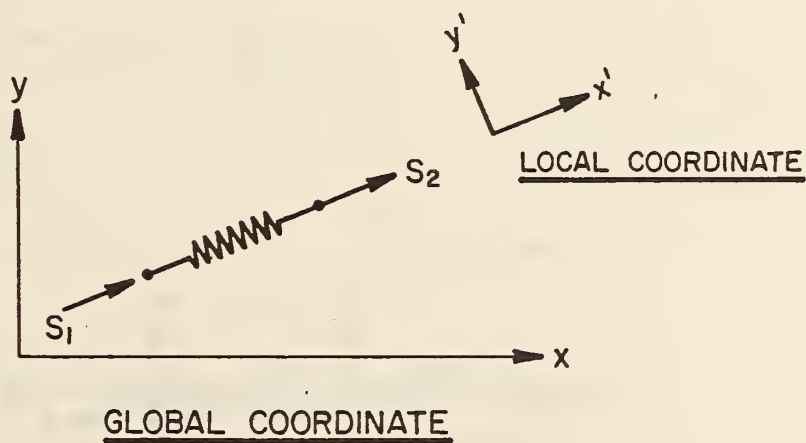


FIG. 3 BOUNDARY ELEMENT



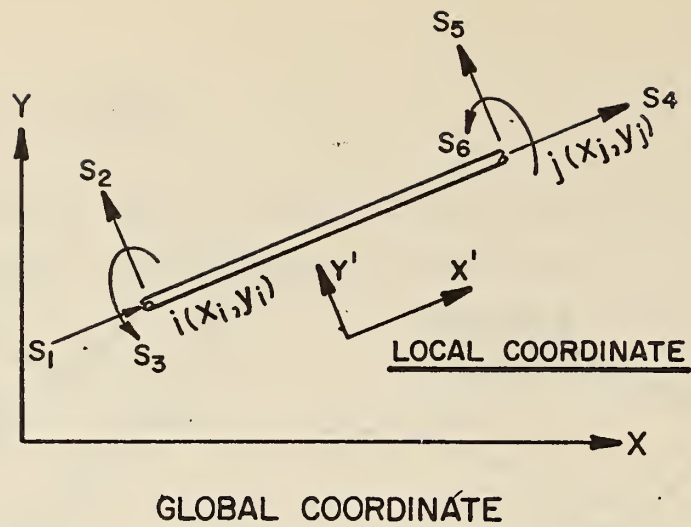


FIG. 4 BEAM ELEMENT COORDINATE SYSTEM

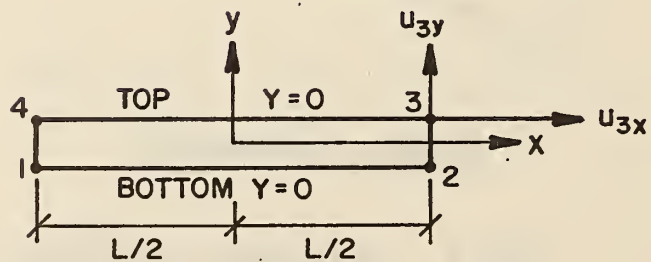
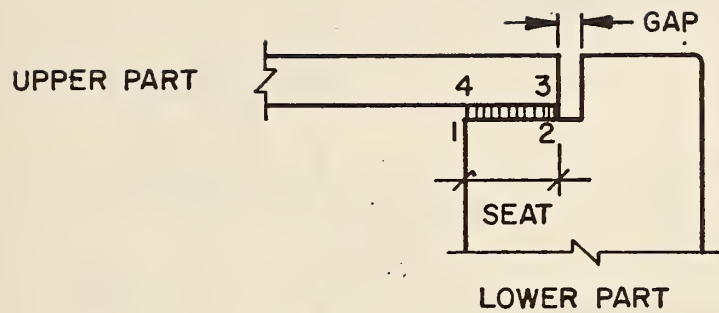
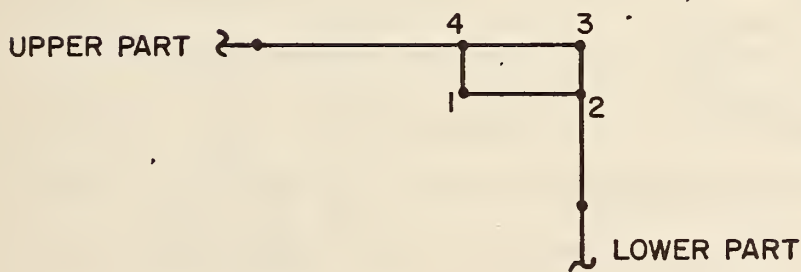


FIG. 5 FRICTIONAL ELEMENT, HEIGHT = 0  
LOCAL COORDINATE



a. PROTOTYPE



b. MODEL

FIG. 6 EXPANSION JOINT ELEMENT

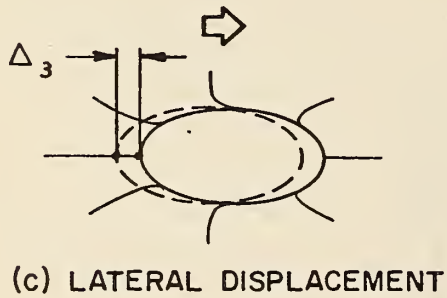
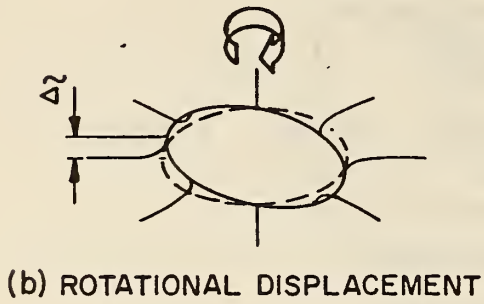
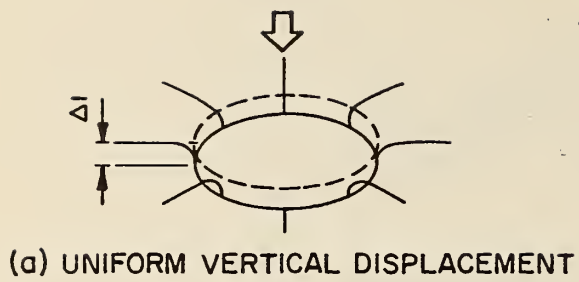


FIG. 7 DISPLACEMENT TYPES

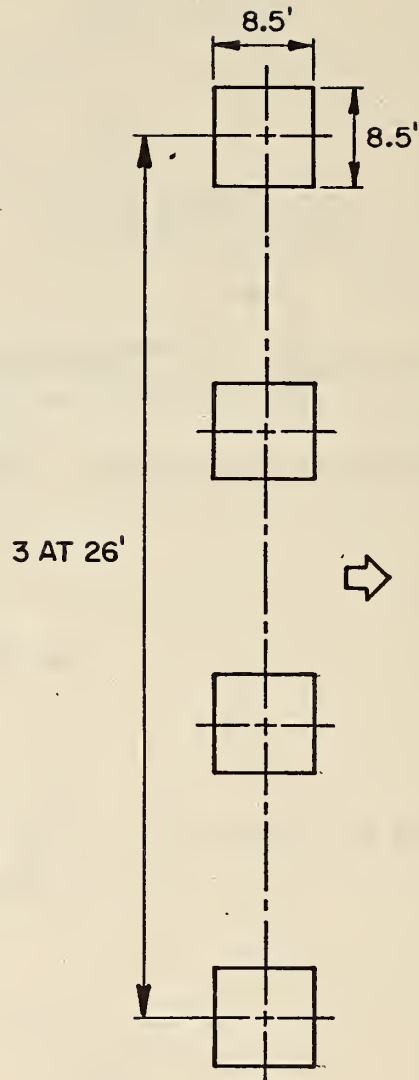


FIG. 8 PIER WITH FOUR COLUMNS

### III MATERIAL PROPERTIES OF SOIL

In this chapter, the pertinent soil material properties used to establish a non-linear finite element model are discussed. The non-linear stress-strain relations, Mohr's envelope and p-q diagram, the concepts of active and passive stresses, and the damping characteristics of soil are described.

#### A. STRESS-STRAIN RELATIONSHIP

Basic to establishing the force-displacement relationships for soil elements as employed in the mathematical model are the stress-strain relationships for the materials involved. These materials include both cohesionless and cohesive soils.

Numerous authors, including Bishop and Henkel, Bishop, Comforth and Seed, have reported procedures for determining the shear modulus of sand [9, 10, 23, 96]. The investigators show that the shear modulus is strongly influenced by confining pressure, strain amplitude, and void ratio. In the present investigation, the equivalent secant shear modulus as determined by extreme points on the hysteresis loop, Fig. 9, is adopted. This modulus can be estimated using the relation proposed by Seed [96], namely,

$$G = 1000 k_2 (\sigma'_m)^{\frac{1}{2}} \quad \text{psf} \quad (38)$$

where  $G$  is the secant modulus of sand,  $\sigma'_m$  is the effective mean stress and  $k_2$  is a parameter which depends upon void ratio  $e$  and strain amplitude

as shown in Fig. 10. Triaxial tests show that  $k_2$  depends only upon void ratio  $e$  at very low strain levels ( $\gamma \leq 10^{-3}$  percent). At intermediate strain levels ( $10^{-3} \leq \gamma \leq 10^{-1}$  percent), it still depends primarily upon void ratio but is also slightly influenced by state of stress and the friction angle  $\phi$ . At very high strain levels,  $k_2$  is essentially a constant which is almost independent of state of stress, friction angle, and the void ratio. Thus for practical purposes, the values of  $k_2$  can be assumed to vary only with strain amplitude and void ratio as shown in Fig. 10.

For prescribed values of void ratio and confining pressure, the stress-strain relationship is non-linear with the shear modulus changing with shear strain. Upon the initiation of yielding the modulus becomes very small. A tangent modulus curve transformed from the equivalent shear modulus curve, Fig. 10, is shown in Fig. 12. Theoretically, one could use a revised tangent modulus over each time interval of a dynamic analysis; however, it is believed to be more practical to use a more simplified form of stress-strain relationship. In the present investigation a trilinear stress-strain relationship, Fig. 13-a, has been adopted with the shear modulus remaining constant during each of three different loading stages. In the initial stage, the soil element is in its geostatic state, i.e. the vertical stress is equal to the weight of soil (per unit area) above the point of interest as given by

$$\sigma_v = \int_0^y w \, dy \quad (39)$$

where  $y$  is the depth and  $w$  is the unit weight of soil. The lateral stress in the principal horizontal direction is



$$\sigma_h = k_0 \sigma_v \quad (40)$$

while in the orthogonal horizontal direction (z) the stress  $\sigma_z$  for plane stress is

$$\sigma_z = 0 \quad (41)$$

and for plane strain is

$$\sigma_z = \mu(\sigma_v + \sigma_h) = \frac{k_0}{1+k_0} (\sigma_v + k_0 \sigma_v) = k_0 \sigma_v = \sigma_h \quad (42)$$

where  $\mu$  is Poisson's ratio. The shear modulus in this stage is evaluated by Eq. (38) with  $k_2$  selected in accordance with the very low strain level shown in Fig. 10. In the second stage the soils in the backfill are no longer in the geostatic state due to loadings from the bridge. In this case the shear modulus is calculated using Eq. (38), but  $k_2$  is revised to be consistent with the maximum shear strain in the element. The third stage occurs after the initiation of yielding in which case the stress-strain relation is evaluated in accordance with a theory of plasticity as described in Chapter IV.

In those cases where curves of  $k_2$  vs.  $\gamma$  as shown in Fig. 10 are unavailable, a bilinear stress-strain relationship is adopted with the initial modulus being estimated by an empirical method and the second stage modulus being calculated by the theory of plasticity as shown in Fig. 13-b.

Turning our attention now to certain clay materials, test data show that at very low strain levels, the shear modulus varies almost linearly with shear strength [112]. In a summary report, Seed has presented a curve of secant shear modulus versus shear strain for

saturated clays [96]. The shear modulus expressed by this curve, Fig. 14, is in the normalized form  $G/s_u$  where  $s_u$  is the undrained shear strength of the material. A curve showing the degradation of secant shear modulus with shear strain, as obtained by a number of investigators, is shown in Fig. 11 [96]. These relationships can be used as a guide for estimating the initial modulus of clay when laboratory test data on the specific material are unavailable.

Fig. 15 gives a tangent modulus curve for clay which is consistent with the secant modulus curve of Fig. 11. Test results show that the shear modulus is essentially independent of the confining pressure. A re-evaluation of shear modulus before the initiation of yielding becomes much less important for this material than for sand. For this reason, a bilinear stress-strain relation has been assumed for cohesive soils in the present investigation. This initial modulus is estimated from the data previously described and the tangent stiffness after yielding is obtained using the same basic procedure as used for sands. No hardening effects after the initiation of yielding are considered.

#### B. MOHR'S ENVELOPE, p-q DIAGRAM

The most widely used yield criterion in soil mechanics is the Mohr-Coulomb criterion which relates the normal stress  $\sigma_f$  and the shear stress  $\tau_f$  at the failure plane by the equation

$$\tau_f = c + \sigma_f \tan \phi \quad (43)$$

where  $c$  is the cohesion of the soil and  $\phi$  is its friction angle. The soil coefficients are usually obtained by conducting triaxial tests at

various confining pressures and by drawing a common tangent line to the resulting Mohr's circles as shown in Fig. 16. It should be noted that since the confining pressure of the triaxial test is uniform, i.e.  $\sigma_2 = \sigma_3$ , the Mohr's circle can be used in its familiar two-dimensional form. Equation (43) when plotted on the  $\sigma$ - $\tau$  plane is called Mohr's yield envelope which implies (1) elastic behavior for a state of stress whose Mohr's circle lies entirely below the envelope, (2) yielding, or impending yielding, for a state of stress whose Mohr's circle has the envelope as its tangent, and (3) that any state of stress whose Mohr's circle crosses the envelope is not permitted.

An alternate way of plotting the results of triaxial tests is to plot the stresses at the plane of maximum shear on the p-q plane, namely,

$$p = \frac{\sigma_1 + \sigma_3}{2} \quad (44)$$

and

$$q = \frac{\sigma_1 - \sigma_3}{2} \quad (45)$$

In Fig. 17, points A, B, and C in the  $\sigma$ - $\tau$  plane represent the stresses on planes of maximum shear. A line drawn through these same points in the p-q plane, as shown in Fig. 18, is called the  $k_f$  line. The equation of this line is

$$q_f = a + p_f \tan \alpha \quad (46)$$

Strength parameters  $c$  and  $\phi$  can be computed from Eq. (46) through the relations

$$\sin \phi = \tan \alpha \quad (47)$$

$$c = a/\cos \phi$$

(48)

### C. ACTIVE AND PASSIVE STRESS

Using the previously defined yield criterion, active and passive soil stresses can be defined as they relate to the backfill pressures exerted on abutment walls. Starting with soil equilibrium in its geostatic state which has principal axes in the vertical and horizontal directions, decrease the horizontal compressive stress continually until the shear strength of the soil is reached and failure occurs. The horizontal compressive stress at the point of failure is active stress. On the other hand, if the horizontal compressive stress is continually increased, the shear strength of the soil will again be reached at a much higher stress level called the passive stress. The Mohr's circles representing these two failure conditions are shown in Fig. 19 where  $\sigma_v$  and  $\sigma_h$  represent the vertical and horizontal stresses, respectively, in the geostatic state and  $\sigma_a$  and  $\sigma_p$  represent the active and passive stresses, respectively. It should be noted here that since the two horizontal stresses are assumed equal, only two stress components are required to describe the stress conditions.

The stress conditions in the  $\sigma$ - $\tau$  diagram of Fig. 19 are again shown in the p-q diagram of Fig. 20, where point A is the geostatic state of stress, point B is the passive state of stress, and point C is the active state of stress. Lines AC and AB are stress paths which depict the successive states of stress which occur in changing from the geostatic condition to the active and passive conditions, respectively.



When applying the concepts of active and passive stresses to more complex stress conditions, certain modifications are needed. For example, the stress conditions of the bridge backfill-soil treated in this investigation is essentially three-dimensional. In this case shear stresses may exist on both vertical and horizontal planes even under gravity loadings. Referring to Figs. 1-A and B for the element coordinates, the Mohr's circle for this condition may be as shown in Fig. 21. Further, it should be noted that if the side slopes of the embankment as seen in Fig. 1-B are not sufficiently flat, the yield plane will show as a line in the y-z plane. In the present study however it is assumed that these slopes are sufficiently flat so that the yield plane shows as a line in the x-y plane. Thus the state of stress at failure as shown on an element of soil in the x-y plane, can be represented by a Mohr's circle tangent to the Mohr's envelope as shown by Circle I in Fig. 22. States of stress in the x-z and y-z planes would be represented by Mohr's circles falling entirely within the above defined circle as shown by Circle II and III in Fig. 22. Because of these restrictions, the problem can be treated as a two-dimensional problem in the x-y plane. Finally, in the present investigation, all stresses vary prior to reaching a state of yield. Based on the previous assumptions, active and passive states can be defined in an equivalent manner. Referring to Fig. 23 where the absolute values of the p and q stresses are plotted, p values at static loading and failure conditions can be compared. If  $|p|$  is assumed to decrease continually with increasing  $|q|$  stress until the Mohr's envelope is reached, active failure occurs. On the other hand, if  $|p|$  is assumed to increase continually with increasing  $|q|$  stress until the envelope is reached, passive failure

occurs. Stresses  $p_a$  and  $p_p$  represent the active and passive stresses in this case.

#### D. DAMPING

Soils, like all materials, exhibit energy dissipation when subjected to cyclic loading. Different methods have been used for measuring damping depending upon the strain levels involved [96]. Forced vibration tests have been used for strain levels in the range  $10^{-4}$  to  $10^{-2}$  percent, free vibration tests have been used for strain levels in the range  $10^{-3}$  to 1.0 percent, and static tests have been used to measure the hysteretic energy absorption for strain levels in the range  $10^{-2}$  to 5 percent. The energy dissipation in the latter case has been expressed in terms of equivalent viscous damping ratios [102, 103].

Experimental evidence shows that two major factors influence the amount of damping exhibited by sands, namely, confining pressure and strain amplitude. Damping in this case tends to decrease with an increase in confining pressure and tends to increase with strain amplitude. Clay materials, on the other hand, exhibit damping which is essentially independent of confining pressure but, like sands, the damping increases with strain amplitude.

In modelling the damping as measured in soils, it has generally been carried out by using an equivalent viscous damping system. An important basic study carried out along these lines, using a wide range of yield values, has been reported by Hudson [47]; see Fig. 24. In this case, the equivalent viscous damping ratio corresponding to elasto-plastic hysteretic damping for a single degree of freedom system

is given.

In the present investigation, hysteretic damping has not been converted to an equivalent viscous form. Rather, it is treated in its true strain dependent form. Since hysteretic damping treated in this manner accounts for energy dissipation only for strain levels above yield, it is necessary to also include viscous damping to represent the low strain level velocity dependent damping. For this purpose, Rayleigh damping has been used in the present investigation.

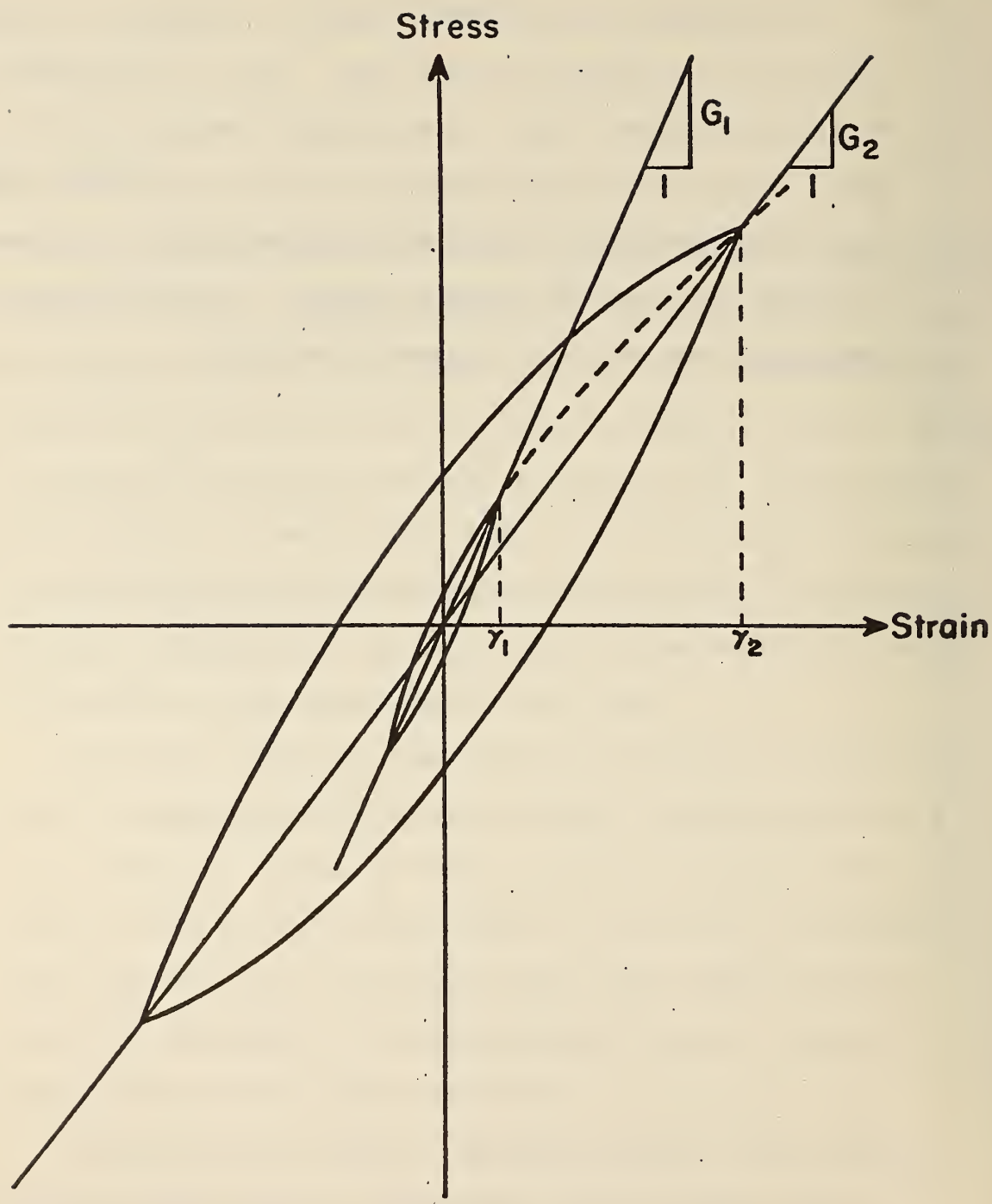


FIG. 9 HYSTERETIC STRESS-STRAIN RELATIONSHIPS AT DIFFERENT STRAIN AMPLITUDES-SECANT MODULUS



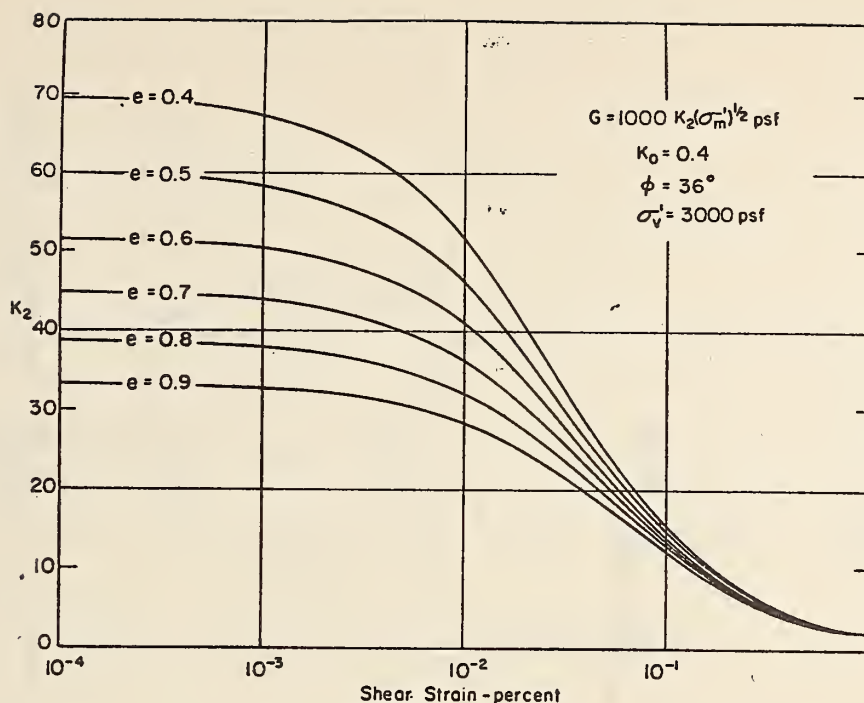


FIG. 10 SECANT SHEAR MODULI OF SANDS AT DIFFERENT VOID RATIOS  
(After Seed and Idriss)

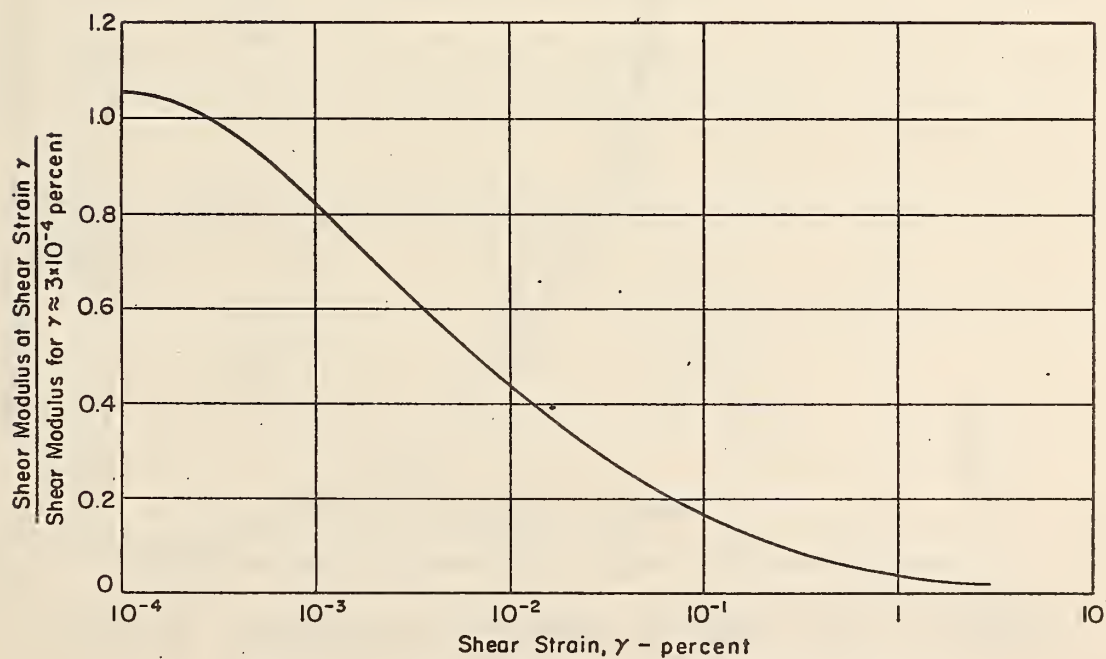


FIG. 11 TYPICAL REDUCTION OF SECANT SHEAR MODULUS  
WITH SHEAR STRAIN FOR SATURATED CLAYS  
(After Seed and Idriss)

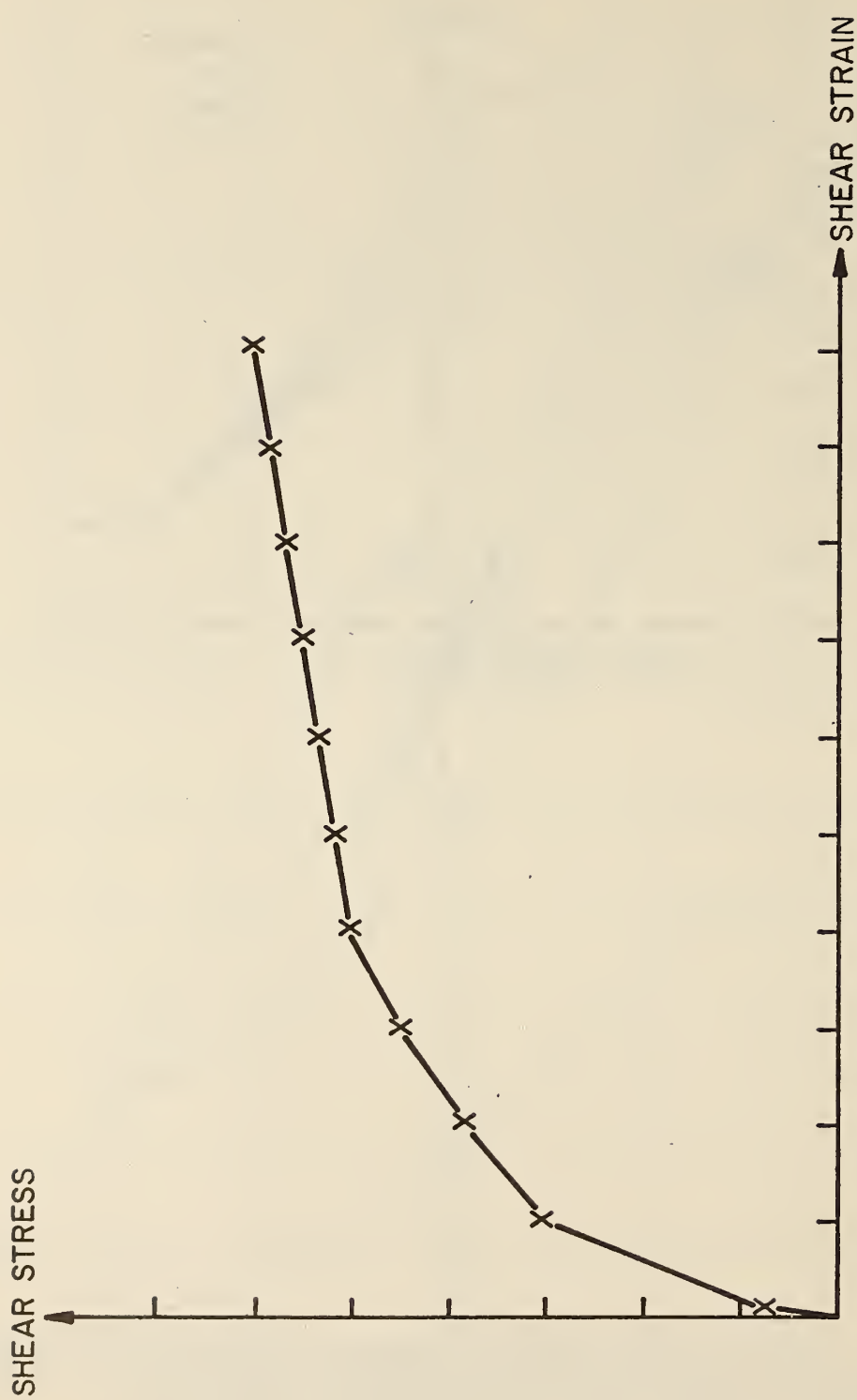
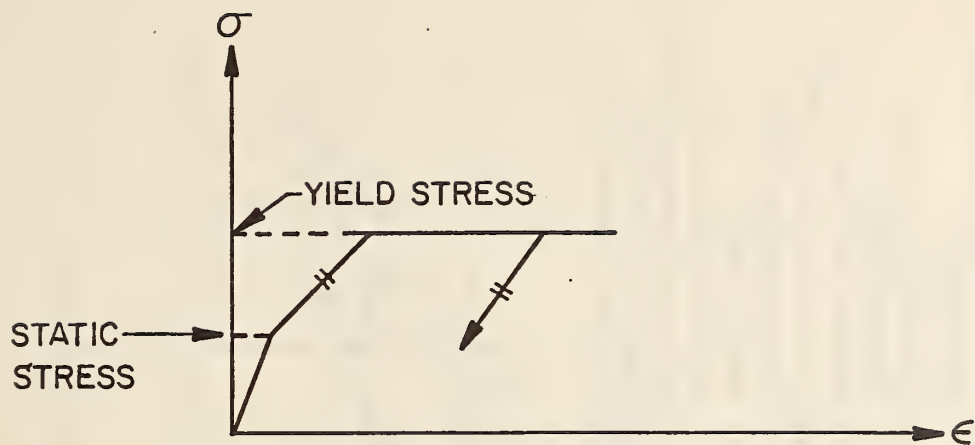
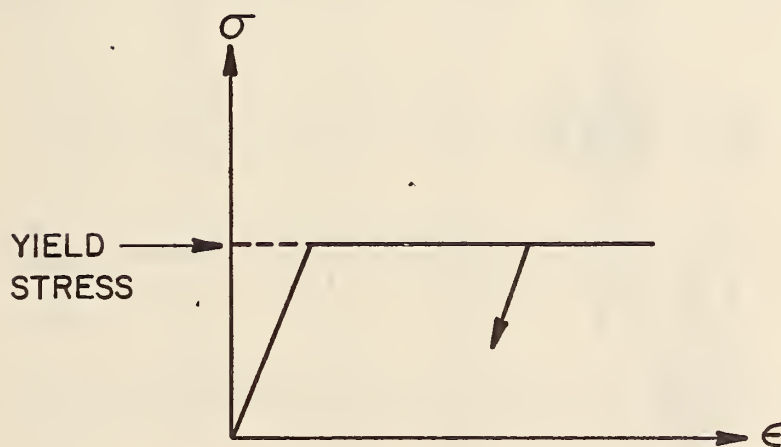


FIG. 12 VARIATION OF TANGENT MODULUS WITH SHEAR STRAIN FOR SAND



(a) TRILINEAR CURVE



(b) BILINEAR CURVE

FIG. 13 IDEALIZED STRESS-STRAIN RELATIONSHIP

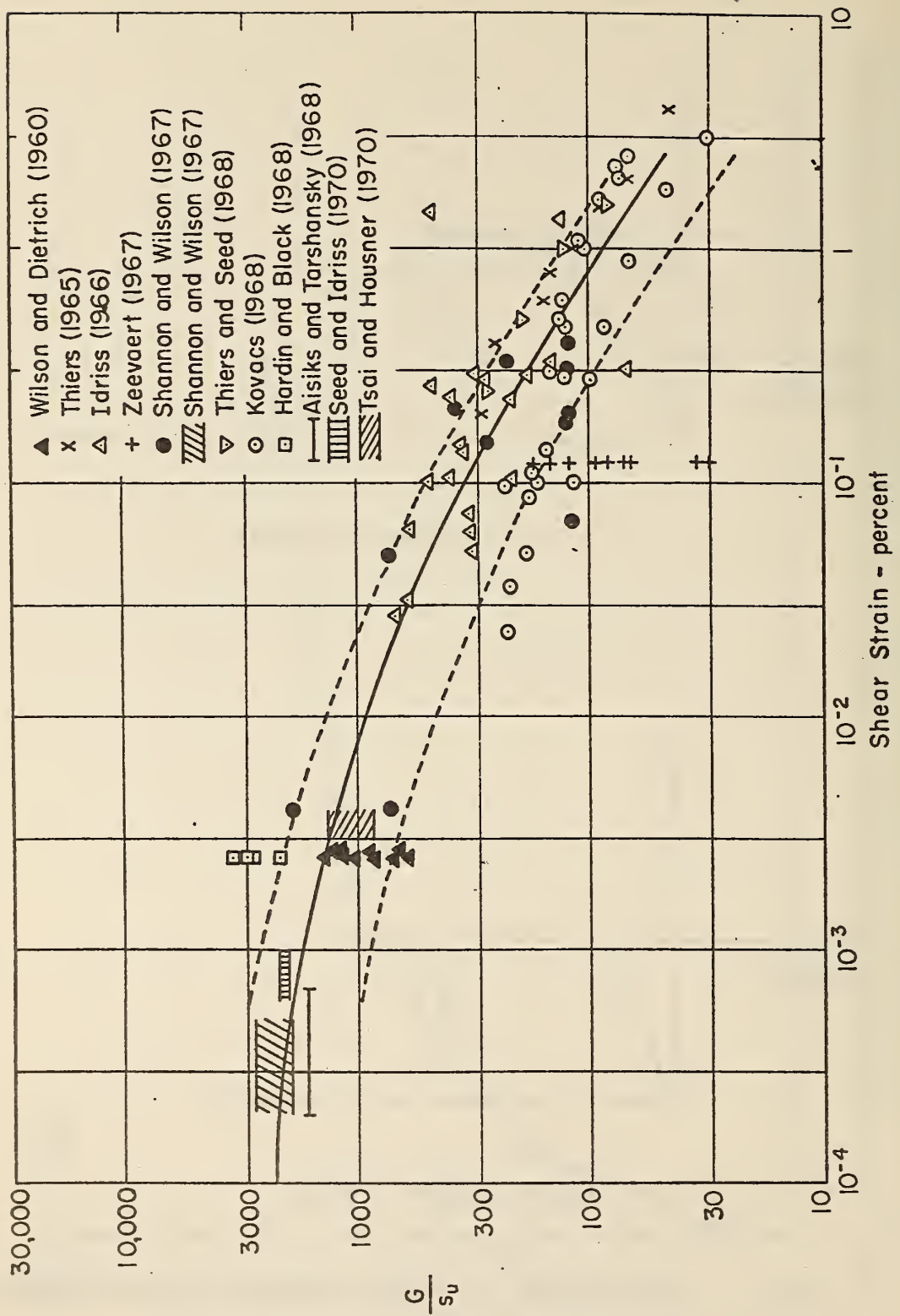


FIG. 14 IN-SITU SECANT SHEAR MODULI FOR SATURATED CLAYS  
(After Seed and Idriss)

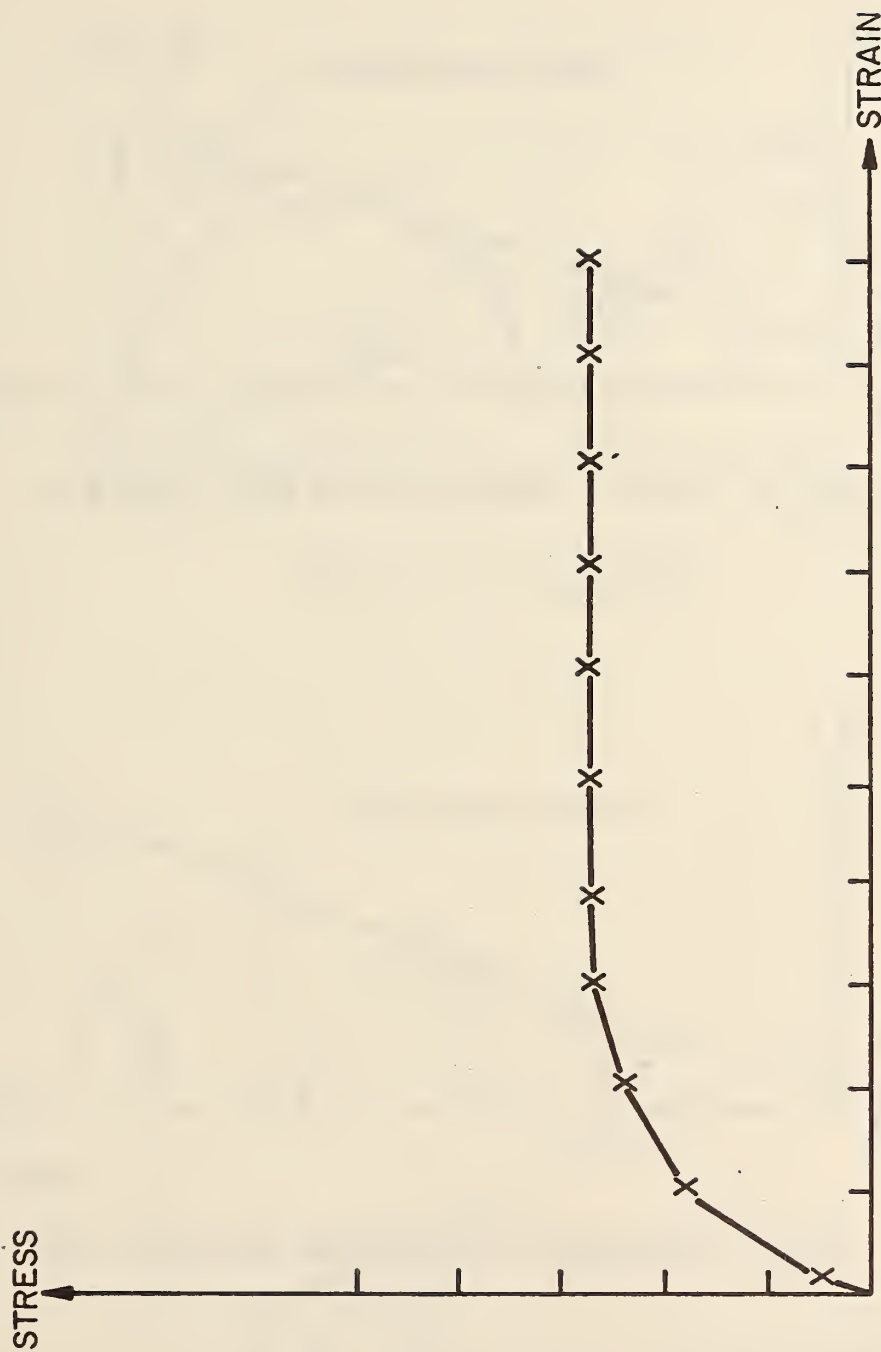


FIG. 15 VARIATION OF TANGENT MODULUS WITH SHEAR STRAIN FOR CLAYS



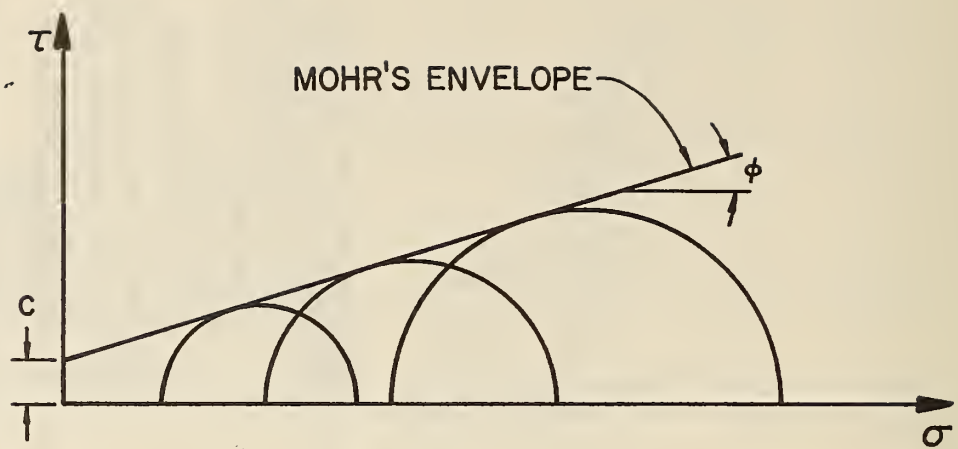


FIG. 16 MOHR'S ENVELOPE FOR SOIL SAMPLE

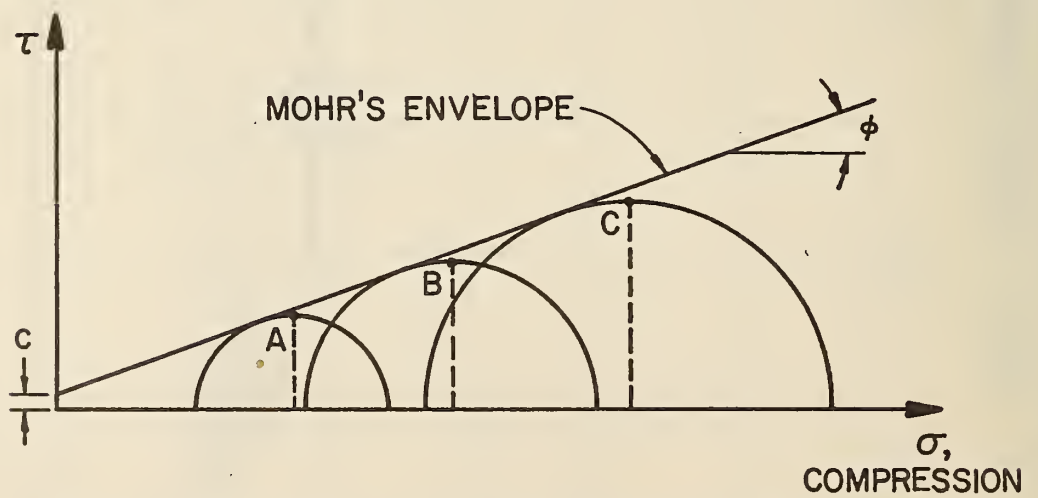


FIG. 17 STRESSES AT MAXIMUM SHEAR PLANE

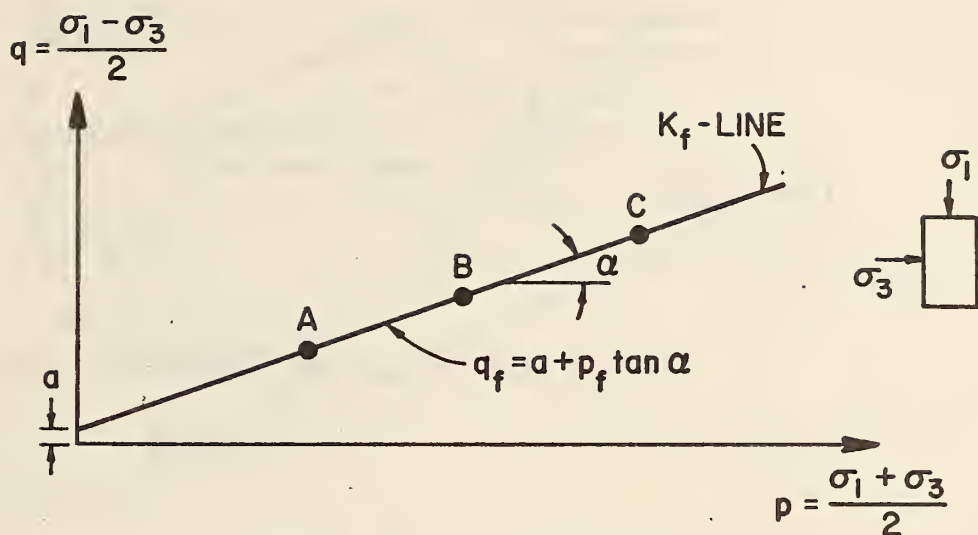


FIG. 18 p-q DIAGRAM

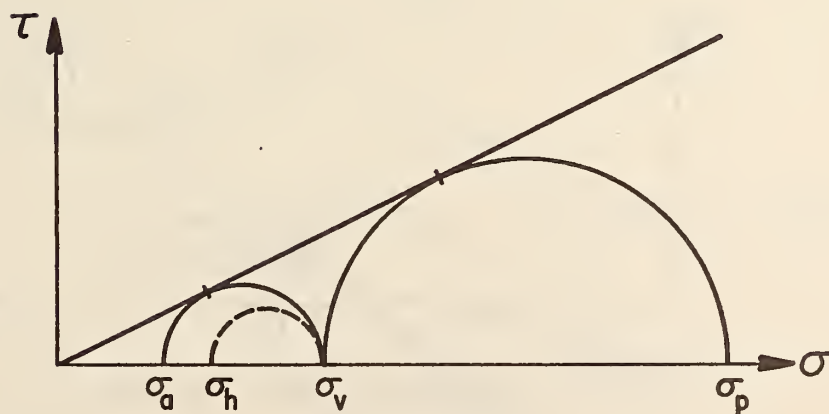


FIG. 19 MOHR CIRCLE

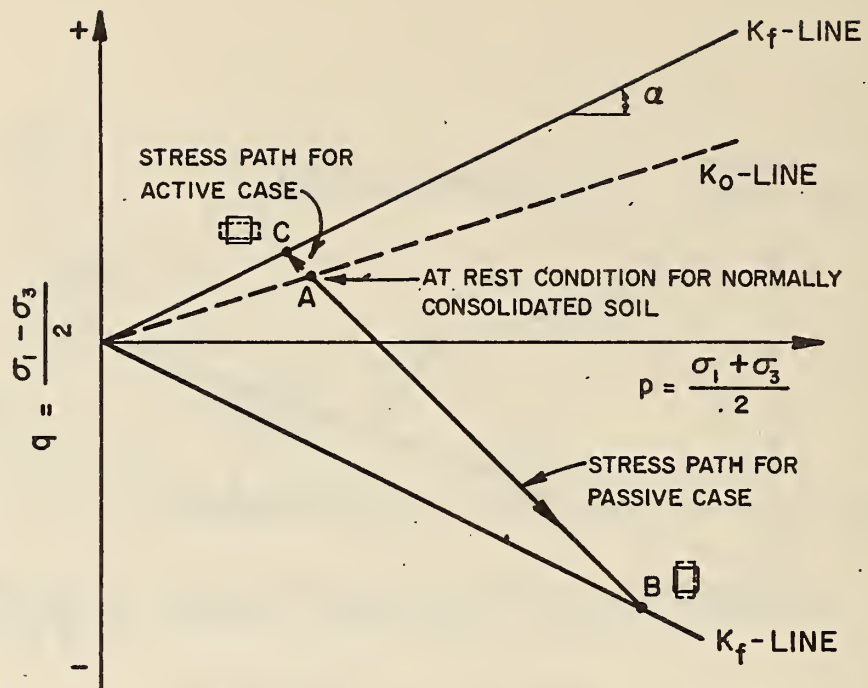


FIG. 20 STRESS PATHS FOR RANKINE ACTIVE AND PASSIVE CONDITIONS

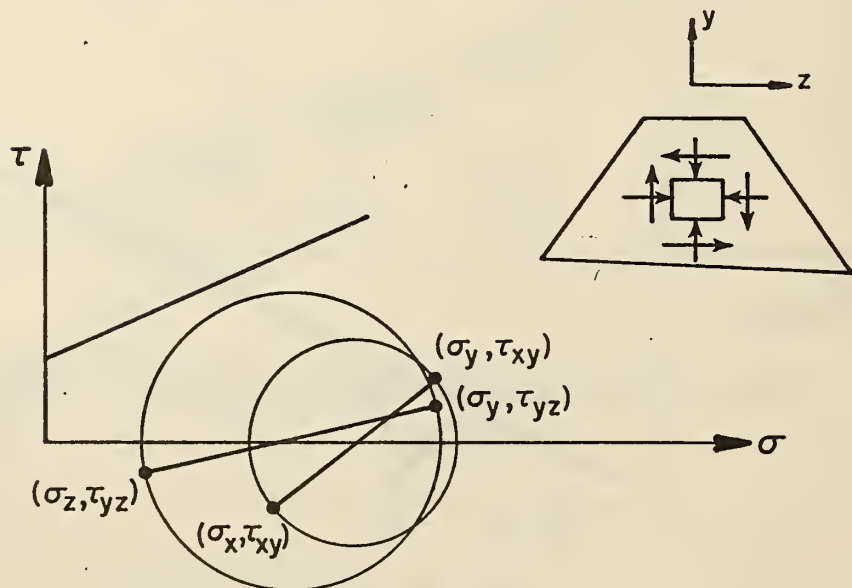


FIG. 21 STRESS CONDITIONS AT FIELD

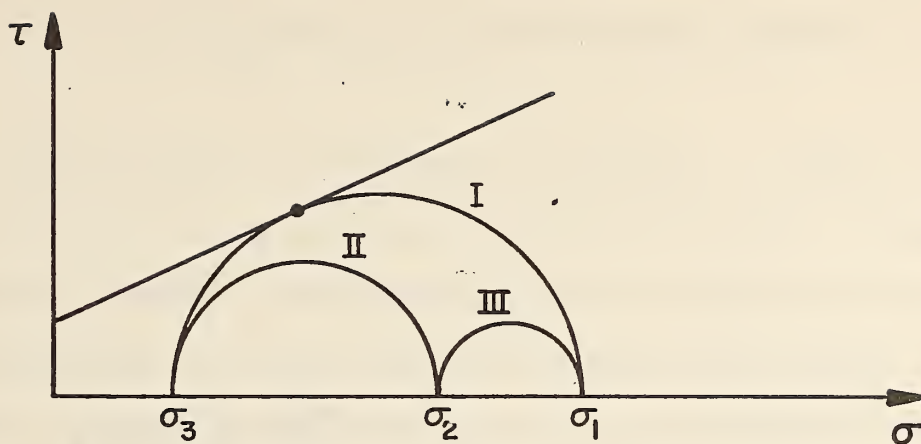


FIG. 22 MOHR CIRCLE IN 3 PLANES

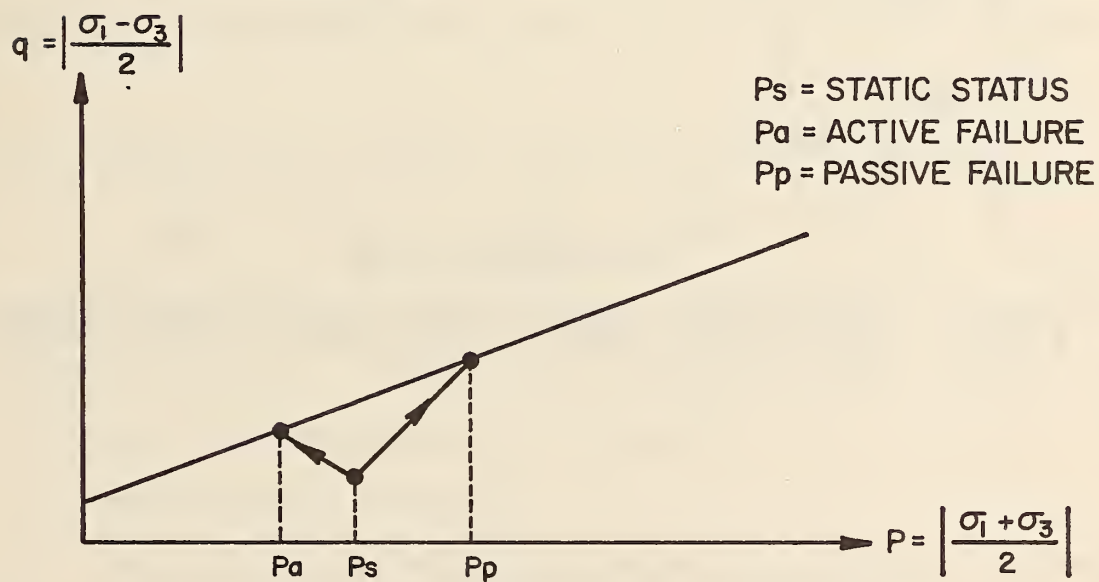


FIG. 23 ACTIVE AND PASSIVE FAILURE

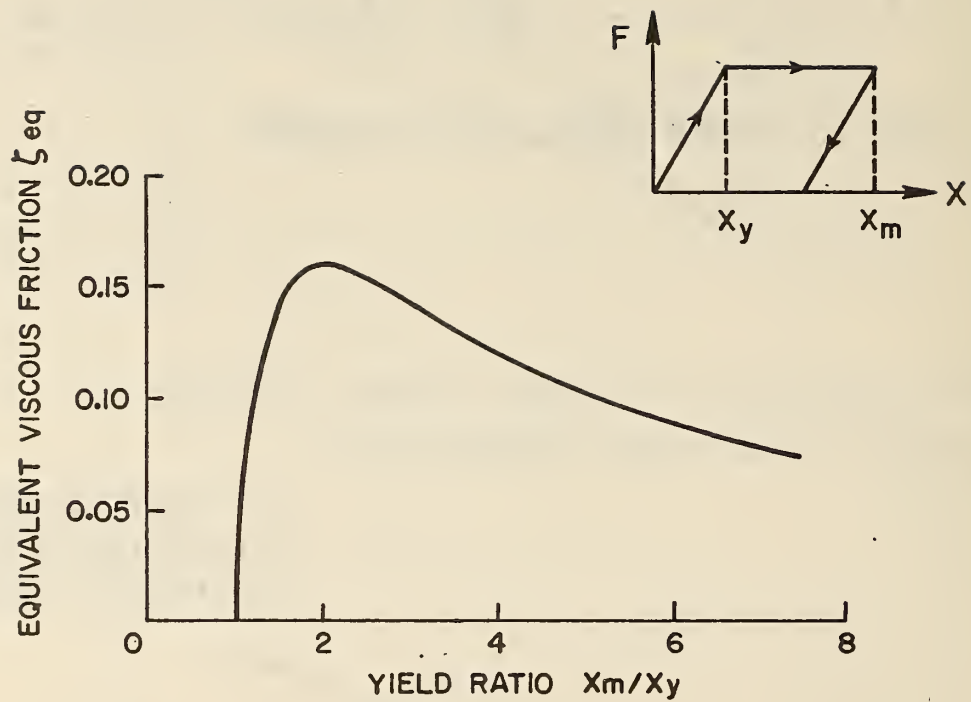


FIG.24 EQUIVALENT VISCOUS FRICTION VS YIELD RATIO



#### IV NON-LINEAR STIFFNESSES OF MODEL ELEMENTS

During periods of low amplitude oscillation, a bridge-soil system can be modelled using the linear elements as described in Chapter II. It may be necessary in this case to treat the friction and expansion joint elements in a piece-wise linear fashion. For a severe earthquake however inelastic deformations may occur in the concrete columns and/or backfill soils, separations and impacts may develop between the abutments and backfills, slippages may take place in the expansion joints, and yielding may take place at the soil boundaries or in the foundation to complicate the behavior.

It is the purpose of this chapter to describe the non-linear behaviors of all elements and to derive their non-linear stiffnesses.

##### A. GENERAL ELASTIC-PERFECTLY PLASTIC STRESS-STRAIN RELATIONS

Presently, extensive literature exists on the theory of plasticity and its application to different types of materials and structural elements [30, 46, 85]. Recently, its application has been extended to soil structures and frame structures as reported by Dibaj and Penzien, and by Porter and Powell [28, 83].

The first step in deriving the stress-strain relations for an elastic-perfectly plastic material is to assume a yield function expressed in terms of the stress space. This stress function can be expressed as

$$f(\tau_{ij}) = 0 \quad (49)$$

By application of the flow rule, the plastic strain increment tensor is derivable from this function using the relation

$$\delta \epsilon_{ij}^P = \lambda \frac{\partial f}{\partial \tau_{ij}} \quad (50)$$

where  $\lambda$  is a non-negative scale factor. The total strain increment tensor is thus decomposed into its elastic and plastic components as expressed by

$$\delta \epsilon_{ij} = \delta \epsilon_{ij}^E + \delta \epsilon_{ij}^P \quad (51)$$

The generalized Hooke's law, relating the increment of stress tensor to the increment of elastic strain tensor, can be written in the form

$$\delta \tau_{ij} = C_{ijkl}^E \delta \epsilon_{kl}^E \quad (52)$$

Using Eq. (51), Eq. (52) can be rewritten as

$$\delta \tau_{ij} = C_{ijkl}^E (\delta \epsilon_{kl} - \delta \epsilon_{kl}^P) \quad (53)$$

For an elastic-perfectly plastic material

$$\delta f = \frac{\partial f}{\partial \tau_{ij}} \delta \tau_{ij} = 0 \quad (54)$$

Substituting Eqs. (53) and (50) into Eq. (54), one obtains

$$\frac{\partial f}{\partial \tau_{ij}} C_{ijkl}^E (\delta \epsilon_{kl} - \delta \epsilon_{kl}^P) = 0 \quad (55)$$

or

$$\frac{\partial f}{\partial \tau_{ij}} C_{ijkl}^E \delta \epsilon_{kl} - \frac{\partial f}{\partial \tau_{ij}} C_{ijkl}^E \frac{\partial f}{\partial \tau_{kl}} \lambda = 0 \quad (56)$$

Solving for  $\lambda$  gives

$$\lambda = h C_{ijkl}^E \frac{\partial f}{\partial \tau_{ij}} \delta \epsilon_{kl} \quad (57)$$

where

$$\frac{1}{h} = C_{ijkl}^E \frac{\partial f}{\partial \tau_{ij}} \frac{\partial f}{\partial \tau_{kl}} \quad (58)$$

Substituting Eq. (57) into Eq. (50) results in the relation

$$\delta \epsilon_{ij}^P = h C_{mnkl}^E \frac{\partial f}{\partial \tau_{mn}} \delta \epsilon_{kl} \frac{\partial f}{\partial \tau_{ij}} \quad (59)$$

A further substitution of this relation into Eq. (53) gives

$$\delta \tau_{ij} = C_{ijkl}^E (\delta \epsilon_{kl} - h C_{ijmn}^E \frac{\partial f}{\partial \tau_{ij}} \frac{\partial f}{\partial \tau_{kl}} \delta \epsilon_{mn}) \quad (60)$$

or

$$\delta \tau_{ij} = C_{ijkl}^E (\delta \epsilon_{kl} - A_{klmn} \delta \epsilon_{mn}) \quad (61)$$

where

$$A_{klmn} = h C_{ijkl}^E \frac{\partial f}{\partial \tau_{ij}} \frac{\partial f}{\partial \tau_{mn}} \quad (62)$$

The final form of the stress-strain relation for elasto-perfectly plastic material can now be written in the form

$$\delta \tau_{ij} = C_{ijkl} \delta \epsilon_{kl} \quad (63)$$

where

$$C_{ijkl} = C_{ijkl}^E - C_{ijmn}^E A_{klmn} \quad (64)$$

and where

$$C_{ijkl}^P = C_{ijmn}^E A_{klmn} \quad (65)$$

## B. SOIL FINITE ELEMENT

The Mohr-Coulomb criterion as stated in Eq. (43) of Chapter III may be expressed in terms of the principal stresses, namely

$$(\sigma_1 - \sigma_3) + (\sigma_1 + \sigma_3) \sin \phi = 2c \cos \phi \quad (66)$$

where  $\sigma_1 \geq \sigma_2 \geq \sigma_3$  with tension as positive. In the case of two dimensional stress in the x,y plane, this relationship takes the form

$$(\sigma_x + \sigma_y) \sin \phi + 2R - 2c \cos \phi = 0 \quad (67)$$

where

$$R = \left[ \left( \frac{\sigma_x - \sigma_y}{2} \right)^2 + (\tau_{xy})^2 \right]^{1/2} \quad (68)$$

is the radius of the failure stress circle as shown in Fig. 25.

1. Tangent Stiffness In Plain Strain - The derivative of tangent stiffness given by Eqs. (49) through (65) will now be presented in matrix form for the case of plain strain. Using the Mohr-Coulomb criterion as the yield function  $f(\tau_{ij})$ , and the index notation for stresses such that  $\tau_{11} = \sigma_x$ ,  $\tau_{22} = \sigma_y$ , and  $\tau_{12} = \tau_{xy}$ , one obtains

$$f = (\tau_{11} + \tau_{22}) \sin \phi + 2 \left[ \left( \frac{\tau_{11} - \tau_{22}}{2} \right)^2 + \tau_{12}^2 \right]^{1/2} - 2c \cos \phi = 0 \quad (69)$$

and

$$q_{ij} = \frac{\partial f}{\partial \tau_{ij}} \quad (70)$$

Equation (50) becomes

$$\{\delta \epsilon^P\} = \lambda \{q\} \quad (71)$$

where

$$\begin{aligned} \{q\}^T &= \langle q \rangle = \langle q_{11} \ q_{22} \ q_{12} \rangle \\ &= \langle [\frac{1}{2} \sin \phi + (\frac{\tau_{11} - \tau_{12}}{R})], [\frac{1}{2} \sin \phi - (\frac{\tau_{11} - \tau_{22}}{R})], \\ &\quad [2 \frac{\tau_{12}}{R}] \rangle \end{aligned} \quad (72)$$

Equation (51) in matrix form can be written as

$$\{\delta \epsilon\} = \{\delta \epsilon^E + \delta \epsilon^P\} \quad (73)$$

where

$$\begin{aligned} \{\delta \epsilon\}^T &= \langle \delta \epsilon \rangle = \langle \delta \epsilon_{11} \ \delta \epsilon_{22} \ \delta \epsilon_{12} \rangle \\ \{\delta \epsilon^P\}^T &= \langle \delta \epsilon^P \rangle = \langle \delta \epsilon_{11}^P \ \delta \epsilon_{22}^P \ \delta \epsilon_{12}^P \rangle \\ \{\delta \epsilon^E\}^T &= \langle \delta \epsilon^E \rangle = \langle \delta \epsilon_{11}^E \ \delta \epsilon_{22}^E \ \delta \epsilon_{12}^E \rangle \\ \{\delta \tau\} &= [C^E] \{\delta \epsilon^E\} \end{aligned}$$

and where

$$\{\delta \tau\}^T = \langle \delta \tau \rangle = \langle \delta \tau_{11} \ \delta \tau_{22} \ \delta \tau_{12} \rangle \quad (74)$$

$$[C^E] = \frac{E}{(1+\nu)(1-2\nu)} \begin{bmatrix} 1-\nu & \nu & 0 \\ \nu & 1-\nu & 0 \\ 0 & 0 & \frac{1-2\nu}{2} \end{bmatrix} \quad (75)$$



$$\lambda = h\{q\}^T [C^E] \{\delta \epsilon\} \quad (76)$$

$$\begin{aligned} \frac{1}{h} &= \{q^T\} [C^E] \{q\} \\ &= \frac{E}{1+\nu} \left[ \frac{\sin^2 \phi}{2(1-2\nu)} + \frac{1}{2} + \frac{3}{2} \frac{\tau_{12}^2}{R^2} \right] \end{aligned} \quad (77)$$

$$\frac{1}{h} = \frac{E B}{1+\nu} \quad (78)$$

where

$$B = \frac{\sin^2 \phi}{2(1-2\nu)} + \frac{1}{2} + \frac{3}{2} \frac{\tau_{12}^2}{R^2} \quad (79)$$

Equations (62) through (65) in matrix form become

$$[A] = h \{q\} \{q\}^T [C^E] \quad (80)$$

$$\{\delta \tau\} = [C] \{\delta \epsilon\} \quad (81)$$

$$\begin{aligned} [C] &= [C^E] - [C^E] [A] \\ &= [C^E] - h [C^E] \{q\} \{q\}^T [C^E] \\ &= [C^E] - [C^P] \end{aligned} \quad (82)$$

Letting

$$\begin{aligned} \{Q\}^T &= \{q\}^T [C^E] \\ &= \frac{E}{1+\nu} \langle Q_1 \ Q_2 \ Q_3 \rangle \\ &= \frac{E}{1+\nu} \left\langle \frac{\sin \phi}{2(1-2\nu)} + \frac{\tau_{11} - \tau_{12}}{4R}, \frac{\sin \phi}{2(1-2\nu)} - \frac{\tau_{11} - \tau_{22}}{4R}, \frac{\tau_{12}}{R} \right\rangle \end{aligned} \quad (83)$$

, the matrix  $[C^P]$  can be expressed in the form

$$\begin{aligned}
[C^P] &= h[C^E] \{q\} \{q\}^T [C^E] \\
&= h\{Q\} \{Q\}^T \\
&= \frac{E}{B(1+\nu)} \begin{bmatrix} Q_1^2 & Q_1 Q_2 & Q_1 Q_3 \\ Q_2 Q_1 & Q_2^2 & Q_2 Q_3 \\ Q_3 Q_1 & Q_3 Q_2 & Q_3^2 \end{bmatrix} \quad (84)
\end{aligned}$$

Finally, the tangent stiffness in explicit matrix notation becomes

$$[C] = \frac{E}{(1+\nu)(1-2\nu)} \begin{bmatrix} 1-\nu & \nu & 0 \\ \nu & 1-\nu & 0 \\ 0 & 0 & \frac{1-\nu}{2} \end{bmatrix} - \frac{E}{B(1+\nu)} \begin{bmatrix} Q_1^2 & Q_1 Q_2 & Q_1 Q_3 \\ Q_2 Q_1 & Q_2^2 & Q_2 Q_3 \\ Q_3 Q_1 & Q_3 Q_2 & Q_3^2 \end{bmatrix} \quad (85)$$

2. Postulate for Application of Tangent Stiffness to the Case of Plane Stress - In order to use the previously derived tangent stiffness for the case of plane stress, one must make two assumptions as follows: (1) no yielding occurs in the third direction and (2) the results of triaxial tests are directly applicable to the case of plain stress. Under these assumptions, the above derivations for plane strain also apply to the case of plane stress except that the matrix  $[C^E]$  is changed to the form

$$[C^E] = \frac{E}{1-\nu^2} \begin{bmatrix} 1 & \nu & 0 \\ \nu & 1 & 0 \\ 0 & 0 & \frac{1-\nu}{2} \end{bmatrix} \quad (86)$$

This results in the following changes

$$\{q\}^T [C^E] \{q\} = \frac{2E}{1-\nu^2} [(1+\nu) \sin^2 \phi + (1-\nu) \left( \frac{\tau_{11} - \tau_{22}}{4R} \right)^2 + (1-\nu) \left( \frac{\tau_{12}}{R} \right)^2] \quad (87)$$

$$\frac{1}{h} = \frac{2EB}{1-\nu^2} \quad (88)$$

$$B = [(1+\nu) \sin^2 \phi + (1-\nu) \left( \frac{\tau_{11} - \tau_{22}}{4R} \right)^2 + (1-\nu) \left( \frac{\tau_{12}}{R} \right)^2] \quad (89)$$

$$\begin{aligned} \{Q\}^T &= \{q\}^T [C^E] \\ &= \frac{E}{1-\nu^2} \langle Q_1 \ Q_2 \ Q_3 \rangle \\ &= \frac{E}{1-\nu^2} \langle \frac{1}{2} (1+\nu) \sin \phi + (1+\nu) \frac{\tau_{11} - \tau_{22}}{4R}, \\ &\quad \frac{1}{2} (1+\nu) \sin \phi - (1+\nu) \frac{\tau_{11} - \tau_{22}}{4R}, (1-\nu) \frac{\tau_{12}}{R} \rangle \end{aligned} \quad (90)$$

$$\begin{aligned} [C^P] &= h[C^E] \{q\} \{q\}^T [C^E] \\ &= h\{Q\} \{Q\}^T \\ &= \frac{E}{2B(1-\nu^2)} \begin{bmatrix} Q_1^2 & Q_1 Q_2 & Q_1 Q_3 \\ Q_2 Q_1 & Q_2^2 & Q_2 Q_3 \\ Q_3 Q_1 & Q_3 Q_2 & Q_3^2 \end{bmatrix} \end{aligned} \quad (91)$$

Finally, one obtains

$$\begin{aligned} [C] &= [C^E] - [C^P] \\ &= \frac{E}{1-\nu^2} \begin{bmatrix} 1 & \nu & 0 \\ \nu & 1 & 0 \\ 0 & 0 & \frac{1-\nu}{2} \end{bmatrix} - \frac{E}{2B(1+\nu)} \begin{bmatrix} Q_1^2 & Q_1 Q_2 & Q_3 \\ Q_2 Q_1 & Q_2^2 & Q_2 Q_3 \\ Q_3 Q_1 & Q_3 Q_2 & Q_3^2 \end{bmatrix} \end{aligned} \quad (92)$$

## C. COLUMN ELEMENT

### 1. Trilinear Yield Surface of the Moment-Axial Force Interaction

Diagram - Moment-axial force interaction curves for the most commonly used sections of reinforced concrete columns are available in handbooks published by the American Concrete Institute [2]. These sections include the spirally reinforced, circular and square columns, and the symmetrically reinforced, rectangular tied columns. Three typical sections are shown in Fig. 27. For other types of sections, a computer program has been developed to obtain the interaction curves by a direct analysis method [105].

There are three controlling points on the interaction curve which can be used to approximate its form using a trilinear relationship. These points are the minimum eccentricity point B, the balanced point C, and the pure moment point D, as shown in Fig. 26. Segment AB having a horizontal slope defines the ultimate axial load capacity as that axial load given by the ACI code for the minimum eccentricity condition [35]. Segment BC defining the compression failure zone connects point B with the balanced point C which corresponding to a concrete strain of 0.003 and a steel strain equal to the yield strain. Finally, segment CD connects point C with point D which corresponds to the yield moment in the presence of no axial load. This latter segment defines the tension failure zone. Since tension seldom occurs in the columns of short bridges, it is not necessary to define the interaction diagram in the negative (tension) region of P. Line segment OD therefore is considered the boundary line for the yield surface which signifies zero tension capacity.

Using the approximate trilinear form of the interaction curve, the normalized yield stress function can be written as

$$f_i(S_1, S_2) = a_i S_1 + b_i S_2 + c_i = 0 \quad (93)$$

where

$$S_1 = \frac{P}{p^2} ; \quad S_2 = \frac{M}{M^2} \quad (94)$$

For line segments AB, BC, and CD, coefficients  $a_i$ ,  $b_i$ , and  $c_i$  are, respectively,

$$\begin{aligned} a_1 &= 1 & a_2 &= \frac{M_1}{M_2} - 1 & a_3 &= \frac{M_3}{M_2} - 1 \\ b_1 &= 0 & b_2 &= 1 - \frac{P_1}{P_2} & b_3 &= 1 - \frac{P_3}{P_2} \\ c_1 &= -\frac{P_1}{P_2} & c_2 &= \frac{P_1}{P_2} - \frac{M_1}{M_2} & c_3 &= \frac{P_3}{P_2} - \frac{M_3}{M_2} \end{aligned} \quad (95)$$

2. Tangent Stiffness - Using the trilinear interaction relationship, the derivation of the elastic-perfectly plastic tangent stiffness of a column follows the same procedure used previously for soils except one must consider that (1) plastic deformations are concentrated at the ends of the element with the deformations taking place independently over zero lengths at each end of the element, (2) plastic deformations are independent of the shear forces present, and (3) the stiffnesses are expressed in terms of element end forces and displacements rather than in terms of stress and strain as in the case of soil elements. In this case, one obtains



$$\{du^P\} = \begin{Bmatrix} du_I^P \\ du_J^P \end{Bmatrix} = \begin{bmatrix} \{q\}_I & \{0\} \\ \{0\} & \{q\}_J \end{bmatrix} \begin{Bmatrix} \lambda_I \\ \lambda_J \end{Bmatrix} = [q] \{\lambda\} \quad (96)$$

where  $du_I^P$  and  $du_J^P$  are the plastic deformation increments at ends I and J of the element, respectively, and  $\lambda_I$  and  $\lambda_J$  are the associated proportionality factors. It follows therefore that

$$\{du^P\}^T = \langle du_1^P \quad du_2^P \quad du_3^P \quad du_4^P \quad du_5^P \quad du_6^P \rangle \quad (97)$$

$$\{q\}_m^T = \left\{ \frac{\partial f_i}{\partial s_j} \right\}_m^T = \langle a_i \quad 0 \quad b_i \rangle_m, \quad m = I \text{ or } J \quad (98)$$

$$\{du\} = \begin{Bmatrix} du_I \\ du_J \end{Bmatrix} = \begin{Bmatrix} du_I^E \\ du_J^E \end{Bmatrix} + \begin{Bmatrix} du_J^P \\ du_J^P \end{Bmatrix} \quad (99)$$

$$\{ds\} = \begin{Bmatrix} ds_I \\ ds_J \end{Bmatrix} = [K^E] \begin{Bmatrix} du_I^E \\ du_J^E \end{Bmatrix} \quad (100)$$

where  $[K^E]$  is the elastic stiffness matrix appearing in Eq. 23. Further, one obtains

$$\{\lambda\} = \begin{Bmatrix} \lambda_I \\ \lambda_J \end{Bmatrix} = [h] [q]^T [K^E] \{du\} \quad (101)$$

$$[h]^{-1} = [q]^T [K^E] [q] \quad (102)$$

$$[A] = [q] [h] [q]^T [K^E] \quad (103)$$

$$\{ds\} = [K] \{du\} \quad (104)$$

$$\begin{aligned}
[K] &= [K^E] - [K^E] [A] \\
&= [K^E] - [K^E] [q] [h] [q]^T [K^E] \\
&= [K^E] - [K^P]
\end{aligned}
\tag{105}$$

3. An Approximation Used in Numerical Iteration - Due to the occurrence of impact upon the frictional element at the interface of soil and abutment wall elements, the time interval used in a dynamic analysis to obtain a stable numerical solution must be quite small. It must be sufficiently small so that "overshooting" of the interaction diagram during a single interval as shown in Fig. 28 is minimized. Even though this interval is kept small, the error introduced into a solution by "overshooting" has been corrected [16, 60, 105].

In the present investigation, a simple procedure has been adopted for the overshooting. If, as shown in Fig. 28, the elastic stress state assumed during an interval moves the applied forces from point A to point B then a transition from an elastic to a yield state is indicated. While the new force vector  $S_{t+\Delta t}$  as represented by point B is adopted without correction, point C which is the intersection of the new stress vector  $S_{t+\Delta t}$  and the yield segment EF is used to calculate the slope of the plastic deformation vector  $du^P$ . This same procedure is used when overshooting occurs at a discontinuity point on the interaction curve as shown in Fig. 29. In this case, the elastic stress state assumed during an interval moves the applied forces from point A' to point B'. The new force vector  $S_{t+\Delta t}$  intersects line EF; thus, the slope of EF is used to calculate the plastic deformation increment. Other investigators have used somewhat different procedures for this

correction [73, 77, 83, 107].

#### D. FRICTIONAL ELEMENT

The non-linear behavior of the frictional element is described in terms of normal and shear stiffnesses  $k_n$  and  $k_s$  during three distinct stages, namely, (1) when reparation occurs, in which case  $k_n = k_s = 0$ , (2) when compression occurs at the interface but the shear strength of the element is not exceeded in which case  $k_n$  and  $k_s$  are assigned high values, and (3) when compression occurs but the shear strength of the element is exceeded in which case  $k_s = 0$  and  $k_n$  retains a high value. The shear yield strength of the element can be defined by the Mohr-Coulomb yield criterion, i.e.,

$$\tau = \sigma \tan \phi_w \quad (106)$$

where  $\phi_w$  is the angle of wall friction between the soil and the abutment wall.

Before discussing the value of  $\phi_w$  to be used, two terms must be defined [63]. Firstly, the constant volume frictional angle is defined by  $\phi_{cv} = \sin^{-1} \left( \frac{\sigma_1 - \sigma_3}{\sigma_1 + \sigma_3} \right)_{cv}$ , where  $\sigma_1$  and  $\sigma_3$  are the axial stress and confining pressure, respectively, in a triaxial test at that stage when the sand strains without further volume change. Secondly, peak friction angle  $\phi$  is defined as the slope of Mohr envelope which is a function of the stresses indicated at the peak of stress-strain curve of a triaxial test.

For backfill against a concrete wall, Lamb suggests that the angle of wall friction  $\phi_w$  is about equal to  $\phi_{cv}$  and that it typically has a

numerical value of about  $30^\circ$  [63]. Seed and Whitman in a discussion of dynamically active pressure against walls suggest that  $\phi_w = \phi/2$  is satisfactory for most practical purposes [97].

#### E. EXPANSION JOINT ELEMENT

The stiffnesses of the expansion joint element can be defined in terms of normal and shear stiffnesses  $k_n$  and  $k_s$  during three stages, (1) when the frictional resistance between the deck and abutment is not exceeded in which case  $k_n$  and  $k_s$  are assigned high values, (2) when the frictional resistance is exceeded, but the gap between deck and abutment as shown in Fig. 6a is not closed, in which case  $k_s = 0$  and  $k_n$  retains a high value, (3) when the frictional resistance is exceeded and the gap is closed in which case, if the relative displacement indicated is consistent with gap closure, high values  $k_n$  and  $k_s$  are retained.

#### F. SOIL BOUNDARY ELEMENT AND EQUIVALENT COLUMN OF FOUNDATION

The non-linear behavior of the soil boundary element and the equivalent column foundation element can be approximated by defining yield levels using standard methods and adopting elasto-plastic hysteretic models. In the present investigation, only elastic behavior has been considered.



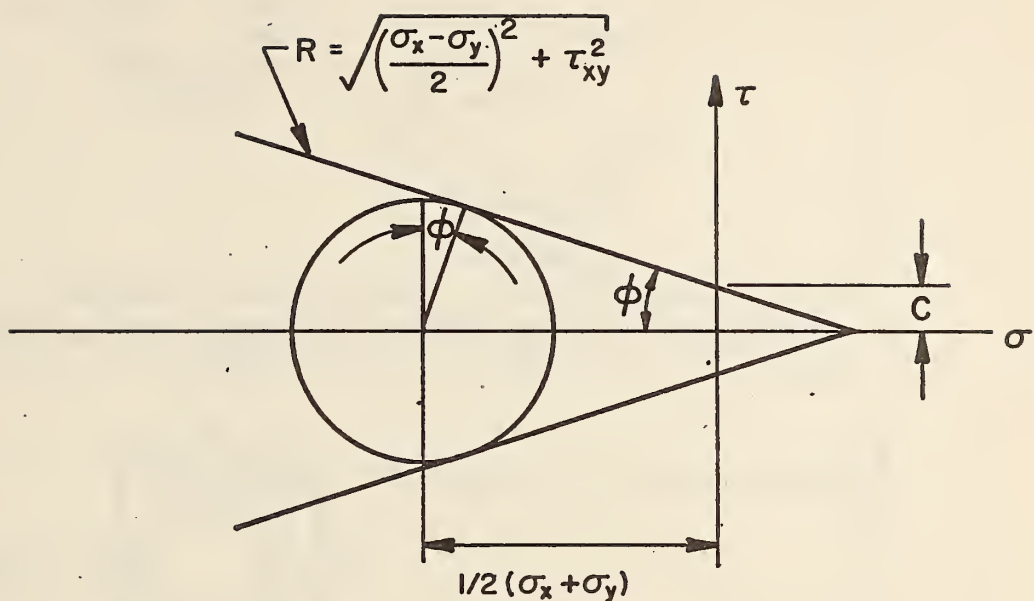


FIG. 25 MOHR-COULOMB YIELD FUNCTION

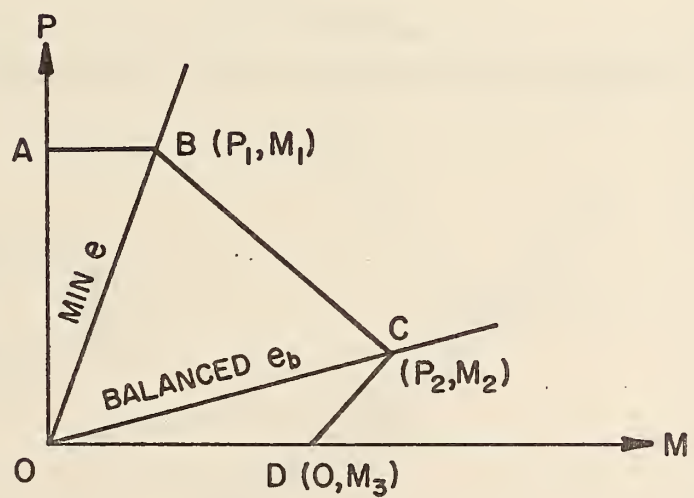
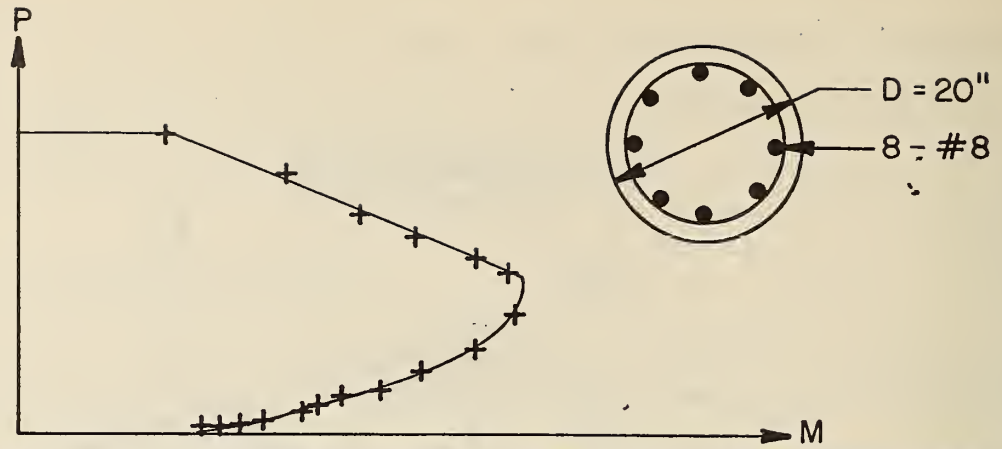
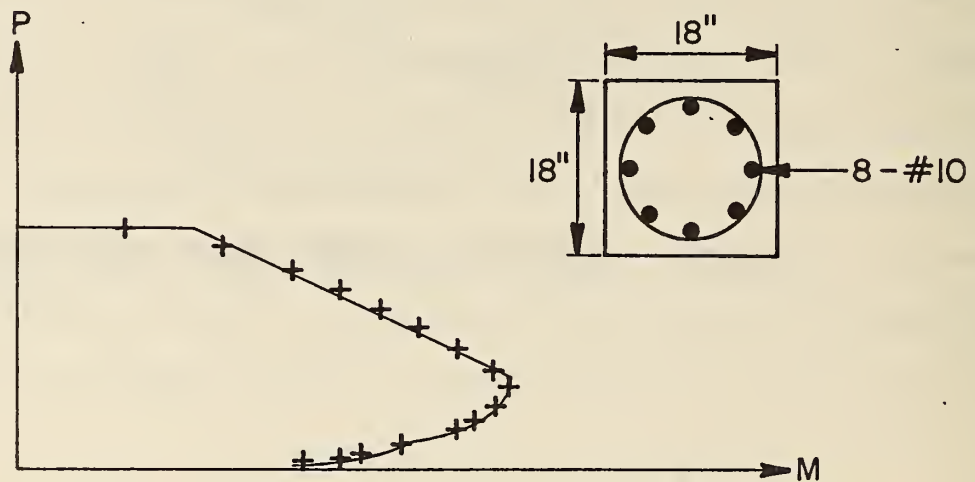


FIG. 26 COLUMN INTERACTION CURVE

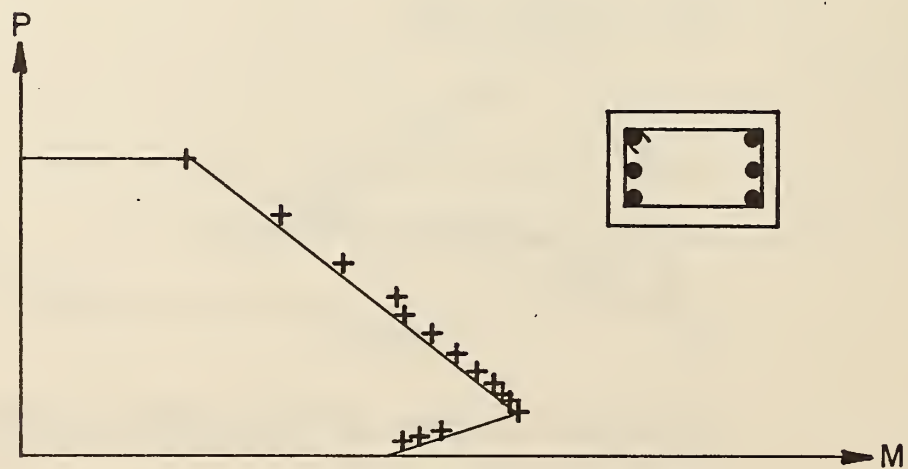




(a) CIRCULAR SECTION WITH BARS CIRCULARLY ARRANGED

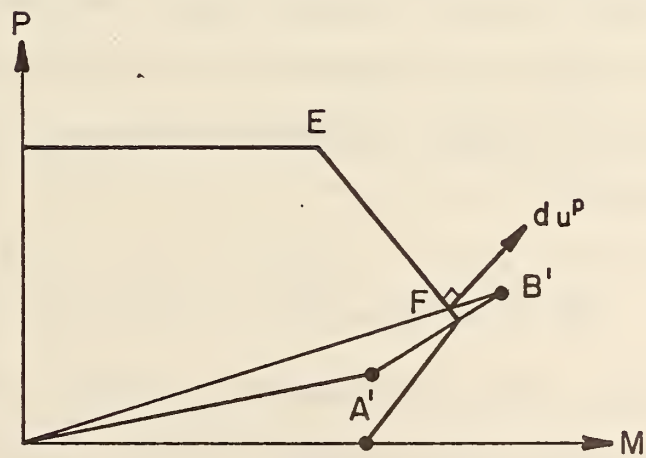
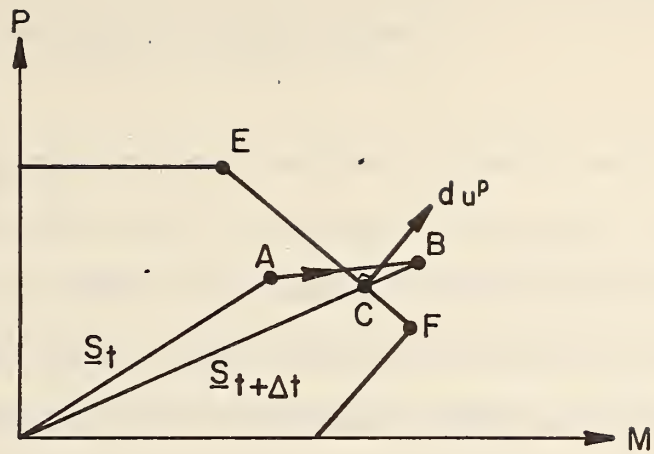


(b) SQUARE SECTIONS WITH BAR CIRCULARLY ARRANGED



(c) RECTANGULAR SECTION

FIG. 27 INTERACTION DIAGRAM OF CONCRETE COLUMN



## V DYNAMIC ANALYSIS PROCEDURES

In the subsequent sections, the nonlinear coupled equations of motion for the discrete parameter soil-structure system are formulated and the method used to establish their associated stiffness, mass, and damping matrices are described. Also presented are the step-by-step integration techniques employed in their solution.

### A. EQUATIONS OF MOTION

Although some previous investigations have considered spacial variations in the earthquake ground motions [27, 32, 43], the present investigation assumes identical motions at all base points of the soil-structural system. This assumption is considered reasonable due to the relatively short lengths of bridges being considered.

The coupled equations of motion at time  $t$  for an  $N$  degree of freedom system subjected to rigid base excitation can be expressed in the matrix form

$$[M] \{\ddot{u}\}_t + [C]_t \{\dot{u}\}_t + [K]_t \{u\}_t = \{R\}_t \quad (107)$$

where  $[M]$  is the constant mass matrix,  $[C]_t$ , and  $[K]_t$  are the time dependent damping and stiffness matrices, respectively, and where  $\{u\}_t$ ,  $\{\dot{u}\}_t$ , and  $\{\ddot{u}\}_t$  are the nodal point displacement, velocity, and acceleration vectors, respectively. The excitation force vector  $\{R\}_t$  due to rigid base motions is given by the relation

$$\{R\}_t = - [M] \{I\} \left( \ddot{u}_{gt}^x + \ddot{u}_{gt}^y \right) \quad (108)$$

where  $\{I\}$  is the unit vector and  $\ddot{u}_{gt}^x$  and  $\ddot{u}_{gt}^y$  are the horizontal and vertical components of ground acceleration.

## B. STIFFNESS MATRIX

The complete stiffness matrix  $[K]_t$  is assembled from the individual element stiffness matrices using the direct stiffness method [22]. The individual element stiffnesses during the elastic and inelastic ranges in each time interval are obtained by the procedures described in Chapters II and IV. The complete stiffness matrix takes on a symmetric banded form; thus, only the diagonal and the off-diagonal terms on one side need be stored in the computer.

## C. MASS MATRIX

The mathematical model used assumes all mass as concentrated at the nodal points. The diagonal mass matrix which results represents a significant saving in computer storage and computational time when compared with similar requirements for the consistent mass matrix [21]. One-third of the mass of each triangular element, one-fourth of the mass of each quadrilateral element, and one-half of the mass of each beam element are lumped at their respective nodal points. No rotational moments of inertia are assigned to these masses. The resulting mass matrix for the complete soil-structural system takes the form

$$[M] = \text{diag} < M_1 \ M_2 \ \dots \ M_n > \quad (109)$$

where  $M_i$  is the mass associated with the  $i$ th degree of freedom and  $n$

is the total number of degrees of freedom present in the system. The static condensation procedure is used to eliminate the degree of freedom of zero rotational masses in the solution of eigenvalues.

#### D. DAMPING MATRIX

Various methods have been used by investigators to determine the viscous damping matrix corresponding to matrix  $[C]_t$  in Eq. (107) [44]. Wilson and Penzien have described two methods for evaluating orthogonal damping matrices [115]. The first method relates the modal damping ratios to the coefficients in the Caughey series form [15]. The second method is a direct approach which expresses the damping matrix as a sum of a series of matrices each of which produces damping in only one particular mode. The second approach has the advantage that prescribed damping ratios in all modes are easily controlled.

The Rayleigh damping matrix which constructs a damping matrix from a scaled linear combination of the mass and stiffness matrices is used in the present investigation. This type of damping matrix has the advantage that it can be calculated directly using the relation

$$[C]_t = \alpha[M] + \beta[K]_t \quad (110)$$

where  $\alpha$  and  $\beta$  are scalar quantities to be prescribed. By properly selecting these scalar values, the damping ratios can be controlled in two normal modes. It can be shown that these quantities are related to the damping ratios ( $\xi$ ) and circular frequencies ( $\omega$ ) of the  $i$ th and  $j$ th normal modes through the equations



$$\alpha = \frac{2 \omega_i \omega_j (\xi_j \omega_i - \xi_i \omega_j)}{(\omega_i^2 - \omega_j^2)} \quad (111)$$

$$\beta = \frac{2 (\xi_i \omega_i - \xi_j \omega_j)}{(\omega_i^2 - \omega_j^2)} \quad (112)$$

Further, it can be shown that if  $\alpha$  and  $\beta$  satisfy Eqs. (111) and (112), the damping ratio in nth normal has the value given by

$$\xi_n = \frac{\alpha + \beta \omega_n^2}{2 \omega_n} \quad (113)$$

In the present investigation, the numerical values of  $\alpha$  and  $\beta$  are determined by using the initial elastic soil-structural system and by prescribing the damping ratios of any two modes of the system. These quantities are then held constant at these values throughout the time history of response including those periods of time when the system responds inelastically.

As shown by Eq. (107), the stiffness matrix varies with time due to nonlinear effects; therefore, the damping matrix also varies with time. Because the stiffnesses in the system decrease considerably during periods of element yielding, the viscous damping present during these periods also decreases. It should be kept in mind, however, that the major sources of energy dissipation during these periods are the hysteresis loops in the force-deformation relations as described in Chapter III.

#### E. STEP-BY-STEP INTEGRATION TECHNIQUES

Having the solution of the coupled equations of motion at time  $t$ , the step-by-step integration procedure allows one to obtain their solution at a later time  $t+\Delta t$ . To develop this procedure, the matrix equation of motion is transformed to its incremental form by subtracting Eq. (107) for time  $t$  from the corresponding equation for time  $t+\Delta t$  as given by

$$[M] (\{\ddot{u}\}_t + \{\Delta\ddot{u}\}_t) + [C]_t (\{\dot{u}\}_t + \{\Delta\dot{u}\}_t) + [K]_t (\{u\}_t + \{\Delta u\}_t) = \{R\}_t + \{\Delta R\}_t \quad (114)$$

In this equation, the incremental quantities represent those changes taking place during the interval  $\Delta t$  following time  $t$ . Thus, one obtains the incremental form

$$[M] \{\Delta\ddot{u}\}_t + [C]_t \{\Delta\dot{u}\}_t + [K]_t \{\Delta u\}_t = \{\Delta R\}_t \quad (115)$$

To find the incremental changes, various procedures can be employed [7, 76]. The differences in these procedures relate to the analytical form of the variation in response over the time interval  $\Delta t$ . In the present investigation, two different analytical forms have been programmed for computer solution, namely, constant acceleration and linear acceleration. These forms lead to the following equations for velocity and displacement at time  $t+\Delta t$  expressed in terms of the state vectors at time  $t$  and the acceleration vector at time  $t+\Delta t$ :

#### Constant Acceleration

$$\{\dot{u}\}_{t+\Delta t} = \{\dot{u}\}_t + \frac{1}{2} \Delta t \{\ddot{u}\}_t + \frac{1}{2} \Delta t \{\ddot{u}\}_{t+\Delta t} \quad (116)$$

$$\{u\}_{t+\Delta t} = \{u\}_t + \Delta t \{\dot{u}\}_t + \frac{1}{4} \Delta t^2 \{\ddot{u}\}_t + \frac{1}{4} \Delta t^2 \{\ddot{u}\}_{t+\Delta t} \quad (117)$$

#### Linear Acceleration

$$\{\dot{u}\}_{t+\Delta t} = \{\dot{u}\}_t + \frac{1}{2} \Delta t \{\ddot{u}\}_t + \frac{1}{2} \Delta t \{\ddot{u}\}_{t+\Delta t} \quad (118)$$

$$\{u\}_{t+\Delta t} = \{u\}_t + \Delta t \{\dot{u}\}_t + \frac{1}{3} \Delta t^2 \{\ddot{u}\}_t + \frac{1}{6} \Delta t^2 \{\ddot{u}\}_{t+\Delta t} \quad (119)$$

Using the following definitions for the incremental vectors

$$\{\Delta \ddot{u}\}_t = \{\ddot{u}\}_{t+\Delta t} - \{\ddot{u}\}_t \quad (120)$$

$$\{\Delta \dot{u}\}_t = \{\dot{u}\}_{t+\Delta t} - \{\dot{u}\}_t \quad (121)$$

$$\{\Delta u\}_t = \{u\}_{t+\Delta t} - \{u\}_t \quad (122)$$

the incremental velocity and acceleration vectors can be expressed in the form

#### Constant Acceleration

$$\{\Delta \ddot{u}\}_t = \frac{4}{\Delta t^2} \{\Delta u\}_t - \{A\}_t \quad (123)$$

$$\{\Delta \dot{u}\}_t = \frac{2}{\Delta t} \{\Delta u\}_t - \{B\}_t \quad (124)$$

where

$$\{A\}_t = \frac{4}{\Delta t} \{\dot{u}\}_t + 2 \{\ddot{u}\}_t \quad (125)$$

$$\{B\}_t = 2 \{\dot{u}\}_t \quad (126)$$

### Linear Acceleration

$$\{\Delta\ddot{u}\}_t = \frac{6}{\Delta t^2} \{\Delta u\}_t - \{A\}_t \quad (127)$$

$$\{\Delta\dot{u}\}_t = \frac{3}{\Delta t} \{\Delta u\}_t - \{B\}_t \quad (128)$$

where

$$\{A\}_t = \frac{6}{\Delta t} \{\dot{u}\}_t + 3 \{\ddot{u}\}_t \quad (129)$$

$$\{B\}_t = 3 \{\dot{u}\}_t + \frac{1}{2} \Delta t \{\ddot{u}\}_t \quad (130)$$

Using these relations, the incremental equation of motion, Eq. (115), can be written in the form

$$[\bar{K}]_t \{\Delta\bar{u}\}_t = \{\Delta\bar{R}\}_t \quad (131)$$

where

$$\{\Delta\bar{R}\}_t = \{\Delta R\}_t + [M] \{A\}_t + C_2 [M] \{B\}_t \quad (132)$$

$$[\bar{K}]_t = [K]_t + C_1 [M] \quad (133)$$

and the actual incremental displacement vector can be expressed as

$$\{\Delta u\}_t = C_3 (\{\Delta\bar{u}\}_t + \beta \{B\}_t) \quad (134)$$

Constants  $C_1$ ,  $C_2$ , and  $C_3$  are given by the relations

### Constant Acceleration

$$C_1 = \frac{2 \alpha \Delta t + 4}{\Delta t^2 + 2 \beta \Delta t} \quad (135)$$

$$C_2 = \alpha - C_1 \beta \quad (136)$$

$$C_3 = \frac{\Delta t}{\Delta t + 2\beta} \quad (137)$$

#### Linear Acceleration

$$C_1 = \frac{3\alpha\Delta t + 6}{\Delta t^2 + 3\beta\Delta t} \quad (138)$$

$$C_2 = \alpha - C_1\beta \quad (139)$$

$$C_3 = \frac{\Delta t}{\Delta t + 3\beta} \quad (140)$$

After computing the incremental displacement vector using Eq. (134), the corresponding incremental acceleration and velocity vectors are determined using Eqs. (123) and (124), or Eqs. (127) and (128), respectively. The displacement, velocity and acceleration vectors at time  $t+\Delta t$  are then evaluated using Eqs. (120), (121) and (122), respectively. The tangent stiffness, strain, and stress for each element can now be calculated for time  $t+\Delta t$ .

An alternative solution of the incremental equilibrium equation, Eq. (115) can be obtained by separating the tangent stiffness matrix  $[K]_t$  into its elastic and plastic parts,  $[K^E]$  and  $[K^P]_t$ , as described in Chapter IV. That term associated with plastic deformation is then transferred to the right hand side of the equation of motion and is treated as an equivalent load vector [21].

In the above described step-by-step integration procedures, the initial displacements and velocities at time  $t = 0$  are assumed equal to zero. The very first incremental acceleration vector is then computed directly from Eq. (115), i.e.,

$$[M] \{\Delta \ddot{u}\}_0 + [C]_0 \{0\}_0 + [K]_0 \{0\}_0 = \{\Delta R\}_0$$



or

$$\{\Delta \ddot{u}\}_0 = [M]^{-1} \{\Delta R\}_0 = [M]^{-1} \{R\}_0 = -\{\ddot{u}_g\}_0$$

The initial forces existing in the elements cannot be assumed zero but must be taken equal to the static gravitational forces since tangent stiffness is dependent upon total force (gravity plus seismic).

While step-by-step integration procedures similar to those described above must be used for nonlinear analyses, they may or may not be used for linear analyses since the mode superposition method is an alternate method which can be used for linear analyses [116]. In the present investigation, it was found computationally convenient to use the step-by-step method for both linear and nonlinear analyses.

#### F. TIME INTERVAL $\Delta t$

The step-by-step integration method is accurate only if the time interval  $\Delta t$  is small compared with the shortest period  $T$  of the soil-structural system and is also small compared with the predominant periods in the excitation. Assuming the latter condition is satisfied, the ratio  $\Delta t/T$  must be selected less than a certain critical value to insure a convergent and stable solution in the case of the linear acceleration method; however, it can be shown that the constant acceleration method is always stable for a linear system [76]. In the present study, the presence of the nonlinear friction elements tend to encourage an unstable response, if the  $\Delta t/T$  ratio is taken too large. Therefore, extreme care must be taken in selecting the numerical value of this ratio. The effects of this particular parameter on dynamic response are discussed

subsequently in Chapter VI.

#### G. EARTHQUAKE INPUT

In the present investigation, the horizontal ground motion was prescribed in accordance with the acceleration time-history shown in Fig. 30. This artificial accelerogram was generated by A. K. Chopra to simulate the ground motions produced by the San Fernando earthquake at the site of the Olive View Hospital located about 6 miles southwest of the epicenter [18]. It has a peak acceleration of 0.5 g and a uniform phase of high intensity shaking for 8' seconds.

The vertical ground motions were assumed zero for the present study, but the computer program has the option to permit input of vertical ground motions.

O.V.H. ACCELEROGRAM

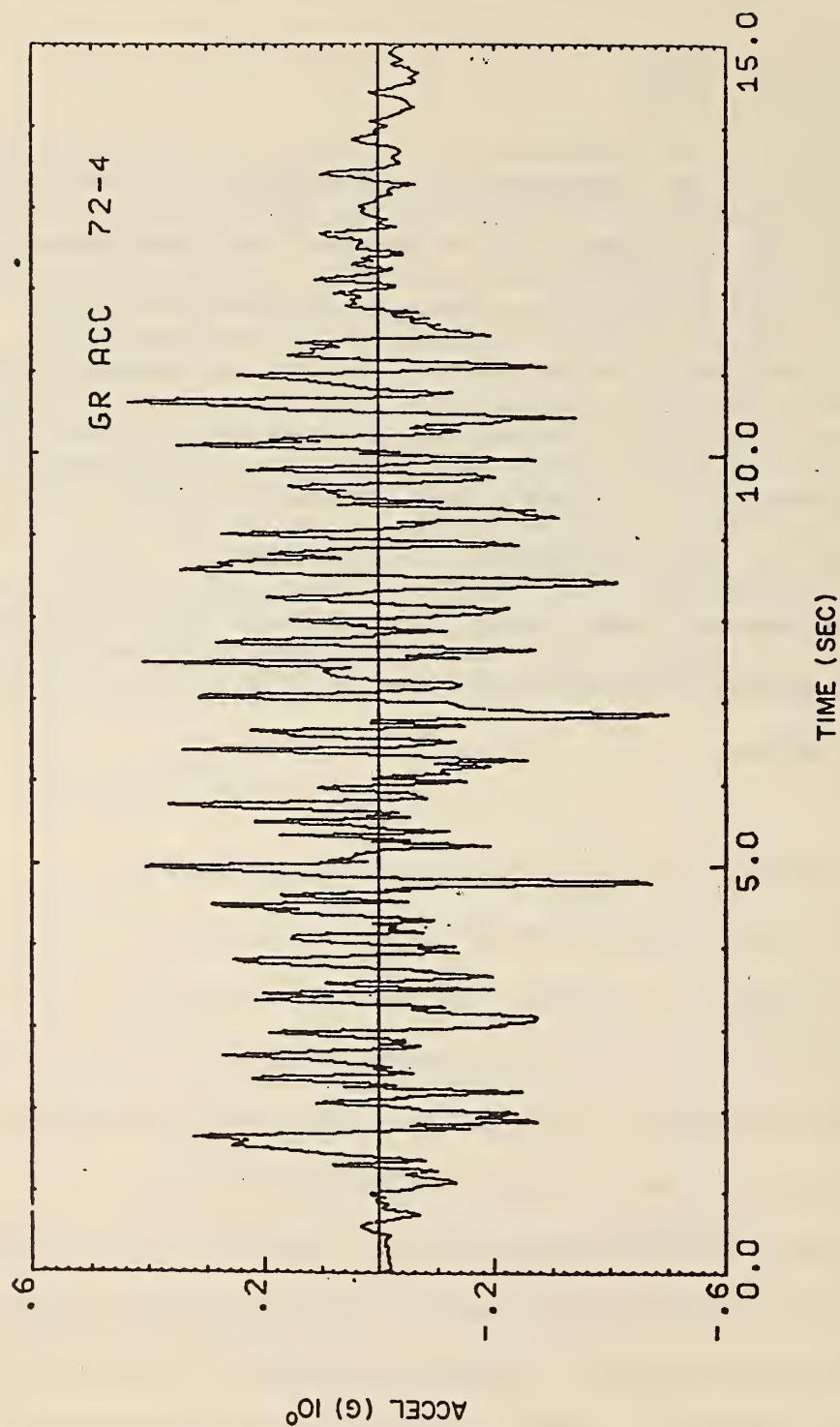


FIG.30 SIMULATED GROUND ACCELERATION RECORD OF THE SAN FERNANDO EARTHQUAKE AT THE OLIVE VIEW HOSPITAL SITE

## VI PARAMETER STUDIES

The previously defined mathematical modelling and dynamic analysis procedures have been applied to a straight version of an existing slightly-curved skewed bridge, namely, the North Connector Undercrossing located approximately 800 ft. northerly of Route 5 - San Fernando Road Interchange in the city and county of Los Angeles. Plan and elvation views of this bridge are shown in Fig. 31 along with cross-sectional views of the decks and the centrally located supporting columns. Figure 32 shows a sectional view of the left abutment with a portion of the backfill of extent  $L$  and height  $H$ .

It is the purpose of this chapter to present the results of dynamic analyses for the North Connector Undercrossing when subjected to one component of earthquake excitation in its longitudinal direction. The ground motions used in this study were the Olive View Hospital accelerations shown in Fig. 30 during the time interval 2-4 seconds. This relatively short duration was chosen to minimize computer time and yet to provide sufficient time for a representative dynamic response to occur. The peak acceleration in this excitation is approximately 0.3 g.

In order to establish an appropriate mathematical model of the entire bridge-soil system, parameter studies were first carried out using a rigid wall with uniform elastic backfill. The complete bridge-soil system was then analyzed with certain parameter variations. The results of these studies along with the results of an integration-time-interval sensitivity analysis are presented in the subsequent sections of this chapter.



## A. RIGID WALL-BACKFILL SYSTEM

1. Lateral Extent of Backfills - To study the longitudinal dimension or extent of backfill required in the mathematical modelling of bridge-soil systems, analyses were conducted using a single rigid wall and a uniform linear-elastic backfill having the properties  $\gamma = 110$  pcf,  $\nu = 0.35$ , and  $G = 10$  ksi. Five cases with  $L/H$  ratios equal to 4.8, 6.0, 10.0, 14.0, and 22.0, as shown in Fig. 33, were used in this investigation. The finite element idealization consists of 5 elements in the vertical direction and a variable number in the horizontal direction. The element length to height ratio  $R = a/b$  was maintained at a constant value equal to 2 throughout the extent of the backfill in Cases 1 and 2 but was maintained only over a distance  $2H$  from the wall in Cases 3, 4, and 5. This ratio was set equal to 4 for all elements beyond the distance  $2H$  in the latter cases. No friction elements were placed between the rigid wall and the backfill in these particular studies and the left vertical boundary of the backfill was assumed free in each case. The fundamental period of the soil system under these conditions is about 0.08 seconds in each case with slight increases occurring with increasing values of  $L/H$  as shown in Table 1.

Assuming rigid body earthquake excitations to occur along the entire base of the backfill and at the rigid-wall vertical-boundary and assuming 5 percent of critical damping in the first two modes of vibration, time histories of response were obtained for all 5 cases. Response quantities of greatest interest were the maximum or peak values of (1) total lateral dynamic force exerted on the rigid wall, and (2) horizontal displacements and accelerations at various location in the backfill.



Figure 34 shows the maximum total lateral dynamic force  $F_d$  exerted on the wall for each of the 5 cases studied. This force is reasonably constant at a value of approximately 14.5 kips over the range studied; i.e.  $4.8 < L/H < 22$ , and is about 3.9 times greater than the average static value which is approximately 3.7 kips. The mean location of the resultant force  $F_d$  was found to be at a distance  $0.52 H$  above the base which is considerably higher than the position of the resultant static force  $F_s$  located at  $0.34 H$ .

The maximum horizontal displacements relative to the moving base at 6 different locations in the backfill are shown in Fig. 35 for all 5 cases. While these displacements are reasonably constant over the range of  $L/H$  studied, large differences are noted from one point to another. The displacements for points 1 and 2 are very small due to the fact they are located only one element away from the rigid wall. Points 3 and 4 which are 5 elements away from the wall experienced much larger displacements than points 1 and 2 and points 5 and 6 at the left boundary experienced even larger displacements. These relative displacements reflect the manner in which the rigid wall boundary effects decay with increasing distance from the wall. The displacements for points 3 and 5 are considerably larger than the corresponding displacements for points 4 and 6, respectively; thus, demonstrating the increase in displacements with vertical distance above the rigid base.

Figure 36 shows the maximum total horizontal acceleration at locations 1-6 for all 5 cases studied. The relative variations of this response quantity with  $L/H$ , horizontal distance from the wall, and vertical distance above the base are similar to those previously described

for horizontal displacement. It should be noted that the average acceleration with  $L/H$  ranges from about 0.5 g for points 1 and 2 to about 1.1 g for point 5. These values represent a rather small amplification of acceleration at points 1 and 2 and a fairly large amplification of the acceleration at point 5 over the peak excitation acceleration of about 0.3 g.

Based on the numerical results shown in Figs. 34-36 and summarized in Table 2, it appears that an  $L/H$  ratio equal to 14 is sufficient for use in any bridge-soil analysis. This ratio may even be reduced to a value of 6 with little loss in accuracy in determining the maximum values of abutment backfill forces. However, this reduction could introduce significant changes in the predicted maximum horizontal accelerations.

2. Length to Height Ratio of Finite Elements - Length to height ratios  $R = a/b$  for the finite elements of the backfill model were rather arbitrarily assigned values as shown in Table 1 for the 5 cases previously defined. To investigate the influence of changing these ratios, 4 new cases as shown in Fig. 37, each having an  $L/H$  ratio equal to 10, are defined. The length to height ratio equals 2 throughout the model for Case 1 and over a distance  $2H$  from the wall for Cases 2, 3, and 4. Beyond  $2H$ , the length to height ratio equals 4, 6, and 10 for Cases 2, 3, and 4, respectively. Five elements are again used in the vertical direction of the model and fixed and free boundaries are prescribed at the right and left ends, respectively. Linear elastic soil properties are again assumed equal to the values previously assigned.

As before, rigid body earthquake excitations are assumed to occur along the entire base of the backfill and 5 percent of critical damping

is assigned to the first two modes of vibration. Time histories of response are obtained for all 4 cases, including (1) total dynamic force exerted on the rigid wall, and (2) horizontal displacements and accelerations at 6 locations in the backfill.

Figure 38 shows total static force  $F_s$  and the maximum total dynamic lateral force  $F_d$  exerted on the wall for each of the 4 cases defined above. This force is fairly constant at a value of approximately 14.5 kips over the range of  $R$  assigned beyond  $x = 2H$  and is about 3.9 times greater than the average static value. The mean location of the resultant force  $F_d$  is at a distance about  $0.52H$  above the base. The average position of the static resultant is  $0.34H$ .

The maximum horizontal displacements relative to the moving base and the maximum total horizontal accelerations at the 6 different locations are shown in Figs. 39 and 40, respectively, for all 4 cases. The results in these figures are quite similar to the results shown the corresponding Figs. 35 and 36. Thus, it is apparent that the changes introduced in  $R$  for  $x > 2H$  have introduced relatively small changes in overall response and that Case 4, Fig. 37, can be considered a reasonable model of the backfill.

Table 3 presents a summary of maximum response for the above described 4 cases.

3. Number of Finite Elements in the Vertical Direction - All previous cases analyzed have used 5 finite elements in the vertical direction of the backfill. To check the adequacy of this number the distributions and resultant magnitudes of the static and dynamic backfill pressures on the rigid retaining wall are compared using 5 and 10 elements



in this direction.

Two cases as defined in Fig. 41 are used for this comparison. Both cases use an L/H ratio equal to 10 and R ratios equal to 2 and 10 for  $x < 2H$  and  $x > 2H$ , respectively. Case 1 uses 5 elements in the vertical direction while Case 2 uses 10 elements.

It is quite clear from the results in Fig. 41 that the distributions and maximum resultant magnitudes of the backfill forces are very similar for Cases 1 and 2 and that the positions of the corresponding resultants almost coincide. Considering this fact and the fact that their time histories (see Fig. 42) are very similar, one may conclude that 5 finite elements in the vertical direction of the backfill is sufficient for engineering purposes.

4. Soil Stiffness - To study the influence of soil stiffness on the dynamic response of the backfill soil system, the finite element model identified as Case 4 in Fig. 37 was analyzed for three soil conditions, namely, a uniform soil modulus equal 10 ksi, a uniform soil modulus equal to 2.5 ksi, and a variable soil modulus in accordance with Eq. (38) for  $K_2 = 50$ . Poisson's ratio  $\nu$  was assumed equal to 0.35 and the unit weight was again assigned the value 110 pcf. These new soil conditions are identified as Cases 1 - 3 in Fig. 43.

While the shapes of the distributions of maximum total wall pressures and their resultant force positions are quite similar for all three cases, the magnitudes of the resultant dynamic wall pressures vary considerably with the soil stiffness condition. This variation ranges from  $F_d = (100)(13.06)$  for Case 3 to  $F_d = (154.0)(13.06)$  for Case 2. Obviously, for the particular excitation used, the less stiff backfill soils produce

higher backfill forces on the rigid wall. If an excitation having a different amplitude distribution with frequency had been used, this observation could be changed considerably. Therefore, one must use caution in interpreting the results of this particular study. It is important to recognize however that soil stiffness can be an important parameter which should be studied using realistic earthquake excitations.

5. Frictional Element Stiffnesses - As pointed out previously, the shear and normal stiffnesses of the frictional elements located between backfill soil and abutment walls are arbitrarily assigned finite but very high values rather than infinite values to avoid discontinuities in their force displacement relations. To study the influences of these stiffnesses on dynamic response, the rigid wall-soil system shown in Fig. 44 was analyzed assuming linear soil behavior. In these studies the shear and normal stiffnesses ( $K_S$  and  $K_N$ ) for each frictional element were assigned equal values ranging from 1 to  $10^9$  ksi.

The total static and total maximum dynamic lateral wall forces ( $F_S$  and  $F_d$ ) obtained in these studies are plotted in Fig. 45 for stiffnesses  $K_S = K_N$  equal to 1,  $10^3$ ,  $10^6$ , and  $10^9$  ksi. As one would expect, these forces are reasonably constant over a wide range of stiffnesses. However, as the stiffnesses approach zero,  $F_S$  and  $F_d$  also approach zero which represent unrealistic values. Theoretically both  $F_S$  and  $F_d$  should approach constant values asymptotically with increasing stiffnesses, however the value of  $F_d$  for  $K_S = K_N = 10^9$  ksi is much larger than for the smaller values of stiffness. This large increase is due to a numerical instability which developed in the analysis procedures and therefore



should be ignored. It appears therefore that realistic wall forces can be obtained by selecting stiffnesses in the range  $10^3 < K_S = K_N < 10^6$  ksi.

Although the asymptotic static value of wall force in Fig. 45 is consistent with values previously presented for cases having no friction elements, the maximum dynamic force of about 40.0 kips is considerably larger than the average value (14.5) previously presented. This increase in dynamic wall force is due to the separations and associated impacts which occur between the backfill soil and the upper part of the rigid wall. Thus it appears that for high intensity excitations, the friction element is essential to realistic modelling.

#### B. INTEGRATION-TIME-INTERVAL SENSITIVITY ANALYSIS

Throughout the rigid wall-backfill parameter studies previously described, the numerical integration time step was assigned a value equal to 0.01 seconds and the constant acceleration method was used which enables response to be stable, but not necessarily convergent, for all modes of vibration. To study the adequacy of using 0.01 seconds for  $\Delta t$ , the rigid wall-soil system defined by Case 4, Fig. 37, was re-analyzed using  $\Delta t = 0.001$  seconds. The total number of degrees of freedom for this system is 90 with the fundamental period being 0.084 seconds and the highest period estimated at 0.0065 seconds. The convergent limit of the ratio of time step duration to period, i.e.  $\Delta t/T$ , is 0.39 for the constant acceleration method. Thus, for  $\Delta t = 0.01$  seconds, the convergent period  $T$  is 0.026 seconds. Since this period corresponds to the period of the 22nd mode of vibration, only the lowest 22 modes are

convergent in the constant acceleration method of analysis when  $\Delta t = 0.01$  seconds. If on the other hand,  $\Delta t = 0.001$  seconds, all modes are convergent.

To check the accuracy of response obtained for the above case using  $\Delta t = 0.01$  seconds, the time histories of lateral dynamic wall force and horizontal acceleration at point No. 1 (see Fig. 40) are obtained for  $\Delta t = 0.001$  and are plotted in Fig. 46 where they can be compared with corresponding results for  $\Delta t = 0.01$  seconds. The vertical acceleration time histories for point No. 1 are plotted in Fig. 47 for  $\Delta t = 0.01$  and  $0.001$  seconds. A summary of the maximum values of response for this case is presented in Table 4.

Obviously, the results of Fig. 46 indicate that a time step interval of  $0.01$  seconds is quite adequate in predicting total lateral wall force and horizontal acceleration time histories. However, the results of Fig. 47 indicate the very low level vertical acceleration time histories caused primarily by very high frequency modal responses cannot be predicted accurately by  $\Delta t = 0.01$  seconds. Since this high frequency response is relatively unimportant from an engineering point of view, it is concluded that  $\Delta t = 0.01$  seconds is adequate for the previously described rigid wall-soil parameter studies and also for the bridge-soil system studies to be described subsequently.

### C. BRIDGE-SOIL SYSTEM

To study the dynamic response of the combined bridge-soil system, 3 mathematical models of the North Connector Undercrossing as shown in Fig. 48, were defined. Model A has fixed boundary conditions at depth H

of the backfills, at the base of abutments, and at the base of all columns. Model B has fixed boundary conditions at depths  $2.2H$  and  $2.5H$  of the backfills, leveling with bases of pier columns, which allows the base of abutments to translate and rotate with the soil system, and fixed boundary conditions are also provided at the base of all columns. Model C has fixed boundary conditions only along the base of the backfills as in Model B. The bases of abutments and columns of this model are attached to equivalent columns representing the foundation flexibility. These equivalent columns of course, have fixed boundary conditions at their bases.

The soil elements in all three models can be assumed linear or nonlinear as desired and friction elements can be included in Models A and C, but not in Model B. The backfills extend a distance  $6H$  in all models as shown. The bridge deck is linear in each model; however, either linear or nonlinear columns can be used. Backfill and foundation soils were assumed to have the properties  $G = 10.0$  ksi,  $\nu = 0.35$ ,  $\gamma = 110$  lb/ft<sup>3</sup>,  $c = 0$ , and  $\phi = 30^\circ$ .

1. Soil Pressures on Abutments - The static and maximum dynamic pressure distributions on one abutment wall for two cases are shown in Fig. 49. The model used for Case 1 is Model A with no friction elements and with all other elements assumed linear. The model used for Case 2 is Model B in its complete linear form. Due to the characteristic response of the bridge-soil system, the static and dynamic pressure distributions are quite different in form in each case. The resultant lateral static force  $F_s$  for Case 2 is about 17% less than for Case 1, due to the change in abutment flexibility and the maximum resultant



dynamic force  $F_d$  for Case 2 exceeds the value for Case 1 by 170%. This latter difference is undoubtedly due to a closer matching of the lower mode periods of vibration for Case 2 with the predominant periods in the excitation. The location of the resultant static force is at about  $H/3$  for Case 1 and at about  $H/2$  for Case 2 while the location of the maximum dynamic resultant force is at about  $0.53H$  and  $0.6H$ , respectively.

Another check on the influence of bridge structure flexibility on the resultant abutment soil forces can be made by comparing the results for Cases 1 and 2 in Fig. 50. In this figure, Case 1 is identical to Case 1 in Fig. 49 but Case 2 is different. Here, Case 2 is actually the same as Case 1 except that the abutment wall and column stiffnesses have been reduced by a factor of 10. It is seen that Case 2 shows a 75% increase in the maximum dynamic resultant force over Case 1 due to the decrease in bridge structure flexibility. This increase is consistent with the similar increase previously noted for Case 2 in Fig. 49. The location of the resultant dynamic lateral force is again at about mid-height. The increase in the resultant static force for Case 2 over the value for Case 1 is due to the increase in rotation (due to deck dead loads) at the top of the abutment caused by the reduced abutment flexibility.

Further results of analysis are shown in Fig. 51 identified as Cases 1, 2, and 3. In this figure, Case 1 is again the complete linear version of Model A. Cases 2 and 3 are also based on Model A but Case 2 has introduced one nonlinearity, namely the friction elements, and Case 3 has employed two nonlinearities - friction elements and nonlinear soil elements. The very large increase in maximum dynamic force  $F_d$  for

Cases 2 and 3 over Case 1 is due primarily to the impact wall forces following separations between wall and backfill.

Finally the results of two additional analyses are shown in Figure 52. Cases 1 and 2 in this figure are based on Model C using friction elements and linear soil elements; however, Case 2 uses the equivalent foundation columns while Case 1 does not. The most significant result to note in Fig. 52 is that force  $F_d$  is more than twice as great for Case 2 over the value shown for Case 1. Again this increase is due to the fact that the more flexible bridge system has a closer matching of frequencies with the predominant frequencies in the excitation.

2. Total Seismic Force Carried by Columns and Abutments - To investigate the maximum total base shear carried by columns and abutments, five cases were analyzed as indicated in Table 5. Case 1 represents the bridge alone with no soil-structure interaction, i.e. Model A, Fig. 48, but with no backfill; Case 2 is Model A with linear backfill and no friction elements; Case 3 is Model B, Fig. 48, with linear backfill; Case 4 is Model A with linear backfill and friction elements; and Case 5 is Model A with non-linear backfill and friction elements. Clearly, the presence of backfill contributes significantly to the maximum total base shear, also it appears from Case 3 that the total base shear increases with overall flexibility which is again evidence of a better matching of the lower natural frequencies with the predominant frequencies in the excitation. The relatively large displacement shown for Case 3 is due to the large flexibility of the system for this case in comparison with the other cases.



D. COMPARISON OF RESULTANT ABUTMENT BACKFILL FORCE OBTAINED BY ANALYSIS AND THE MONONOBE-OKABE METHOD

One commonly used formula in calculating the resultant dynamic lateral force on the abutment wall is the Mononobe-Okabe formula [53, 55, 97].

This formula has the following form

$$P_p = (1-K_v) \cdot r \cdot x \cdot K_{Ep} \quad (141)$$

where

$P_p$  = Passive earthpressure at depth  $x$

$K_v$  = vertical seismic coefficient

$\gamma$  = Unit weight of soil

$x$  = arbitrary depth

$K_{Ep}$  = Passive earthpressure coefficient during earthquake

The coefficient  $K_{Ep}$  is given by

$$K_{Ep} = \frac{\cos^2 (\phi - \theta_0 + \theta)}{\cos \theta_0 \cdot \cos \theta^2 \cdot \cos (\theta - \theta_0) \left[ 1 - \sqrt{\frac{\sin \phi \cdot \sin (\phi + \alpha - \theta_0)}{\cos (\theta - \theta_0) \cdot \cos (\theta - \alpha)}} \right]^2} \quad (142)$$

where

$\phi$  = Angle of friction of soil

$\theta_0 = \tan^{-1} \frac{K_h}{1-K_v}$

$K_h$  = Horizontal seismic coefficient

$\theta$  = Angle between the backline of the wall and the vertical line

$\alpha$  = Angle between ground surface and the horizontal line

Using  $\phi = 30^\circ$ ;  $\theta = 0^\circ$ ;  $\theta_0 = \tan^{-1} \frac{0.1}{1-0.0} = 6^\circ$ ;  $\alpha = 0^\circ$ ;  $\gamma = 110 \text{ lb/ft}^3$

$$K_{Ep} = 2.86$$

The earthpressure at bottom of wall is

$$p_p = (1-0.0) * 110 * 13.5 * 2.86 = 4.25 \text{ K/ft}^2$$

and the total lateral force on the wall is

$$F_d = \frac{1}{2} * 13.5 * 4.25 = 28.6 \text{ K/ft}$$

Using the non-linear form of Model A, Fig. 48, or Case 3 of Fig. 51, analysis gives

$$F_d = 35.0 \text{ K/ft}$$

This analytical result is a higher value than that formula given by the Monobe-Okabe. The position of the resultant force is assumed a distance  $H/3$  above the base when using the formula; however, the analysis shows it to be  $0.44H$  above the base. This higher position given by an analysis is consistent with other investigations [97, 117].

Table 1 Details of Rigid Wall Systems for Study of Lateral Extent

Case	L/H	Subdivision of System	Fundamental Period (Sec.)	<ol style="list-style-type: none"> <li>1. Time step for all cases is 0.01 sec.</li> <li>2. Damping ratio is 0.05 for first two modes</li> <li>3. <math>G = 10.0</math> ksi</li> </ol>
1	4.8	R=2 Uniformly	0.0825	
2	6.0	R=2 Uniformly	0.0838	
3	10.0	R=2 for $x < 2H$ R=4 for $x > 2H$	0.0846	
4	14.0	R=2 for $x < 2H$ R=4 for $x > 2H$	0.0848	
5	22.0	R=2 for $x < 2H$ R=4 for $x > 2H$	0.0849	

Table 2 Comparison of Responses of Rigid Wall System at Different Lateral Extent, Using Case 5 as a Basis for Calculating the Percentage

Case	$F_s$	$F_d$	$A_i$						$U_i$					
			$A_1$	$A_2$	$A_3$	$A_4$	$A_5$	$A_6$	$U_1$	$U_2$	$U_3$	$U_4$	$U_5$	$U_6$
1	99.1	105.8	100.3	98.9	124.4	116.8	97.4	96.2	115.2	104.1	115.9	115.1	98.4	97.6
2	99.1	103.3	100.2	100.1	115.8	110.2	106.8	103.1	108.9	102.5	110.5	109.7	107.3	104.7
3	100	99.4	98.9	99.5	102.3	99.5	117.3	113.2	99.1	99.2	94.8	96.7	113.5	110.9
4	100	97.9	97.9	98.9	104.5	99.0	98.8	100.3	98.2	97.5	99.4	99.3	100.3	100.2
5	100	100	100	100	100	100	100	100	100	100	100	100	100	100
Case 5 in Absolute Value	3.73	14.54	1.90	1.88	2.21	1.96	4.23	2.87	1.12	1.21	4.65	2.99	8.75	5.31
Kips			$\text{in/sec}^2 \times 10^2$						$\text{in} \times 10^{-2}$					

1.  $A_i$  and  $U_i$  are the Maximum Acceleration and Displacement at point  $i$  respectively
2.  $F_s$  and  $F_d$  are the Static and Maximum Dynamical Lateral Forces.

Table 3 Comparison of Responses of Rigid Wall System With Different Length to Height Ratio  $R = a/b$ , Using Case 1 as Basis for Calculating the Percentage

Case	F <sub>s</sub>	F <sub>d</sub>	A <sub>1</sub>	A <sub>2</sub>	A <sub>3</sub>	A <sub>4</sub>	A <sub>5</sub>	A <sub>6</sub>	U <sub>1</sub>	U <sub>2</sub>	U <sub>3</sub>	U <sub>4</sub>	U <sub>5</sub>	U <sub>6</sub>
	8													
1	100	100	100	100	100	100	100	100	100	100	100	100	100	100
2	100	98.8	98.9	99.5	99.6	97.0	97.3	100	97.4	99.2	97.6	97.6	95.8	97.4
3	100	99.0	98.4	98.9	97.4	93.0	92.2	97.2	94.7	97.5	95.1	94.3	89.7	93.1
4	100	98.6	98.4	99.5	99.1	96.0	75.9	87.4	97.4	99.2	100.4	99.0	75.0	80.5
Case	Kips		in/sec <sup>2</sup> x 10 <sup>2</sup>					INCH x 10 <sup>-2</sup>						
1 in														
Abso-	3.73	14.63	1.90	1.88	2.27	2.01	5.10	3.25	1.14	1.21	4.52	2.96	10.36	6.05
lute														
Value														

1.  $A_i$  and  $U_i$  are the maximum acceleration and displacement at point  $i$  respectively

2.  $F_s$  and  $F_d$  are the static and maximum dynamical lateral force

3. Refer to Fig. 37 for details of subdivision



Table 4 Comparison of Responses of Rigid Wall System With  $R = 2$  for  $x < 2H$   
and  $R = 10$  for  $x > 2H$  at Different Time Step. Using Case 2 as basis

Case	Time Step	$F_s$	$F_d$	$A_{1h}$	$A_{1v}$	$A_{2h}$	$A_{2v}$	$A_{3h}$	$A_{3v}$
	Sec	%							
1	0.01	100	99.0	96.4	233.3	96.0	109.0	95.3	82.1
2	0.001	100	100	100	100	100	100	100	100
Case 2 in Absolute Value	Sec	Kips		in/sec <sup>2</sup> x 10 <sup>2</sup>					
	0.001	3.725	14.58	1.94	0.056	2.01	0.041	2.98	0.51

1.  $F_s$ ,  $F_d$  are the static and maximum dynamical lateral forces
2.  $A_{1h}$ ,  $A_{1v}$  are the maximum horizontal and vertical acceleration at point i.

Table 5 Comparison of Maximum Total Seismic Force on the Bridge With or Without Soil Interaction

Case	Bridge Model	$A_x$	$U_x$ %	$F_{max}$	Remarks
1	Bridge alone	100	100	100	1. $F_{max}$ is the maximum total seismic force on the bridge
2	linear bridge-soil system, abutment base fixed	73	140	168	2. $A_x$ , $U_x$ is the horizontal acceleration and displacement at the center of deck at the time of $F_{max}$
3	linear bridge-soil system, abutment on soil	237	1120	205	
4	Bridge-soil system, linear soil, non-linear friction	138	186	276	3. Case 2 - Fig. 48-A, no friction element
5	Bridge-soil system, non-linear soil and friction	163	151	225	Case 3 - Fig. 48-B
Case 1	Absolute Value	g's	INCH $10^{-2}$	KIPS	Case 4, 5 - Fig. 48-A, with friction element
		0.50	3.63	408.0	

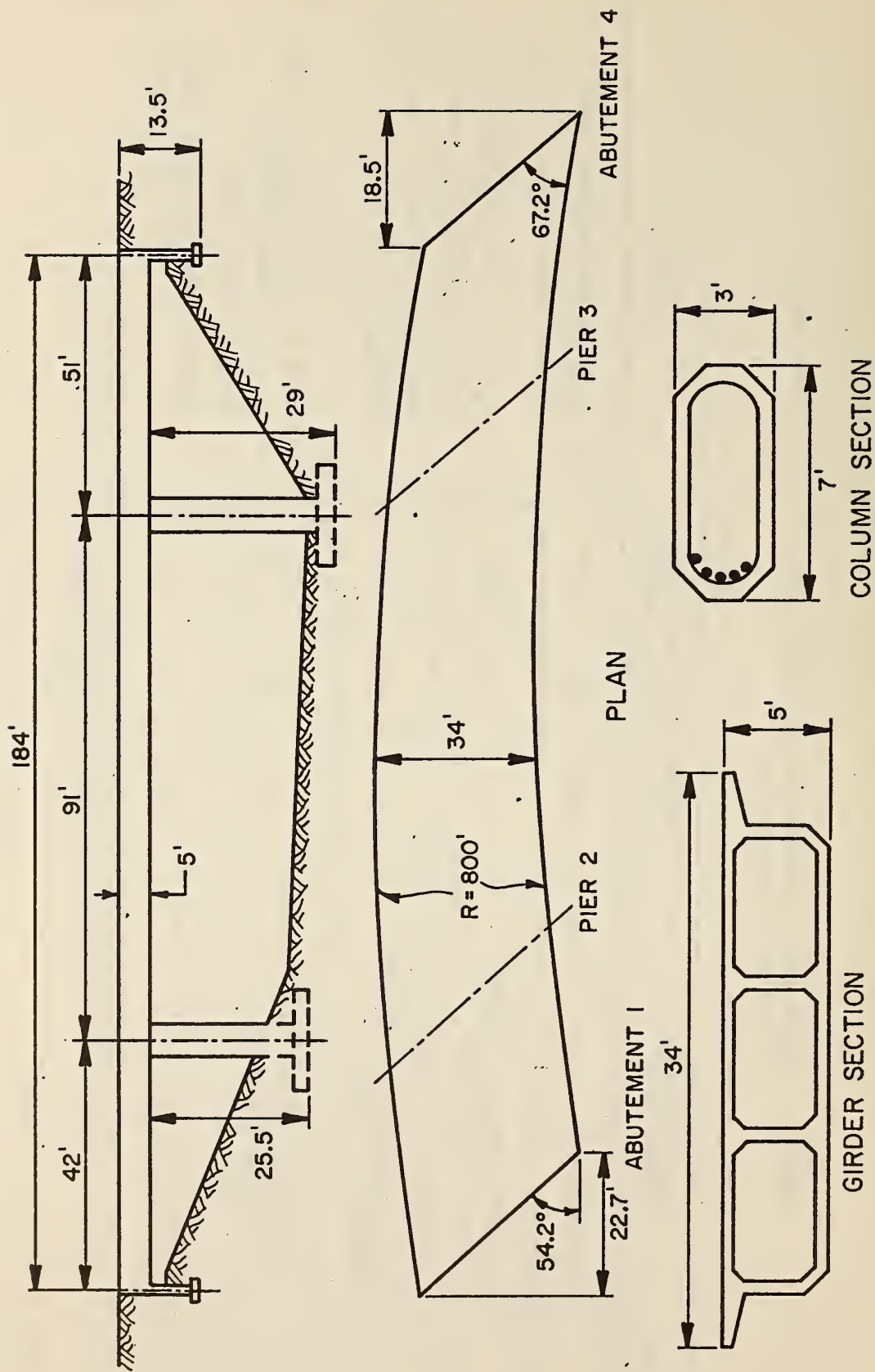


FIG. 31 GENERAL PLAN OF NORTH CONNECTOR UNDERCROSSING

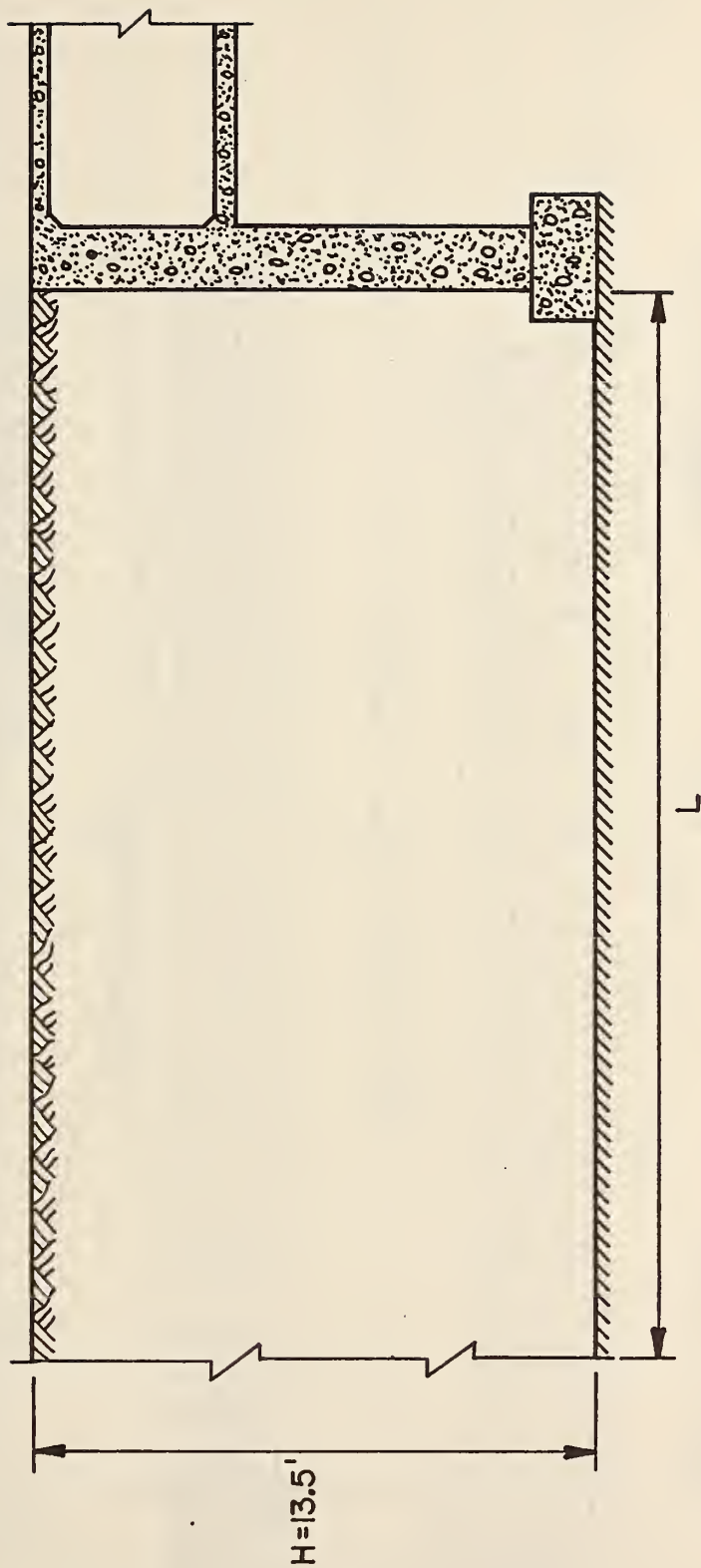
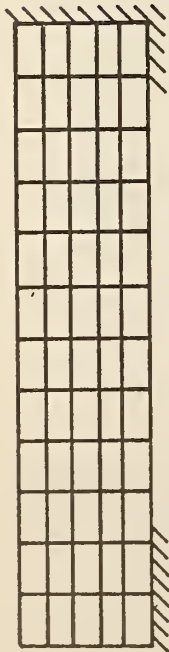
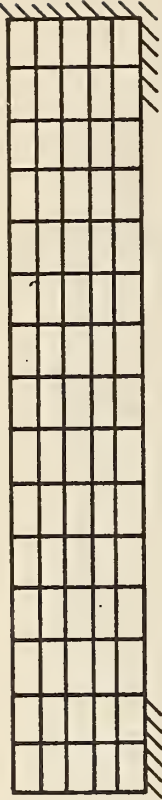


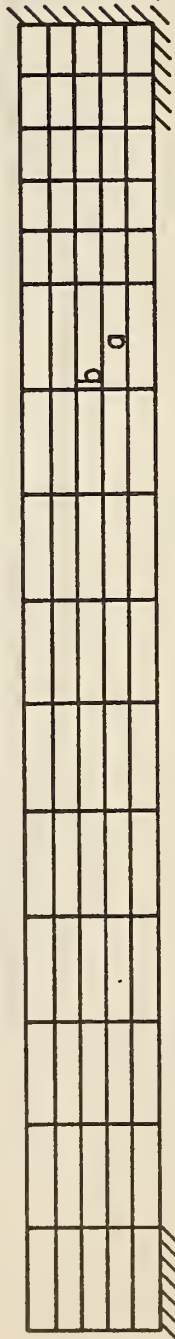
FIG. 32 ABUTMENT AND BACKFILLS



CASE 1  $L/H = 4.8$



CASE 2  $L/H = 6.0$



CASE 3  $L/H = 10.0$

$$R = a/b$$



CASE 4  $L/H = 14.0$



CASE 5  $L/H = 22.0$

FIG.33 RIGID WALL SYSTEM FOR STUDYING THE EFFECTS  
OF LATERAL EXTENT OF BACKFILLS



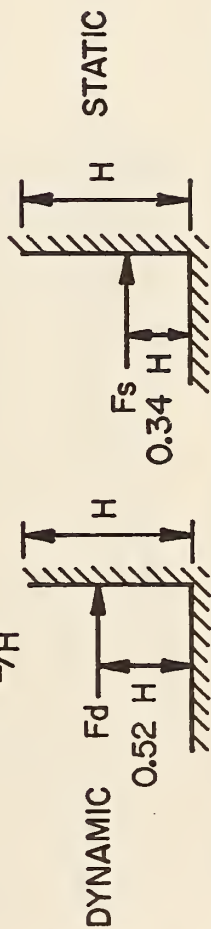
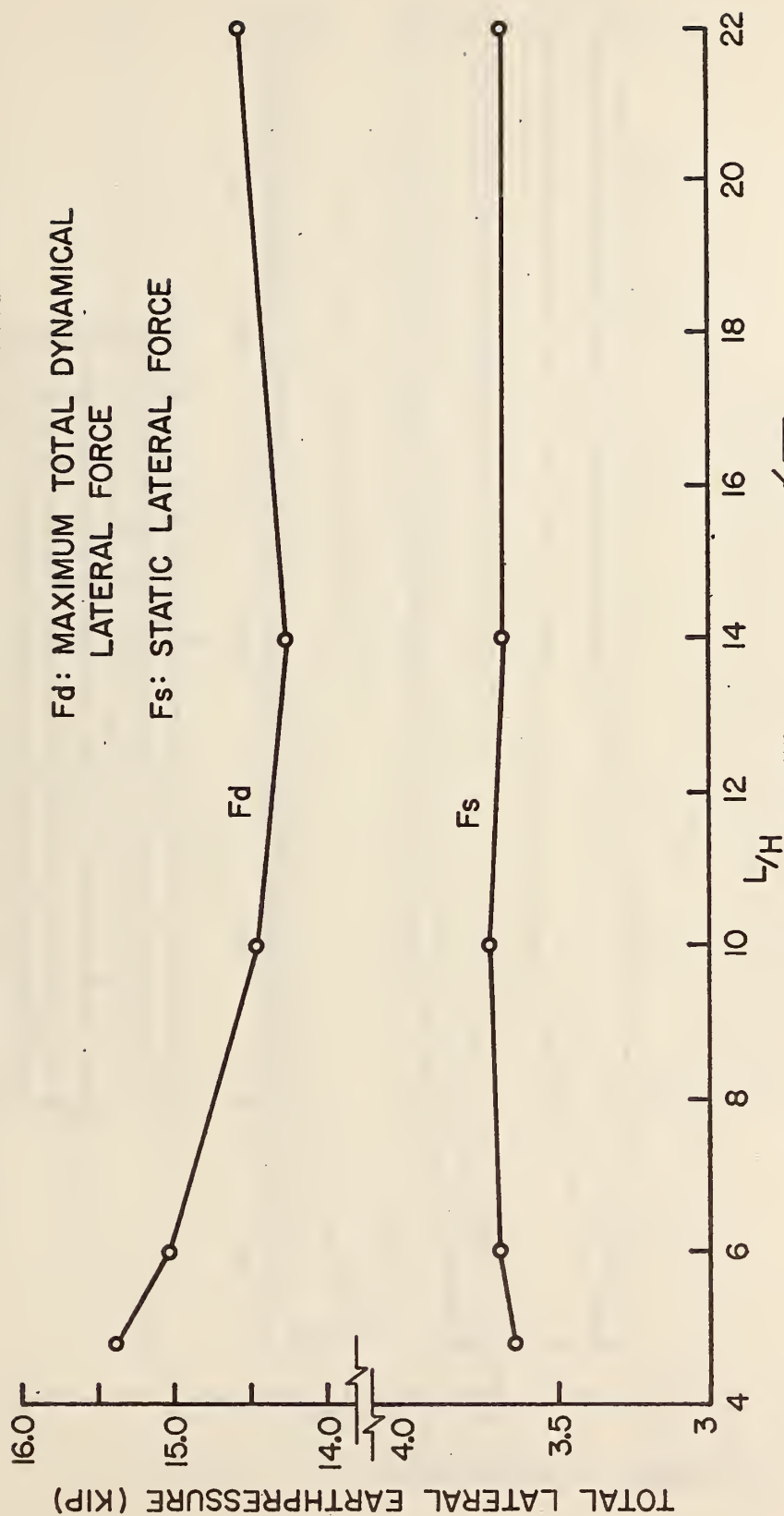


FIG. 34 STATIC AND MAXIMUM DYNAMICAL TOTAL LATERAL EARTH PRESSURE FOR DIFFERENT LATERAL EXTENT  $L/H$

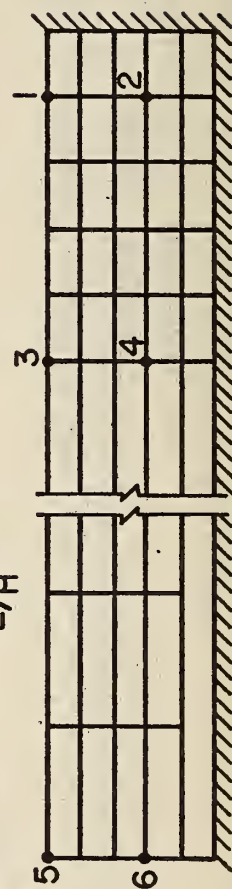
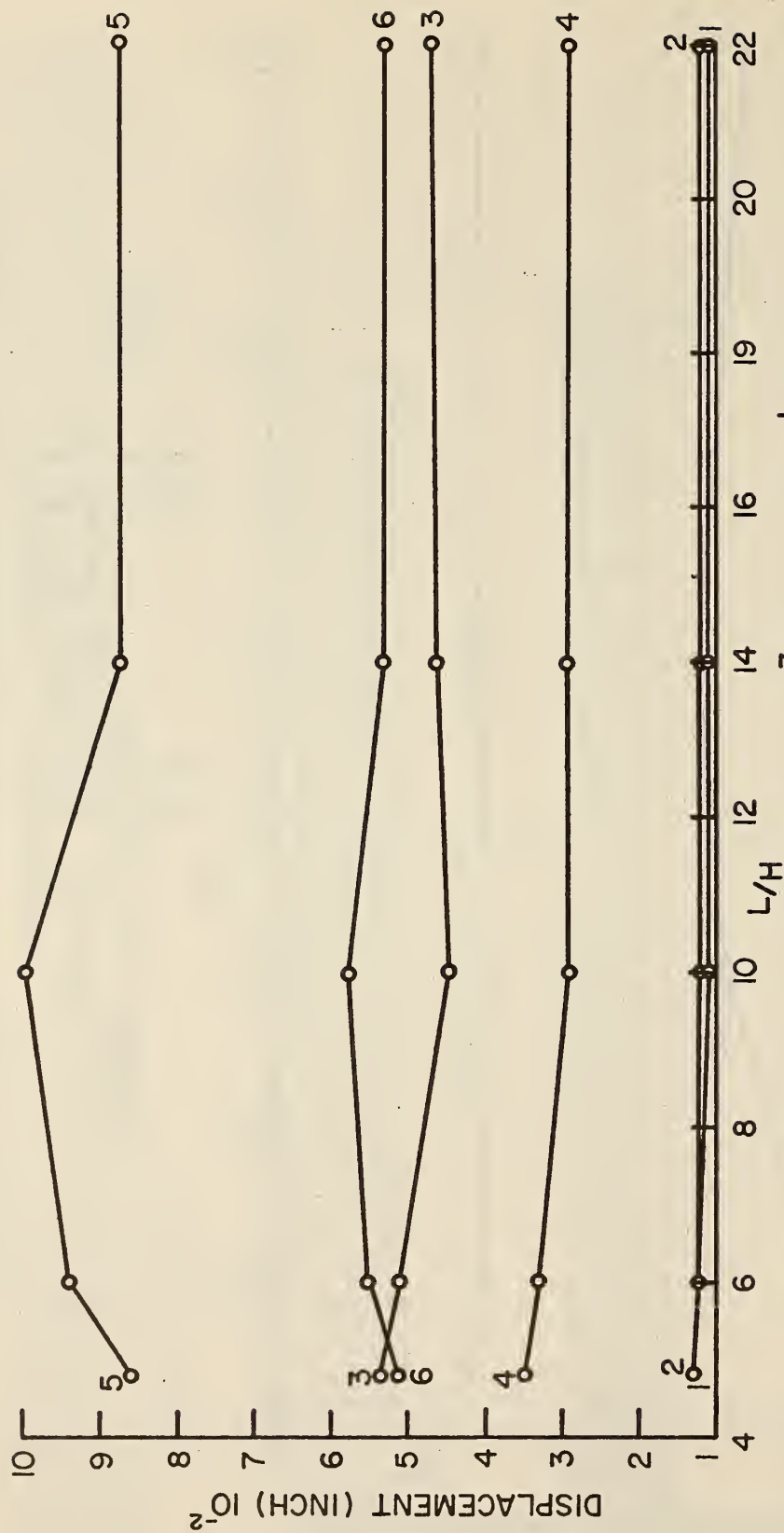


FIG. 35 MAXIMUM HORIZONTAL DISPLACEMENT AT POINTS 1 TO 6 FOR DIFFERENT LATERAL EXTENT  $L/H$

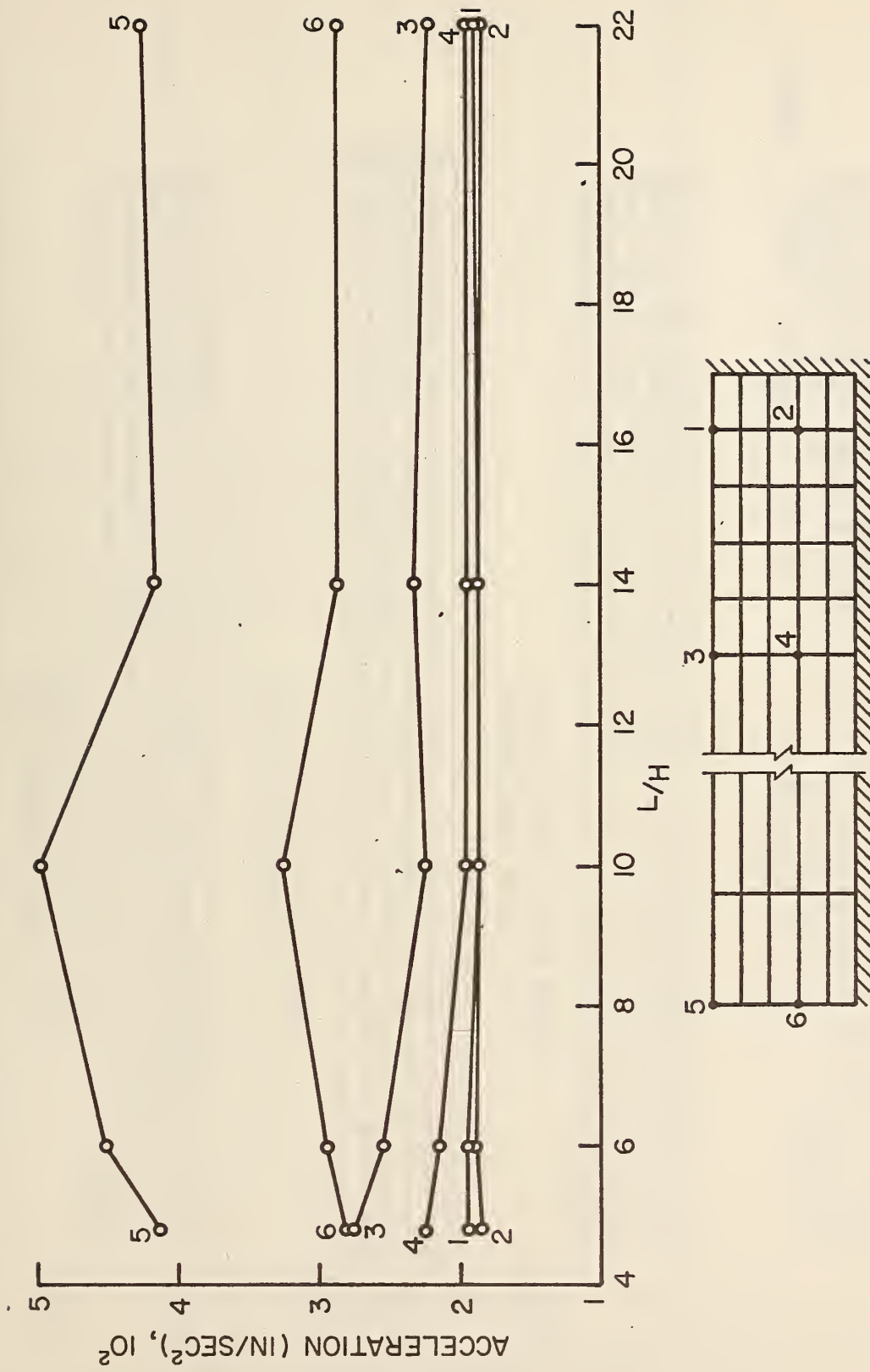


FIG.36 MAXIMUM HORIZONTAL ACCELERATIONS AT POINTS 1 TO 6 FOR DIFFERENT LATERAL EXTENT L/H

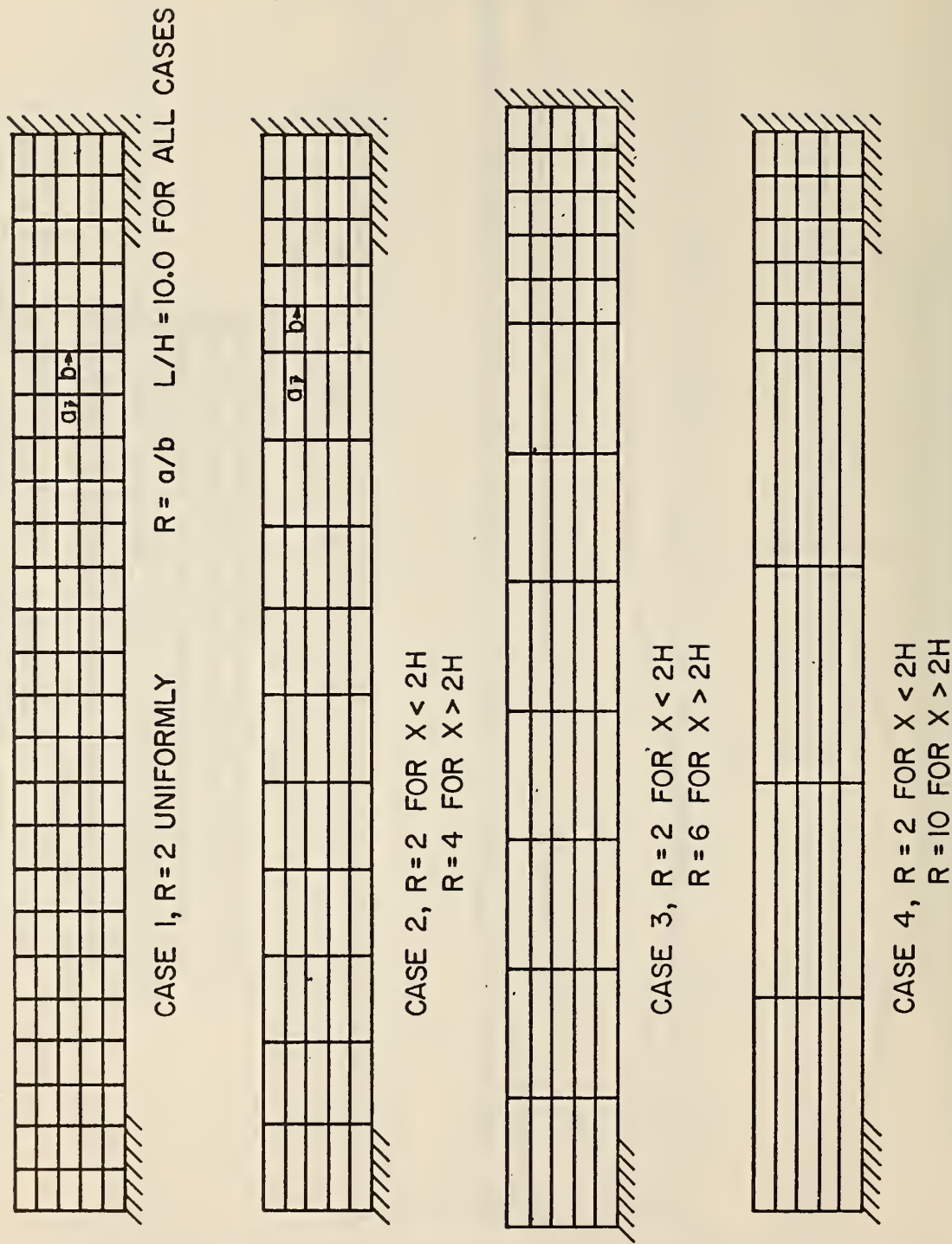


FIG. 37 FINITE ELEMENT MODEL FOR STUDYING THE LENGTH TO HEIGHT RATIO  $R$

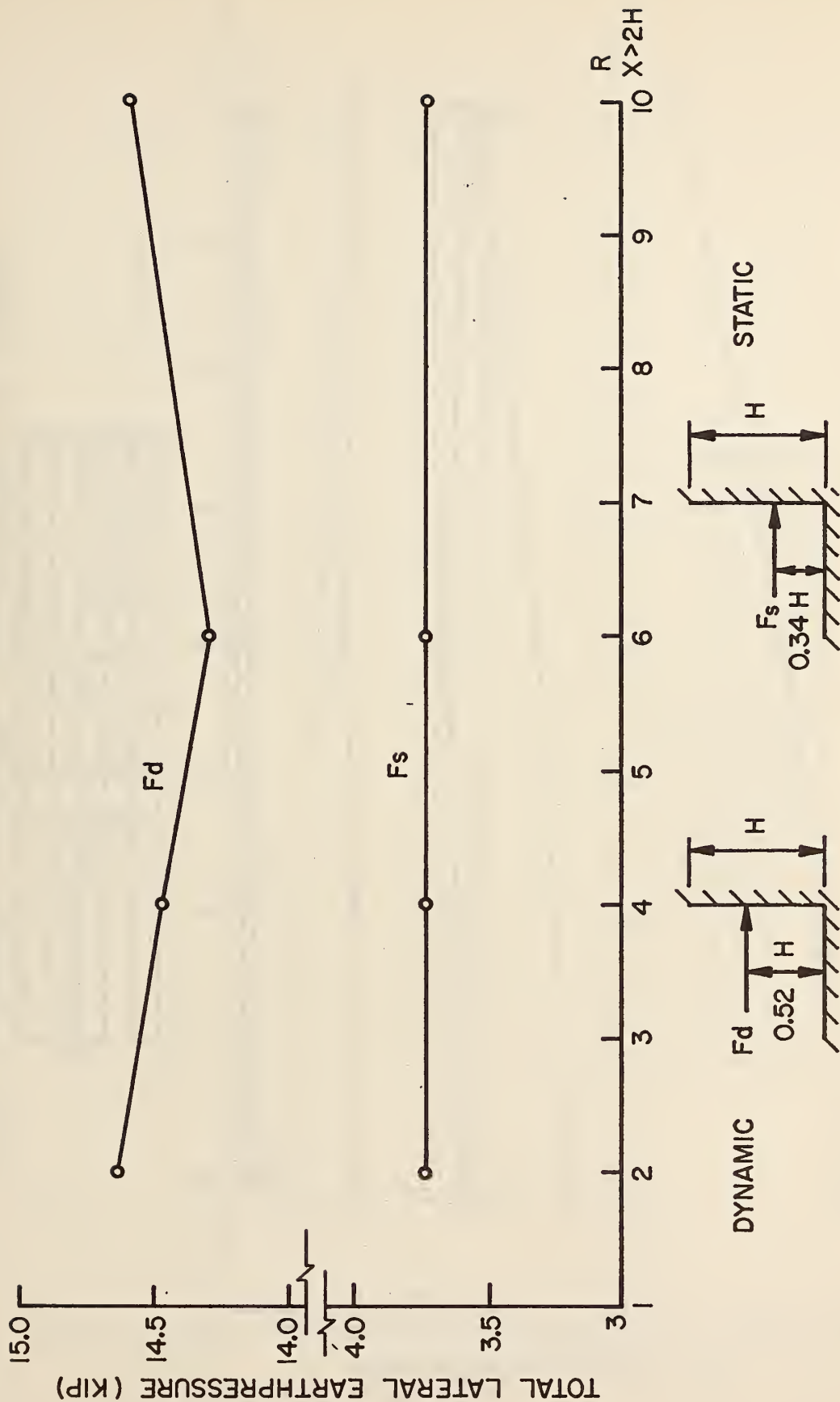


FIG.38 STATIC AND MAXIMUM DYNAMICAL TOTAL LATERAL PRESSURE FOR DIFFERENT ELEMENT SIZE  $R = a/b$





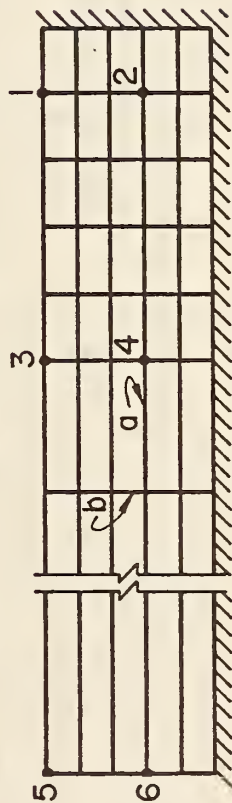
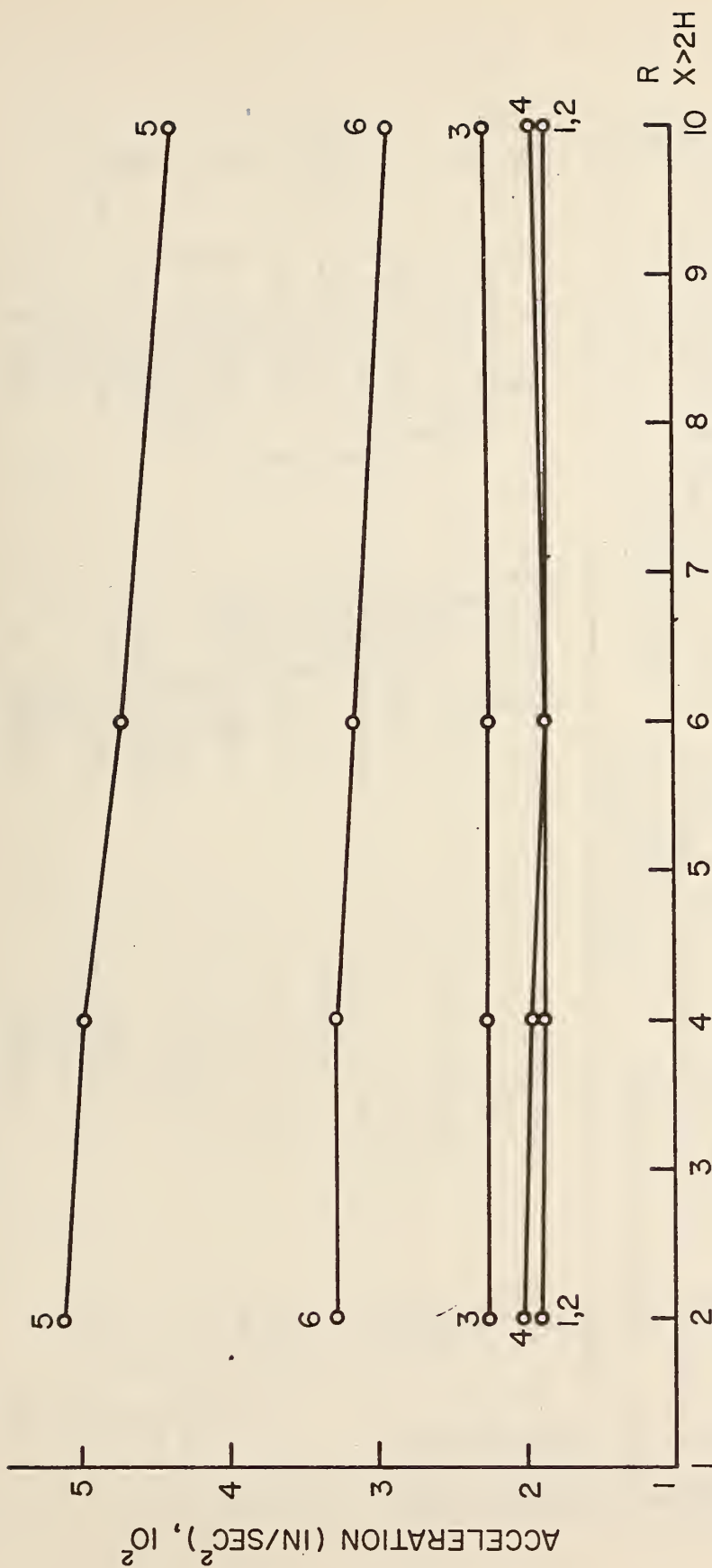


FIG. 40 MAXIMUM HORIZONTAL ACCELERATION AT POINTS  
1 TO 6 FOR DIFFERENT ELEMENT SIZE  $R = a/b$

CASE	TOTAL LAYERS	SUBDIVISION	F <sub>s</sub>	F <sub>d</sub>	REMARKS
1	5	R = 2 FOR X < 2H R = 10 FOR X > 2H	95.2	94.2	1. F <sub>s</sub> , F <sub>d</sub> ARE THE STATIC AND MAXIMUM DYNAMIC LATERAL FORCES
2	10	L/H = 10	100	100	2. CASE 2 AS BASIS FOR CALCULATING PERCENTAGES
CASE 2, ABSOLUTE VALUES			KIPS		
			3.91	15.32	

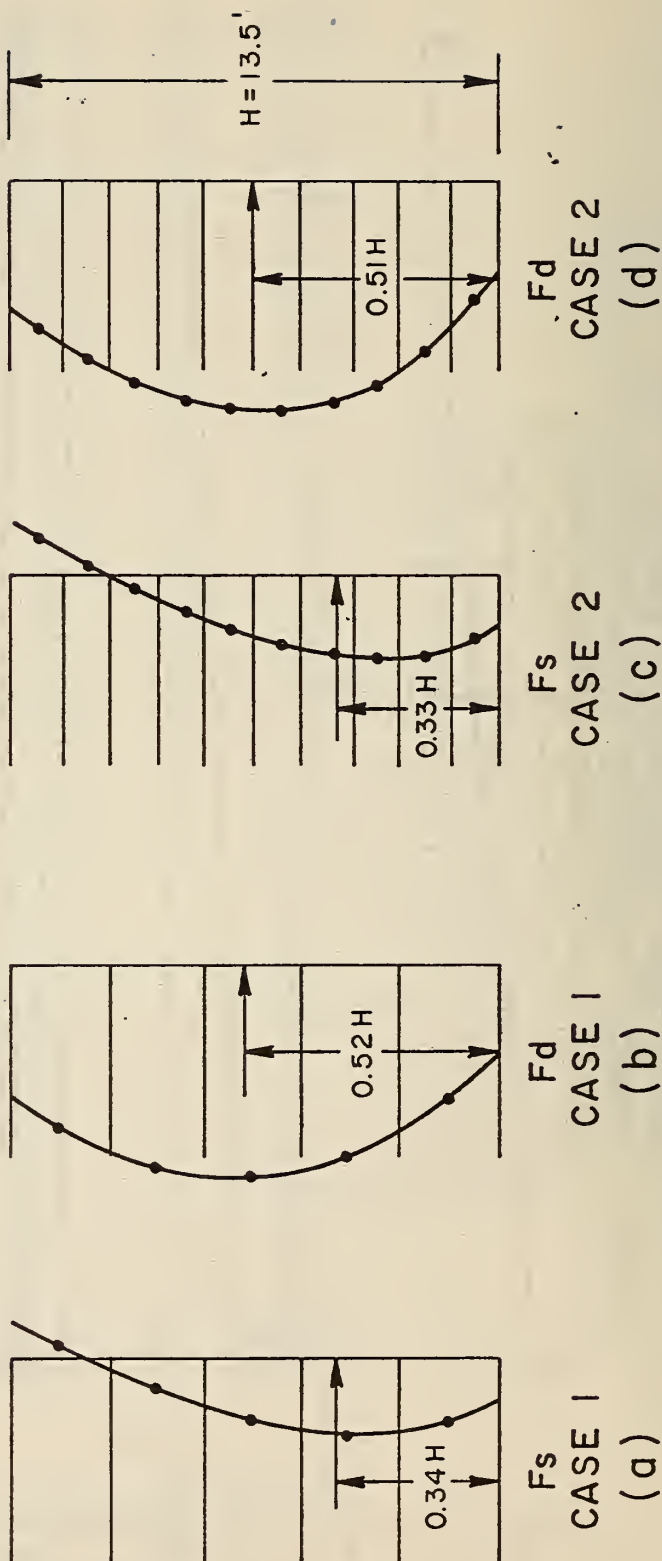
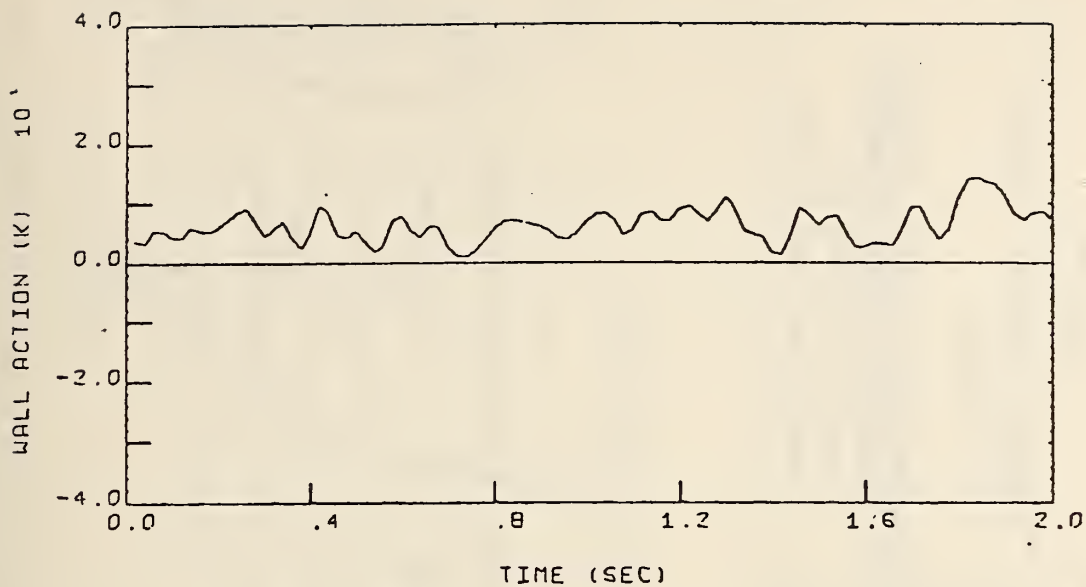
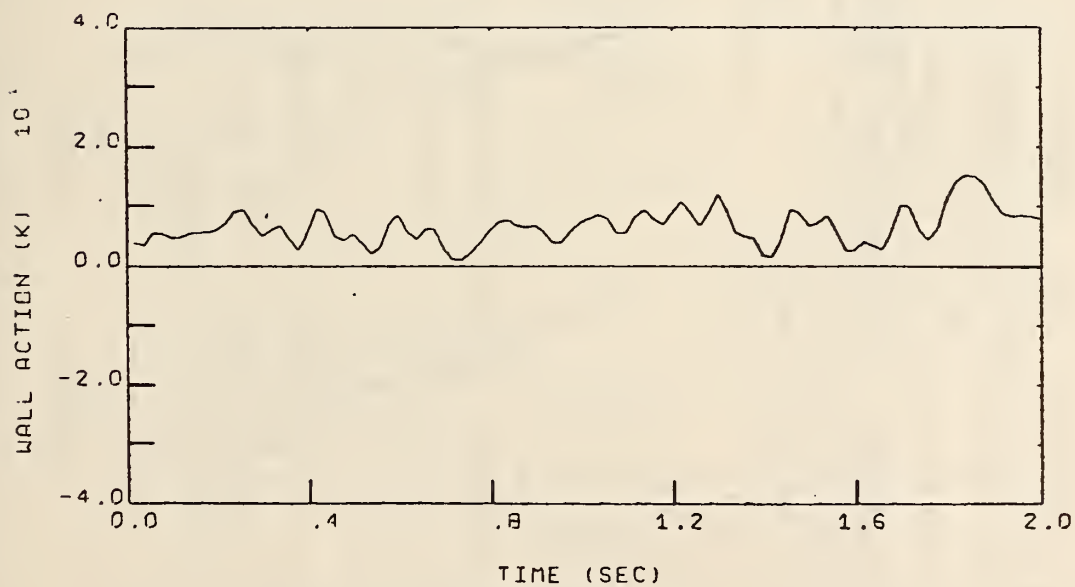


FIG. 41 STATIC AND MAXIMUM DYNAMICAL PRESSURE DISTRIBUTION WITH DIFFERENT NUMBER OF LAYERS - RIGID WALL SYSTEM



(a) 5 LAYERS



(b) 10 LAYERS

FIG. 42 TOTAL LATERAL EARTH PRESSURE - RIGID WALL SYSTEM

CASE	SUBDIVISION	SOIL PROPERTY	Fs	Fd	REMARKS
1	R=2 FOR $X < 2H$	G=10.0 UNIFORM	101.3	110.5	1. REFER TO FIG. 37 , CASE 4 FOR MODEL  2. CASE 3, THE NON-UNIFORM MODULUS CASE AS BASES FOR CALCULATING THE PERCENTAGE FOR $K_2 = 50$
2	R=10 FOR $X > 2H$	G = 2.5 UNIFORM	101.3	154.0	
3	L/H = 10.0	$G = 1000 \cdot K_2 (\sigma_m)^{1/2}$	100	100	
CASE 3, ABSOLUTE VALUE			KIPS		
			3.67	13.06	

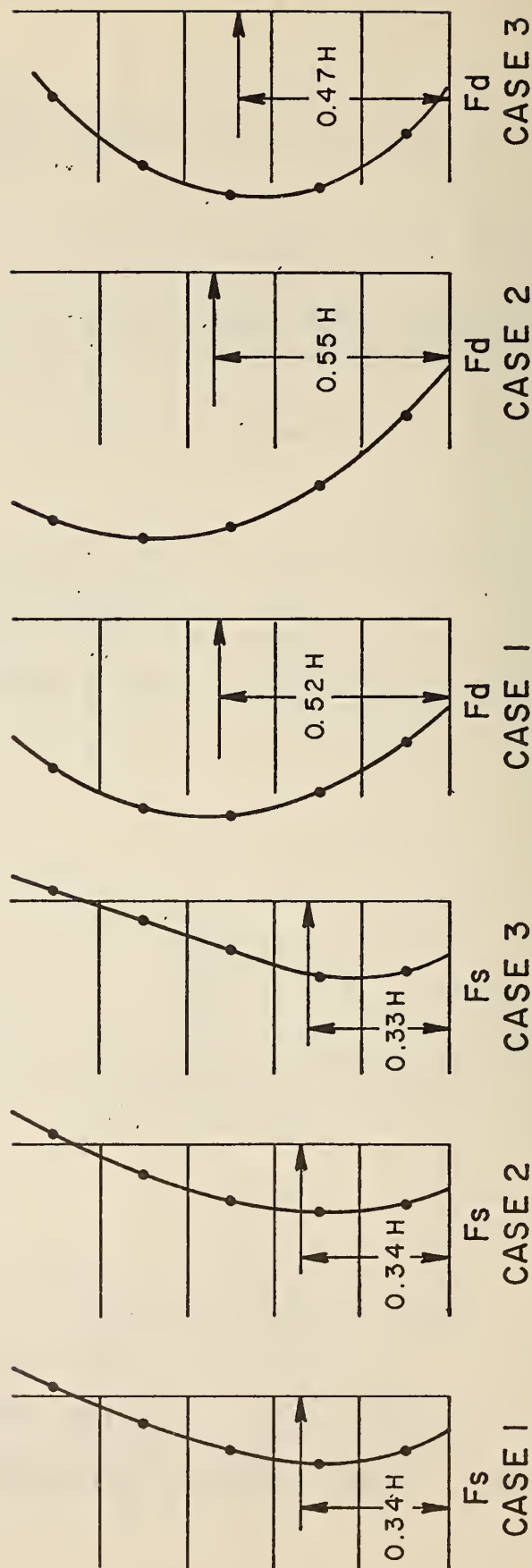
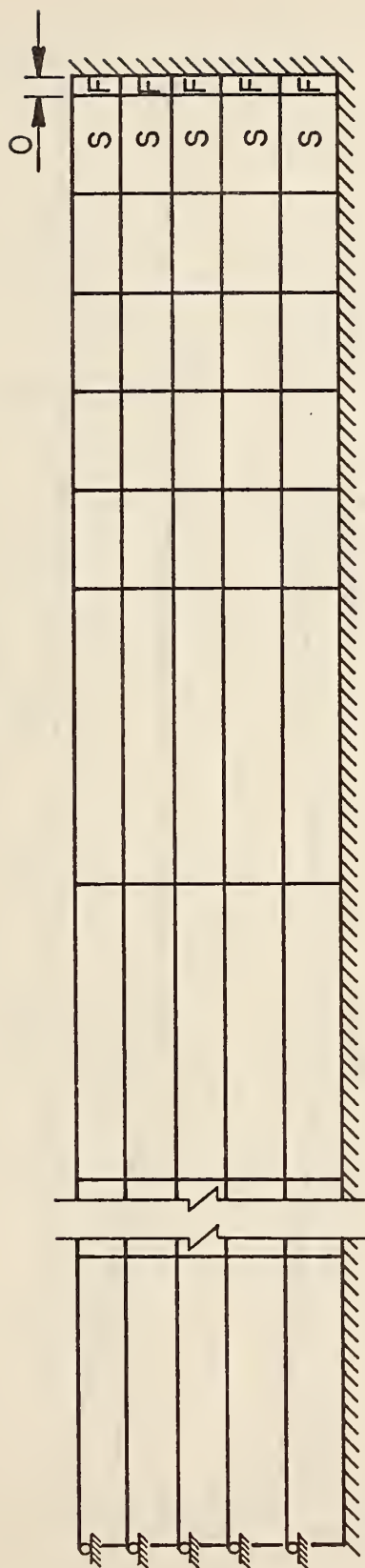


FIG. 43 STATIC AND MAXIMUM DYNAMICAL PRESSURE DISTRIBUTION WITH DIFFERENT SOIL PROPERTIES - RIGID WALL SYSTEM





$R \approx 2$  FOR  $X < 2H$   
 $R \approx 6$  FOR  $X > 2H$   
 $L/H = 115/13.5 = 8.5$   
 $G = 10.0$  KSI

$K_S = K_N$  RANGING  $1, 10^3, 10^6, 10^9$  KSI  
 F: THE FRICTIONAL ELEMENTS NEAR WALL  
 S: SOIL ELEMENT

FIG. 44 MODEL FOR STUDYING FRICTIONAL ELEMENT, RIGID WALL SYSTEM

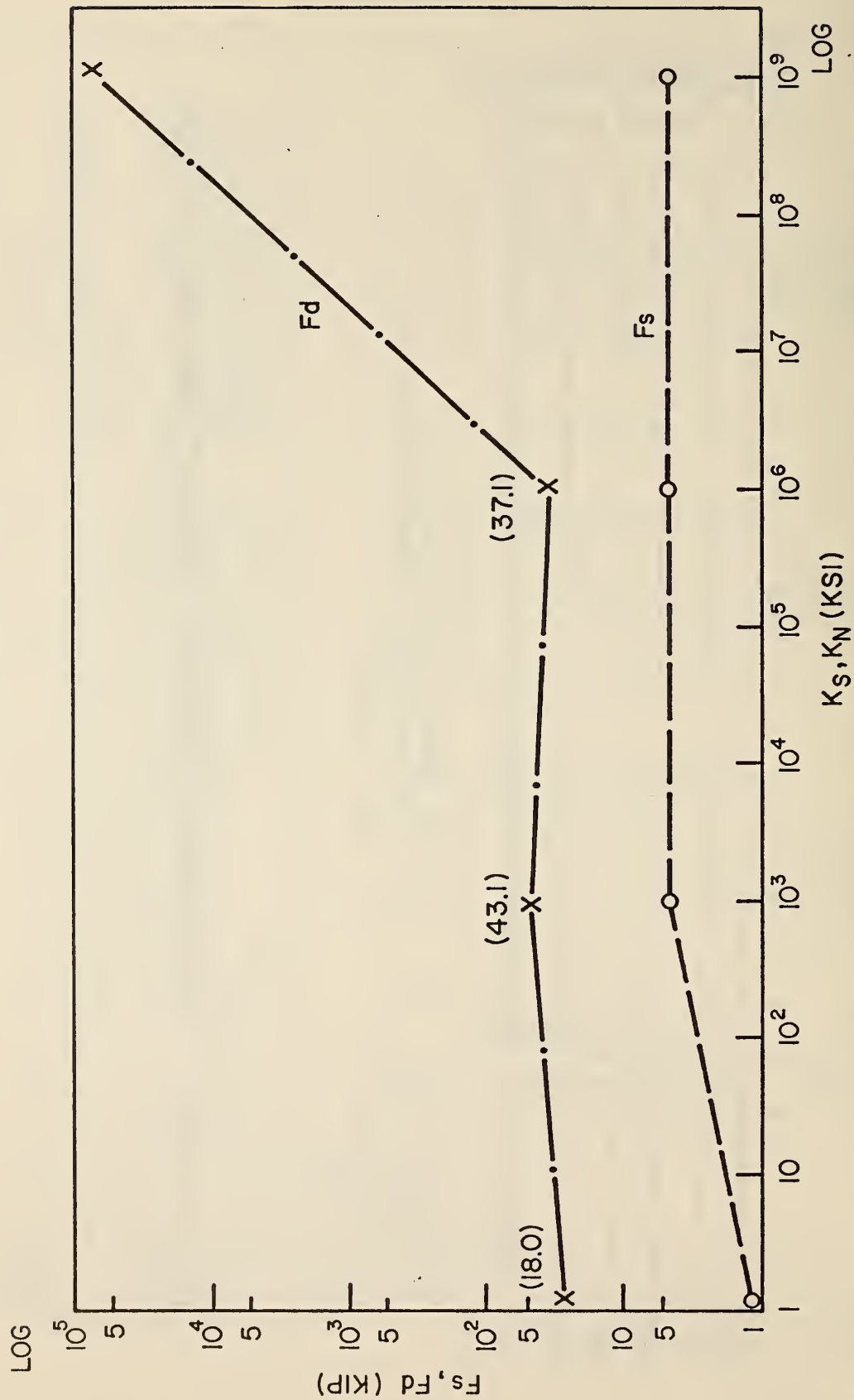


FIG. 45 EFFECT OF STIFFNESS OF FRICTIONAL ELEMENT ON  
TOTAL LATERAL FORCE - RIGID WALL SYSTEM

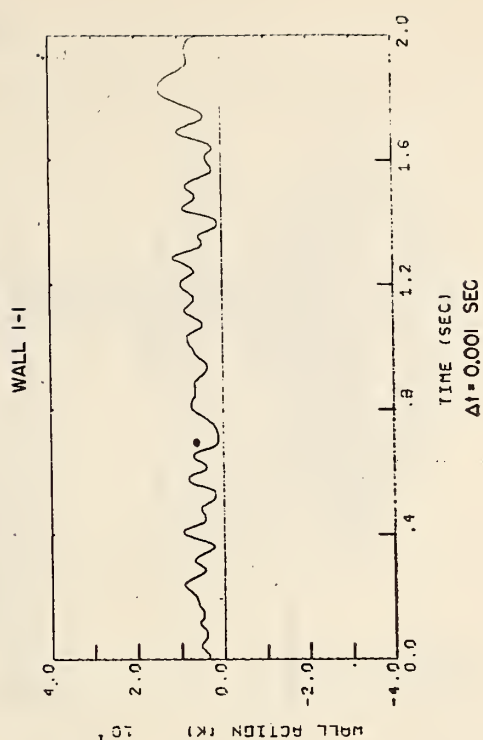
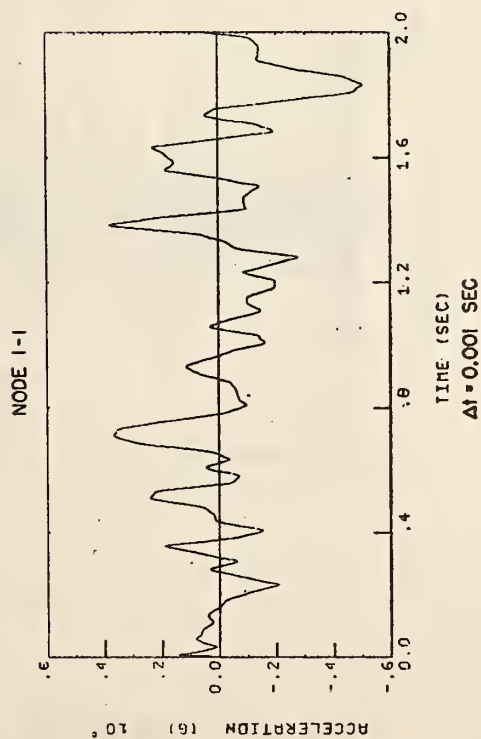
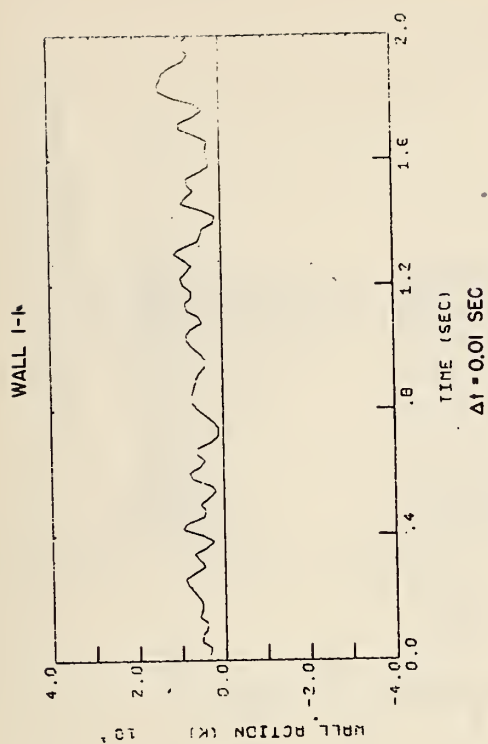
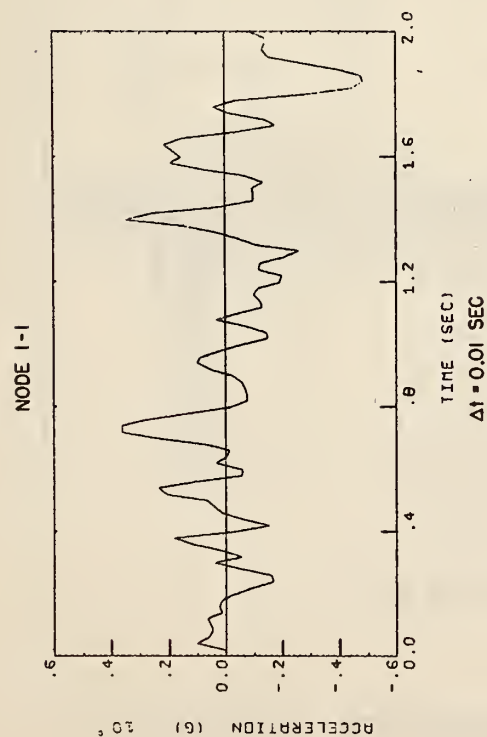
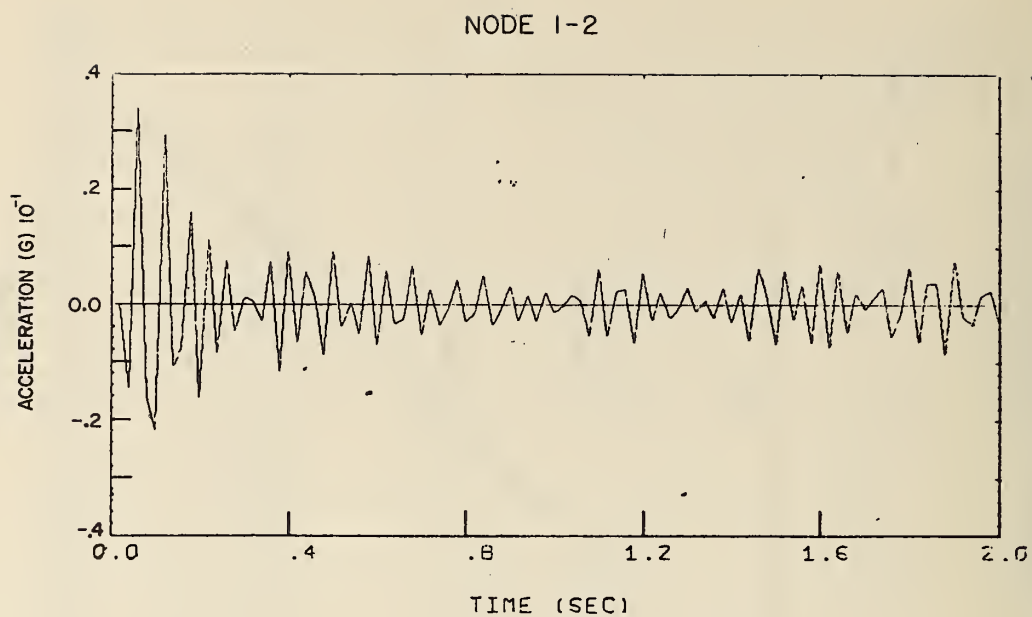
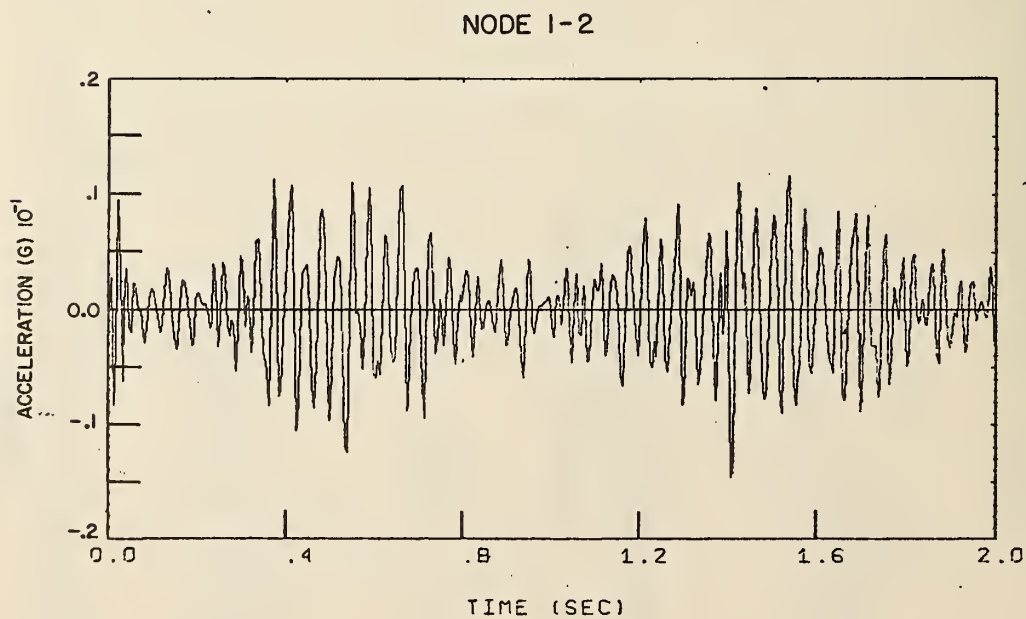


FIG. 46 LATERAL FORCE AND HORIZONTAL ACCELERATION AT POINT NO. 1 - RIGID WALL SYSTEM



(a)  $\Delta t = 0.01$  SEC



(b)  $\Delta t = 0.001$  SEC

FIG. 47 VERTICAL ACCELERATION AT POINT NO. 1

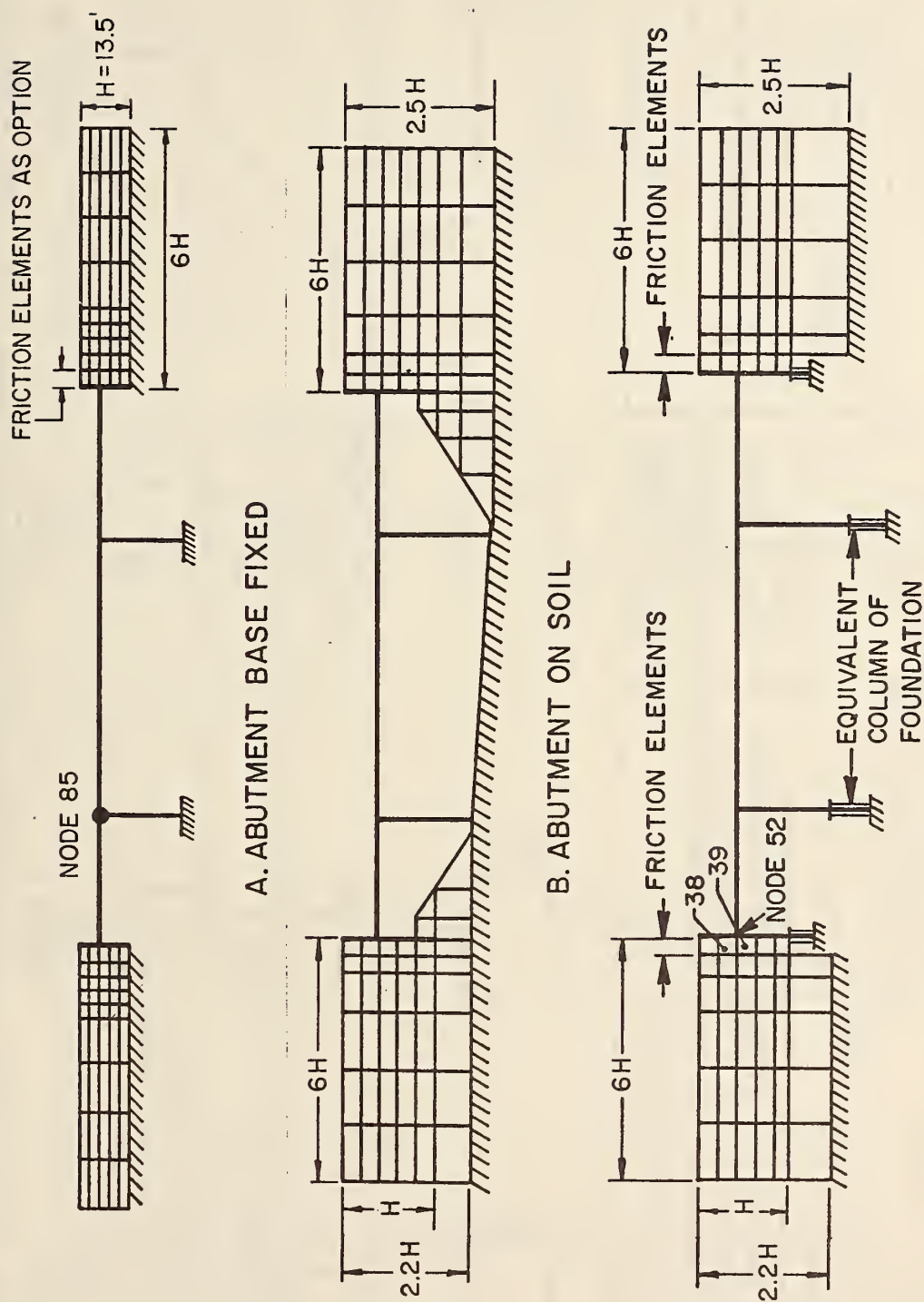
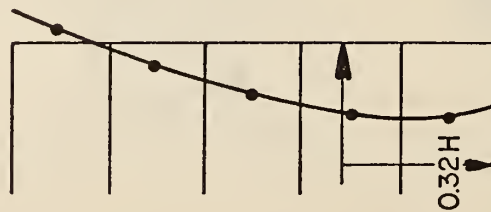


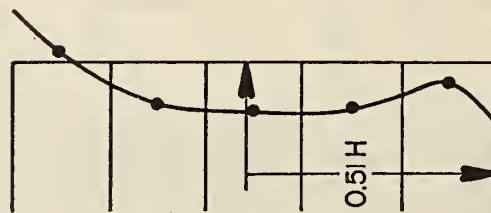
FIG. 48 NORTH CONNECTOR UNDERCROSSING, BRIDGE-SOIL SYSTEMS



CASE	SYSTEM	MOVEMENT AT ABUTMENT BASE	F <sub>s</sub>	F <sub>d</sub>	REMARKS
			%		
1	BRIDGE - SOIL SYSTEM FIXED BASE	NO MOVEMENT	100	100	1. ALL SOILS ARE ASSUMED UNIFORM, WITH G=10 KSI  2. CASE 1, REFER TO FIG. 48 - A CASE 2, REFER TO FIG. 48 - B
2	BRIDGE - SOIL SYSTEM COLUMN ON SOIL	ROTATION AND TRANSLATION	83.0	270.0	
CASE 1 , ABSOLUTE VALUE			KIPS		
			3.42	6.32	



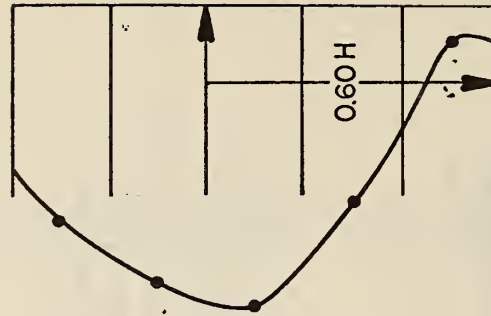
F<sub>s</sub>  
CASE 1



F<sub>s</sub>  
CASE 2



F<sub>d</sub>  
CASE 1



F<sub>d</sub>  
CASE 2

FIG. 49 STATIC AND MAXIMUM DYNAMICAL PRESSURE DISTRIBUTION WITH DIFFERENT  
BOUNDARY CONDITIONS AT THE BASE OF ABUTMENT

CASE	SYSTEM	PERIOD, SEC.		Fs	Fd		REMARKS
		1 st.	10 th.		%		
1	BRIDGE- SOIL SYSTEM FIXED BASE	0.195	0.063	100	100		1. ALL SOILS ARE ASSUMED UNIFORM, WITH G = 10 KSI  2. REFER TO FIG.48-A FOR THE MODEL
2	SAME AS 1, EXCEPT WITH SOFTER SUB- STRUCTURE	0.232	0.076	120.0	175.0		
CASE 1 , ABSOLUTE VALUE				KIPS			
				3.42	6.32		

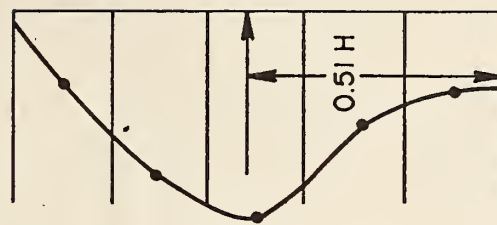
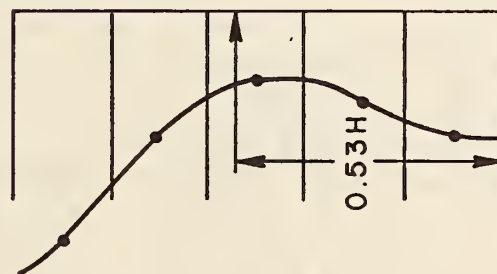
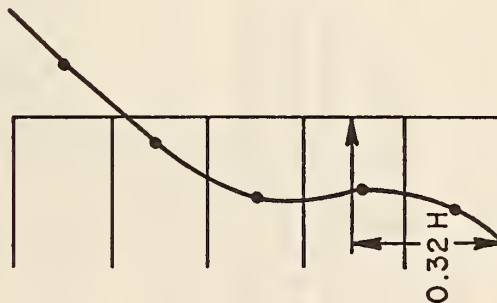
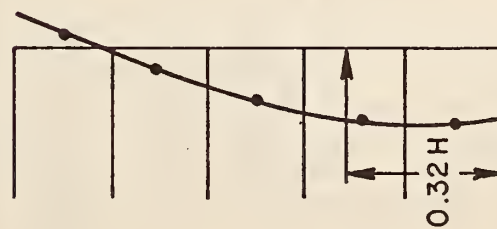


FIG.50

STATIC AND MAXIMUM DYNAMICAL PRESSURE DISTRIBUTION OF BRIDGE-SOIL SYSTEM WITH DIFFERENT SUBSTRUCTURES

CASE 1

CASE 2

CASE 1

CASE 2



CASE	SYSTEM	FOUNDATION	Fs	Fd	REMARKS
1	BRIDGE - SOIL SYSTEM WITH NON - LINEAR FRICTION ELEMENT, THE REST IS LINEAR	FIXED AT TOP OF EQ.COL.	100	100	1. REFER TO FIG. 48-C FOR MODEL
2		WITH EQUIVALENT COLUMN	129.0	225.0	
CASE 1, ABSOLUTE VALUES			KIPS		
			3.30	15.3	

SCALE DOWN 1/2 FOR Fd

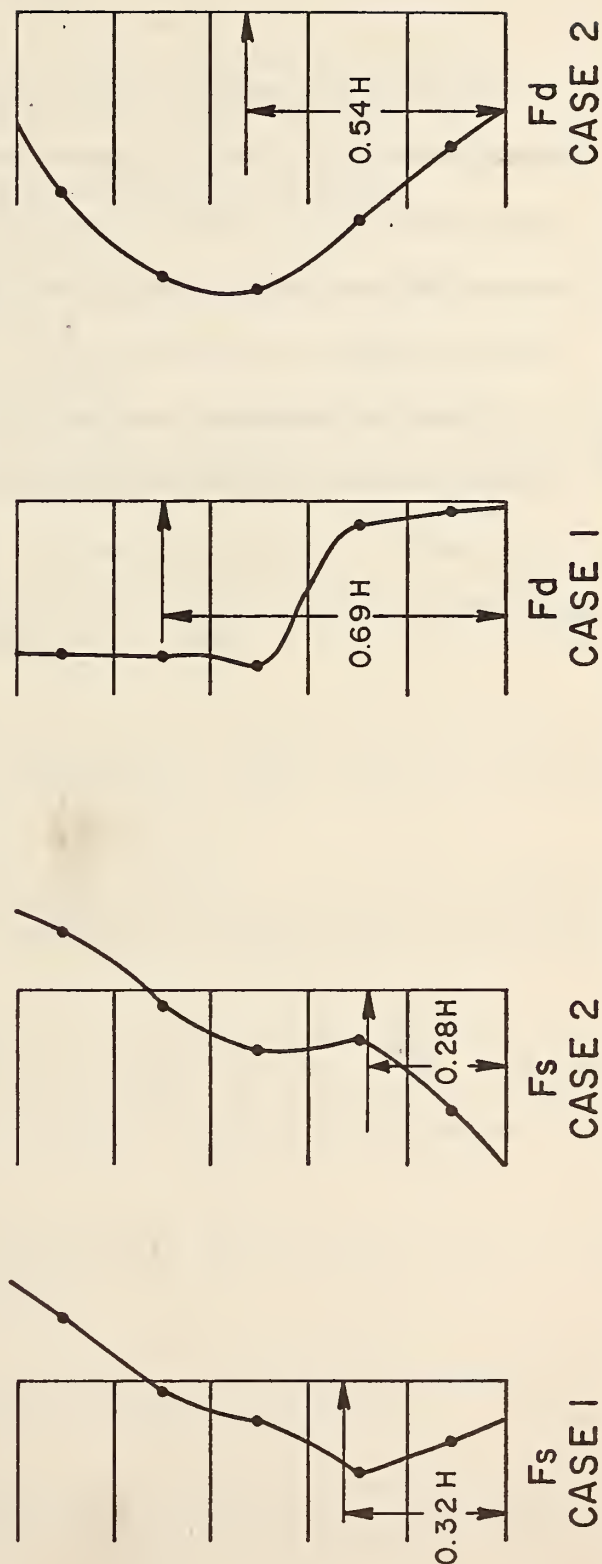


FIG. 52 STATIC AND MAXIMUM DYNAMICAL PRESSURE DISTRIBUTION OF BRIDGE - SOIL SYSTEM WITH DIFFERENT FOUNDATION

## VII GENERAL CONCLUSION

Based on the results of this investigation, it is concluded that soil-structure interaction effects must be considered when analyzing the dynamic response of short, stiff, single or multiple span bridges. The mathematical modelling and computer programs presented herein provide an effective means of conducting such analyses.

Since the numerical results obtained in this investigation are very limited, caution should be exercised when interpreting them in a quantitative sense. Further analyses are recommended to complete the parameter studies.



## BIBLIOGRAPHY

1. AASHO (1969)  
"Standard Specification for Highway Bridges," 10th Ed.
2. ACI (1970)  
"Ultimate Strength Design Handbook," Vol. 2, Columns, Special Publication No. 17A, American Concrete Institute.
3. ACI-ASCE Committee 326 (1962)  
"Shear and Diagonal Tension," Journal, ACI, Proc. 59, Jan. 1962, Feb. 1962 and March 1962.
4. Ang, H. S., Chang, G. C. (1967)  
"Numerical Calculation of Inelastic Plane Structure Soil Interaction," Proceedings International Symposium on Wave Propagation and Dynamic Properties of Earth Materials, New Mexico, Aug. 23-25, 1967, pp 393-410.
5. Arnold, R. N., Bycroft, G. N., and Warburton, G. B. (1955)  
"Forced Vibration of Body on an Infinite Elastic Solid," Journal of Applied Mechanics, Transaction, ASME, Vol. 77, pp 391-401.
6. Basavanna, B. M. (1970)  
"Dynamic Earth Pressure Distribution Behind Retaining Walls," 4th Symposium on Earthquake Engineering, Indian Society of Earthquake Technology, Nov. 14-16, 1970, pp 311-320.
7. Bathe, K. J., and Wilson, E. L. (1973)  
"Stability and Accuracy Analysis of Direct Integration Methods," International Journal of Earthquake Engineering and Structural Dynamics, Vol. 1.
8. Bertero, P. F., Fratessa, S. A., Mahin, J. H., Sexton, A. C., Scordelis, E. L., Wilson, E. L., Wyllie, L.A., Seed, H. B., and Penzien, J., Chairman (1970) "Seismic Analysis of the Charaima Building, Caraballeda, Venezuela," EERC 70-4, Earthquake Engineering Research Center, University of California, Berkeley.
9. Bishop, A. W., and Henkel, D. L. (1957)  
"The Measurement of Soil Properties in the Triaxial Test," Edward Arnold Ltd., London, 2nd Ed.
10. Bishop, A. W. (1966)  
"The Strength of Soils as Engineering Materials," 6th Rankine Lecture, Geotechnique, Vol. 16, No.2, pp 91-130.
11. Broms, B. B., and Ingelson, I. (1971)  
"Earthpressure Against the Abutments of a Rigid Frame Bridge," Geotechnique, Vol. 21, No. 1, March, 1971, pp 15-28.

12. Bull, Keith D. (1972)  
"Seismic Design of Highway Structure," Journal of the Structure Division, ASCE, Vol. 98, No. ST8, Proc. paper 9135, Aug. 1972, pp 1741-1755.
13. California State, the Department of Public Works, Division of Highways - Bridge Department, "Bridge Planning and Design Manual." (1966)
14. California State, the Department of Public Works, Division of Highways - Bridge Department (1963), "Manual of Bridge Design Practice."
15. Caughey, T. K. (1960)  
"Classical Normal Modes in Damped Linear Dynamic Systems," Journal of Applied Mechanics, Vol. 27, Trans. ASME, Vol. 82, Series E, pp 269-271.
16. Chi, H. M., and Powell, G. H. (1973)  
"Computational Procedure for Inelastic Finite Element Analysis," SESM 73-2, Department of Civil Engineering, University of California, Berkeley, January 1973.
17. Chopra, A. K., and Perumalswani, P. R. (1969)  
"Dam-Foundation Interaction During Earthquake," Proc. 4th World Conference of Earthquake Engineering, Vol. III, A6-37.
18. Chopra, A. K., Bertero, V. V., and Mahin, S. (1973)  
"Response of the Olive View Medical Center Main Building During the San Fernando Earthquake," Proceedings, 5th World Conference on Earthquake Engineering, Rome, June 1973.
19. Chopra, A. K. (1970)  
"A Computer Program for Earthquake Analysis of Dams," EERC 70-5, Earthquake Engineering Research Center, University of California, Berkeley, Sept. 1970.
20. Christian, I. J. (1966)  
"Plane Strain Deformation Analysis of Soil," Report by MIT, Department of Civil Engineering to U.S. Army Engineering Water Experimental Station.
21. Clough, R. W., and Bathe, K. J. (1972)  
"Finite Element Analysis of Dynamic Response," of "Advances in Computational Methods in Structural Mechanics and Design," Edited by Oden, J. T., Clough, R. W., and Yamamoto, Y., UAH Press, The University of Alabama in Huntsville, Huntsville, Alabama, pp 153-180.
22. Clough, R. W. (1965)  
"The Finite Element Method in Structural Mechanics," Chapter 7 of "Stress Analysis," Ed. O. C. Zienkiewicz and G. S. Hoister, Wiley, 1965.
23. Cornforth, D. H. (1964)  
"Some Experiments on the Influence of Strain Conditions on the

Strength of Sand," Geotechnique, Vol. 14, 1964, pp 143-167.

24. Cornforth, D. H. (1961)  
"Plane Strain Failure Characteristics of a Saturated Sand," Ph.D. Thesis, University of London
25. Desai, C. S., and Abel, J. F. (1972)  
"Introduction to the Finite Element Method," Van Nostrand Reinhold Company.
26. Dezfulian, H. (1969)  
"Seismic Response of Soil Deposits Underlain by Inclined Boundaries," Ph.D. Thesis, Department of Civil Engineering, University of California, Berkeley.
27. Dibaj, M., and Penzien, J. (1967)  
"Dynamic Response of Earth Dams to Traveling Waves," Report No. TE 67-3, Soil Mechanics and Bitumous Material Research, University of California, Berkeley, August 1967.
28. Dibaj, M., and Penzien, J. (1969)  
"Non-Linear Seismic Response of Earth Structures," EERC 69-2, Earthquake Engineering Research Center, University of California, Berkeley, January, 1969.
29. Duke, C. M., and Leeds, D. J. (1963)  
"Response of Soils, Foundations and Earth Structures," Bulletin of the Seismological Society of America, Vol. 53, No. 2, pp 309-357.
30. Drucker, D. C. (1960)  
"Plasticity," Proceedings 1st Symposium Naval Structural Mechanics, pp 407-455.
31. Duns, C. S., and Butterfield, R. (1967)  
"The Dynamic Analysis of Soil-Structure Systems Using the Finite Element Method," Proceedings International Symposium on Wave Propagation and Dynamic Properties of Earth Materials, New Mexico, Aug. 23-25, 1967, pp 59-70.
32. Ewing, W. M., Jardetzky, W. S., and Press, F. (1957)  
"Elastic Waves in Layered Media," McGraw-Hill Book Company, Inc., N. Y.
33. Farhoomand, I., and Wilson, E. (1971)  
"A Non-Linear Finite Element Code for Analyzing the Blast Response of Underground Structures," U.S. Army Engineer Waterways Experiment Station, Contract Report N-71-1, January 1971
34. Farhoomand, I. (1970)  
"Non-Linear Stress Analysis of 2-Dimensional Solids," Ph.D. Thesis, Department of Civil Engineering, University of California, Berkeley, June 1970.



35. Ferguson, P. M. (1973)  
"Reinforced Concrete Fundamentals," 3rd Ed., 1973, John Wiley & Sons, Inc.
36. Finn, W. D. Liam, and Reimer, R. B.  
"Effect of Soil Structure Interaction on Seismic Responses," Soil-Mechanics Series No. 14, Department of Civil Engineering, University of British Columbia.
37. Fleming, J. F., Screwvala, F. N., and Konder, R. L. (1965)  
"Foundation Superstructure Interaction Under Earthquake Motion," Proc. 3rd World Conference of Earthquake Engineering, New Zealand, 1965, pp I-22-30.
38. Gallagher, R. H. (1964)  
"A Correlation Study of Methods of Matrix Structural Analysis," New York, Macmillan.
39. Gerrand, C. M., and Harrison, W. J. (1971)  
"Stresses and Displacements in a Loaded Orthorhombic Half Space," "The Analysis of a Loaded Half Space Comprised of Anisotropic Layers," "Circular Loads Applied To a Cross-Anisotropic Half Space," Division of Applied Geomechanics Technique Paper, No. 8, 9 and 10, Commonwealth Scientific and Industrial Research Organization, Australia.
40. Ghaboussi, J., and Wilson, E. L. (1973)  
"Finite Element for Rock Joints and Interfaces," Journal of the Soil Mechanics and Foundation Division, ASCE, Proc. paper 10095, Vol. 99, No. SM10, Oct. 1973.
41. Goodman, R. E., and Taylor, R. L. (1968)  
"A Model for the Mechanics of Jointed Rock," Journal of the Soil Mechanics and Foundation Division, ASCE, Proc. Paper 5937, Vo. 94, No. SM3, May 1968.
42. Goto, H., and Kaneta, K. (1960)  
"Analysis With an Application to Seismic Design of Bridge Piers," Proceedings, the 2nd World Conference on Earthquake Engineering, Tokyo, Vol. 2, pp 1449-1463.
43. Grant, F. S., and West, G. F.  
"Interpretation Theory in Applied Geophysics," McGraw-Hill, New York, 1964.
44. Hart, G. C., and Collin, J. D. (1972)  
"Study of Modeling of Structural Damping Matrice," Society of Automotive Engineers, Oct. 1972.
45. Harr, M. E. (1966)  
"Foundation of Theoretical Soil Mechanics," McGraw-Hill.

46. Hill, R. (1950)  
"The Mathematical Theory of Plasticity," Oxford.
47. Hudson, D. E. (1965)  
"Equivalent Viscous Friction for Hysteretic Damping Systems With Earthquake-Like Excitation," Proc. 3rd World Conference on Earthquake Engineering, Vol. 2, part II, pp 185-202.
48. Ichihara, M. (1965)  
"Dynamic Earth Pressure Measured by a New Testing Apparatus," Proceedings, 6th International Conference on Soil Mechanics and Foundation Engineering, Montreal, Canada, Sept. 1965, Vol. 2, pp 386-390.
49. Idriss, I. M. (1968)  
"Finite Element Analysis for Seismic Response of Earth Dams," Journal of the Soil Mechanics and Foundation Division, ASCE, Vol. 94, No. SM3.
50. Idriss, I. M. (1968)  
"Response of Earth Banks During Earthquakes," Journal of the Soil Mechanics and Foundation Division, ASCE, Vol. 93, SM4, 1968.
51. Idriss, I. M., and Seed, H. B. (1968)  
"Seismic Response of Horizontal Soil Layers," Journal of the Soil Mechanics and Foundation Division, ASCE, Vol. 94, No. SM4, Proc. Paper, 6043, July, 1968, pp 1003-1031.
52. Ishii, Y., Arai, M., and Tsuchida, H. (1960)  
"Lateral Earthpressure in an Earthquake," Proceedings, 2nd World Conference on Earthquake Engineering, Tokyo, Japan, July 1960, Vol. 1, pp 211-228.
53. Iwasaki, T., Penzien, J., and Clough, R. (1972)  
"Literature Survey - Seismic Effects on Highway Bridges," EERC 71-11, Earthquake Engineering Research Center, University of California, Berkeley, Nov. 1972.
54. Jacobsen, L. S. (1930)  
"Steady Forced Vibration as Influenced by Damping," Transaction, ASME, Vol. 52, Part 1, APM 52-15, pp 169-181.
55. The Japan Society of Civil Engineers (1968)  
"Earthquake Resistant Design for Civil Engineering Structures - Earth Structures and Foundation in Japan."
56. Jennings, P. C. (1967)  
"Forced-Deflection Relations From Dynamic Tests," Journal of the Engineering Mechanics Division, ASCE, Vol. 93, No. EM2, Proc. paper 5199, Apr. 1967, pp 115-129.



57. Jennings, P. C. (1968)  
"Equivalent Viscous Damping for Yielding Structures," Journal of the Engineering Mechanics Division, ASCE, Vol. 94, No. EM1, Feb. 1968, pp 103-116.
58. Jennings, P. C., and Bielak (1972)  
"Dynamics of Building-Soil Interaction," EERL 72-01, California Institute of Technology, Earthquake Engineering Research Laboratory, April 1972.
59. Jennings, P. C., and Wood, J. H. (1971)  
"Earthquake Damage to Freeway Structures," Chapter 6 of "Engineering Features of the San Fernando Earthquake, February 9, 1971," EERL 71-02, California Institute of Technology, Earthquake Engineering Research Laboratory, June 1971.
60. Kanaan, A., and Powell, G. H. (1973)  
"General Purpose Computer Program for Inelastic Dynamic Response of Plane Structures," EERC 73-6, Earthquake Engineering Research Center, University of California, Berkeley.
61. Konder, R. L., and Zelasko, J. S.  
"A Hyperbolic Stress-Strain Formulation for Sands," proc. 2nd American Conference Soil Mechanics Foundation Engineering, Vol. 1, pp 289-324.
62. Khanna, J. (1969)  
"Elastic Soil-Structure Interaction," proc. of the 4th World Conference on Earthquake Engineering, Santiago, Chile, 1969, Vol. 3, pp A 6-143-152.
63. Lambe, T. W., and Whitman, R. V. (1969)  
"Soil Mechanics," John Wiley and Sons, Inc.
64. Lastrico, R. M. (1970)  
"Effects of Site and Propagation Path on Recorded Strong Earthquake Motion," Ph.D. Thesis, University of California, Los Angeles.
65. Lew, H. S., Legendacker, E. V., and Dikkers, R. D. (1971)  
"Damages to Bridges and Highways," Chapter 7 of United States, Department of Commerce, Building Science Series 40, Dec. 1971.
66. Lysmer, J., and Kuhlemeyer, R. L. (1969)  
"Finite Dynamic Model for Infinite Media," Journal of the Engineering Mechanics Division, ASCE, Vol. 95, No. EM4, proc. paper 6719, August 1969, pp 859-877.
67. Lysmer, J., and Duncan, J. M. (1969)  
"Stresses and Deflections in Foundations and Pavements," Department of Civil Engineering, Institute of Transportation and Traffic Engineering, University of California, Berkeley, 4th Ed. 1969.

68. Matsuo, H. (1941)  
"Experimental Studies on the Distribution of Lateral Earthpressure in Earthquake," Journal of the Japan Society of Civil Engineers, Vol. 27, No. 2, 1941.
69. Matsuo, H., and Ohara, S. (1960)  
"Lateral Earthpressure and Stability of Quay Walls During Earthquake," proc. 2nd World Conference on Earthquake Engineering, Tokyo, Japan, Vol. 1, July 1960, pp 165-181.
70. Marcal, P. V. (1965)  
"A Stiffness Method for Elastic-Plastic Problems," International Journal of Mechanics Science, Vol. 7, No. 4, Apr. 1965, pp 229-238.
71. McCormick, J. M., and Salvadori (1964)  
"Numerical Methods in Fortran," Prentice-Hall, Inc., New Jersey.
72. Minami, T. (1972)  
"Elasto-Plastic Earthquake Response of Soil-Building System," Ph.D. Thesis, University of California, 1972.
73. Morris, G. A., and Fenves, S. J. (1967)  
"A General Procedure for the Analysis of Elastic and Plastic Frameworks," Structural Research Series No. 325, Civil Engineering Studies, University of Illinois, Urbana, Illinois, Aug. 1967.
74. Mononobe, N., and Matsuo, H. (1929)  
"On the Determination of Earthpressure During Earthquake," proc., World Engineering Congress, Tokyo, 1929, Vol. IX, paper no. 388, pp 177-186.
75. Nandakaumaran, P., and Prakash, S. (1970)  
"The Problem of Retaining Walls in Seismic Zones," 4th Symposium on Earthquake Engineering, Indian Society of Earthquake Technology, Nov. 1970, pp 307-310.
76. Newmark, N. M. (1959)  
"A Method of Computation for Structural Dynamics," proc. ASCE, Vol. 85, No. EM3, 1959.
77. Nigma N. C. (1970)  
"Yielding in Framed Structures Under Dynamic Loads," Journal of the Engineering Mechanics, ASCE, Vol. 96, No. EM5, Oct. 1970, pp 687-709.
78. Niwa, Shin (1960)  
"An Experimental Study of Oscillating Earth Pressure Acting on a Quay Wall," 2nd World Conference on Earthquake Engineering, Tokyo, 1960, pp 281-296.
79. Ohara, S. (1960)  
"Experimental Studies of Seismic Active and Passive Earthpressure," proc., 3rd Japan Earthquake Engineering Symposium, Tokyo, Nov. 1960.

80. Okabe, S. (1926)  
"General Theory of Earthpressure," Journal of Japanese Society of Civil Engineering.
81. Parmelee, R. A. (1967)  
"Building-Foundation Interaction Effect," proc. ASCE, Vol. 93, No. EM2, Apr. 1967, pp 131-152.
82. Penzien, J. (1970)  
"Soil-Pile Foundation Interaction," "Earthquake Engineering," R. L. Wiegel, Coordinating Editor, Prentice-Hall.
83. Porter, F. L., and Powell, G. H. (1971)  
"Static and Dynamic Analysis of Inelastic Frame Structures," EERC 71-3, Earthquake Engineering Research Center, University of California, Berkeley, 1971.
84. Poulos, H. G. (1971)  
"Behavior of Laterally Load Piles: I - Single Pile, II - Pile Group," Journal of the Soil Mechanics and Foundation Division, ASCE, Vol. 97, No. SM5, proc. paper 8092, May 1971, pp 711-751.
85. Prager, W. (1955)  
"The Theory of Plasticity: A Survey of Recent Achievements," proc. Institute of Mechanical Engineering, Vol. 169, 1955, pp 41-52.
86. Przemieniecki, J. S. (1968)  
"Theory of Matrix Structural Analysis," McGraw-Hill.
87. Radhakrishnan, N., and Reese, L. C. (1970)  
"A Review of Application of Finite Element Method of Analysis to Problems in Soil and Rock Mechanics," Soil and Foundation, Vol. X, No. 3, The Japanese Society and Foundation Engineering, Sept. 1970, pp 95-112.
88. Reddy, A. S., and Valsangkar, A. J. (1970)  
"General Solutions for Laterally Loaded Pile in Elastic-Plastic Soil," Soil and Foundation, The Japanese Society of Soil Mechanics and Foundation Engineering, Vol. X, No. 3, Sept. 1970, pp 66-80.
89. Richart, F. E., Hall, J. R., and Woods, R. D. (1970)  
"Vibration of Soils and Foundations," Prentice-Hall, Inc.
90. Richart, F. E., Jr. (1963)  
"Foundation Vibration," Transaction of ASCE, Vol. 127, 1962, Part 1, pp 863-878.
91. Richart, C. F. (1958)  
"Elementary Seismology," W. F. Freeman and Co.
92. Ross, G. A., Seed, H. B., and Migliaccio, R. (1969)  
"Bridge Foundation Behavior in Alaska Earthquake, Journal of Soil



93. Sarrazin, Mauricio A. (1972)  
"Dynamic Soil-Structure Interaction," Journal of the Structural Division, ASCE, Vol. 98, No. ST7, proc. paper 9026, July 1972, pp 1525-1544.
94. Scholes, A., and Strover (1971)  
"The Piecewise-Linear Analysis of Two Connecting Structures Including the Effects of Clearance at the Connections," International Journal for Numerical Methods in Engineering, Vol. 3, No. 10, 1971, pp 45-52.
95. Seed, H. B., and Idriss, I. M. (1969)  
"The Influence of Soil Conditions on Ground Motions During Earthquakes," Journal of Soil Mechanics and Foundation Division, ASCE, Vol. 95, No. SM1, Jan. 1969.
96. Seed, H. B., and Idriss, I. M. (1969)  
"Soil Modulus and Damping Factors for Dynamic Response Analysis," EERC 70-10, Earthquake Engineering Research Center, University of California, Berkeley, Dec. 1970.
97. Seed, H. B., and Whitman, R. V. (1970)  
"Design of Earth Retaining Structures for Dynamic Loads," Specialty Conference "Lateral Stress in the Ground and Design of Earth-Retaining Structures," Sponsored by Soil Mechanics and Foundation Division, ASCE, Ithaca Section, Cornell University, June 22-24, 1970.
98. Seed, H. B. (1972)  
"Dynamic Characteristics of Soil-Structure System," Conference on Planning and Design of Tall Building, Lehigh University, Aug. 1972.
99. Shackel, B. (1968)  
"Damping Characteristics of Soils," proc. 4th Conference, Australia Road Research Board, Vol. 4, part 2, pp 1126.
100. Shepherd, R., and Charlson, A. W. (1971)  
"Experimental Determination of the Dynamic Properties of a Bridge Structure," Bulletin Seismological Society of America, 1971, Vol. 61(6), pp 1529-1548.
101. Shepherd, R., and Sidwell, G. K. (1973)  
"Investigation of the Dynamic Properties of Fine Concrete Bridges," 4th Australasian Conference on the Mechanics of Structures and Materials, University of Queensland Brisbane, August 1973, pp 261-268.
102. Silver, M., and Seed, H. B. (1969)  
"The Behavior of Sands Under Seismic Loading Conditions," EERC 69-10, Earthquake Engineering Research Center, University of California, Berkeley, Dec. 1969.

103. Taylor, P. W. (1971)  
"The Properties of Soils Under Dynamic Stress Conditions With Applications to the Design of Foundation in Seismic Stress," Ph.D. Thesis, School of Engineering, University of Auckland, Nov. 1971.
104. Tschebotanoff, G. (1949)  
"Large Scale Earthpressure Tests With Model Flexible Bulkheads," Bureau of Yards and Docks, Department of the Navy.
105. Tseng, W. S., and Penzien, J. (1973)  
"Analytic Investigation of the Seismic Response of Long Multiple Span Highway Bridge," EERC 73-12, Earthquake Engineering Research Center, University of California, Berkeley, June 1973.
106. Valera, J. E. (1968)  
"Seismic Interaction of Granular Soils and Rigid Retaining Structures," Ph.D. Thesis, Department of Civil Engineering, University of California, Berkeley.
107. Wen, R. K., and Farhoomand, F. (1970)  
"Dynamic Analysis of Inelastic Space Frames," Journal of the Engineering Mechanics Division, ASCE, Vol. 96, No. EM5, Oct. 1970, pp 667-686.
108. Whitman, R., Roesset, J., and Dobry, R. (1972)  
"Accuracy of Model Superposition for One-Dimensional Soil Amplitude Analysis," Structural Publication, No. 351, Department of Civil Engineering, School of Engineering, Massachusetts Institute of Technology, 1972.
109. Whitman, R. (1972)  
"Dynamic Soil-Structure Interaction," Structural Publication No. 352, Department of Civil Engineering, School of Engineering, Massachusetts Institute of Technology.
110. Whitman, R. V., Miller, E. T., and Moore, P. J. (1964)  
"Yielding and Locking of Confined Sand," Journal of the Soil Mechanics and Foundation Division, ASCE, Vol. 90, No. SM4, proc. paper 3966, July 1964, pp 57-84.
111. White, D. F., and Enderby, L. R. (1970)  
"Finite Element Stress Analysis of a Non-Linear Problem: A Connecting-Rod eye by Means of pin," Journal of Strain Analysis, Vol. 5, No. 1, January 1970, pp 41-48.
112. Wilson, S. D., and Dietrich, R. J. (1960)  
"Effect of Consolidation Pressure on Elastic and Strength Properties of Clay," proc., Research Conference on Shear Strength of Cohesive Soils, ASCE, Boulder, Colorado, 1960.



- 113. Wilson, E. L. (1968)  
"A Computer Program for the Dynamic Stress Analysis of Underground Structure," Report No. 68-1, SESM, Department of Civil Engineering, University of California, Berkeley, Jan. 1968.
- 114. Wilson, E. L. (1969)  
"A Method of Analysis for the Evaluation of Foundation-Structure Interaction," proc. 4th World Conference on Earthquake Engineering, Santiago, Chile, 1969, Vol. 3, pp A 6-87-99.
- 115. Wilson, E. L., and Penzien, J. (1972)  
"Evaluation of Orthogonal Damping Matrices," International Journal for Numerical Method in Engineering, Vol. 4, Jan. 1972, pp 5-10.
- 116. Wilson, E. L., and Clough, R. W. (1962)  
"Dynamic Response by Step-by-Step Matrix Analysis," proc., Symposium on the Use of Computers in Civil Engineering, Lisbon, Portugal, 1962.
- 117. Wood, J. H. (1973)  
"Earthquake-Induced Soil Pressures on Structures," EERL 70-05, Ph.D. Thesis, California Institute of Technology, May 1973.
- 118. Yong, R. N., and McKyes, E. (1971)  
"Yield and Failure of a Clay Under Triaxial Stress," Journal of the Soil Mechanics and Foundation Division, ASCE, Vol. 97, No. SMI, proc. paper 7790, Jan. 1971, pp 159-176.
- 119. Zienkiewicz, O. C. (1971)  
"The Finite Element Method in Engineering Science," McGraw-Hill, Inc.

## APPENDIX

### Computer Program Listings

















```

SUBROUTINE FBECOL (XX,YY,AMASS,NT,FEN)
*****
      CALCULATE THE BEAD LOAD AND F-E-N OF CONCRETE
*****
      DIMENSION XX(2),YY(12)

      LENGTH=BL
      N=NT/2-XX(1)
      MY=YY(2)-YY(1)
      BL=SOAT(HL*0.2+VL*0.2)
      BL=ABS(BL)
      H=ABS(HL)
      FEN=HL*0.2*WT/12.0
      WT=BL*WT/72.0
      AMAS=BL*AMASS/2.0
      FEN=FEN/12.-0.100E+0
      AMAS=AMASS/12000.0
      RETURN
END

```

```

SUBROUTINE ESSEPS1X,YPARASO,PARACO,PARAFR,PARAEK,PARABO,COPROP,
      1,IBC,C,BCL,O1,O2,O3,D4,O5,NUMAT5,NUMATC,
      2,NUMATP,NUMATE,NUMATB,NURGE,NPLAN)
      3
      4
      5
      6
      7
      8
      9
      10
      11
      12
      13
      14
      15
      16
      17
      18
      19
      20
      21
      22
      23
      24
      25
      26
      27
      28
      29
      30
      31
      32
      33
      34
      35
      36
      37
      38
      39
      40
      41
      42
      43
      44
      45
      46
      47
      48
      49
      50
      51
      52
      53
      54
      55
      56
      57
      58
      59
      60
      61
      62
      63
      64
      65
      66
      67
      68
      69
      70
      71
      72
      73
      74
      75
      76
      77
      78
      79
      80
      81
      82
      83
      84
      85
      86
      87
      88
      89
      90
      91
      92
      93
      94
      95
      96
      97
      98
      99
      100
      101
      102
      103
      104
      105
      106
      107
      108
      109
      110
      111
      112
      113
      114
      115
      116
      117
      118
      119
      120
      121
      122
      123
      124
      125
      126
      127
      128
      129
      130
      131
      132
      133
      134
      135
      136
      137
      138
      139
      140
      141
      142
      143
      144
      145
      146
      147
      148
      149
      150
      151
      152
      153
      154
      155
      156
      157
      158
      159
      160
      161
      162
      163
      164
      165
      166
      167
      168
      169
      170
      171
      172
      173
      174
      175
      176
      177
      178
      179
      180
      181
      182
      183
      184
      185
      186
      187
      188
      189
      190
      191
      192
      193
      194
      195
      196
      197
      198
      199
      200
      201
      202
      203
      204
      205
      206
      207
      208
      209
      210
      211
      212
      213
      214
      215
      216
      217
      218
      219
      220
      221
      222
      223
      224
      225
      226
      227
      228
      229
      230
      231
      232
      233
      234
      235
      236
      237
      238
      239
      240
      241
      242
      243
      244
      245
      246
      247
      248
      249
      250
      251
      252
      253
      254
      255
      256
      257
      258
      259
      260
      261
      262
      263
      264
      265
      266
      267
      268
      269
      270
      271
      272
      273
      274
      275
      276
      277
      278
      279
      280
      281
      282
      283
      284
      285
      286
      287
      288
      289
      290
      291
      292
      293
      294
      295
      296
      297
      298
      299
      300
      301
      302
      303
      304
      305
      306
      307
      308
      309
      310
      311
      312
      313
      314
      315
      316
      317
      318
      319
      320
      321
      322
      323
      324
      325
      326
      327
      328
      329
      330
      331
      332
      333
      334
      335
      336
      337
      338
      339
      340
      341
      342
      343
      344
      345
      346
      347
      348
      349
      350
      351
      352
      353
      354
      355
      356
      357
      358
      359
      360
      361
      362
      363
      364
      365
      366
      367
      368
      369
      370
      371
      372
      373
      374
      375
      376
      377
      378
      379
      380
      381
      382
      383
      384
      385
      386
      387
      388
      389
      390
      391
      392
      393
      394
      395
      396
      397
      398
      399
      400
      401
      402
      403
      404
      405
      406
      407
      408
      409
      410
      411
      412
      413
      414
      415
      416
      417
      418
      419
      420
      421
      422
      423
      424
      425
      426
      427
      428
      429
      430
      431
      432
      433
      434
      435
      436
      437
      438
      439
      440
      441
      442
      443
      444
      445
      446
      447
      448
      449
      450
      451
      452
      453
      454
      455
      456
      457
      458
      459
      460
      461
      462
      463
      464
      465
      466
      467
      468
      469
      470
      471
      472
      473
      474
      475
      476
      477
      478
      479
      480
      481
      482
      483
      484
      485
      486
      487
      488
      489
      490
      491
      492
      493
      494
      495
      496
      497
      498
      499
      500
      501
      502
      503
      504
      505
      506
      507
      508
      509
      510
      511
      512
      513
      514
      515
      516
      517
      518
      519
      520
      521
      522
      523
      524
      525
      526
      527
      528
      529
      530
      531
      532
      533
      534
      535
      536
      537
      538
      539
      540
      541
      542
      543
      544
      545
      546
      547
      548
      549
      550
      551
      552
      553
      554
      555
      556
      557
      558
      559
      560
      561
      562
      563
      564
      565
      566
      567
      568
      569
      570
      571
      572
      573
      574
      575
      576
      577
      578
      579
      580
      581
      582
      583
      584
      585
      586
      587
      588
      589
      590
      591
      592
      593
      594
      595
      596
      597
      598
      599
      600
      601
      602
      603
      604
      605
      606
      607
      608
      609
      610
      611
      612
      613
      614
      615
      616
      617
      618
      619
      620
      621
      622
      623
      624
      625
      626
      627
      628
      629
      630
      631
      632
      633
      634
      635
      636
      637
      638
      639
      640
      641
      642
      643
      644
      645
      646
      647
      648
      649
      650
      651
      652
      653
      654
      655
      656
      657
      658
      659
      660
      661
      662
      663
      664
      665
      666
      667
      668
      669
      670
      671
      672
      673
      674
      675
      676
      677
      678
      679
      680
      681
      682
      683
      684
      685
      686
      687
      68
```



```

00 313 I=1,MUMATF
ESGEP5.33
ESGEP5.34
AKN=PARAFR11,I
ESGEP5.35
AKN=PARAFR12,I
0311,I)=AKS/3.0
ESGEP5.36
0312,I)=AKN/3.0
ESGEP5.37
0313,I)=AKS/6.0
ESGEP5.38
0314,I)=AKN/6.0
ESGEP5.39
313 CONTINUE
410 CONTINUE
C
C EXPANSION JOINT NODAL FORCE-DISPLACEMENT RELATIONSHIP IN LOCAL COORDINATE SYSTEM
IFIMUNATF .EQ. 0) GO TO 411
EXPANIMATE .EQ. 0) GO TO 411
ESGEP5.113
ESGEP5.114
AKN=PARAFR11,I
ESGEP5.115
AKN=PARAFR12,I
0311,I)=AKS/3.0
ESGEP5.116
0312,I)=AKN/3.0
ESGEP5.117
0313,I)=AKS/6.0
ESGEP5.118
0314,I)=AKN/6.0
ESGEP5.119
ESGEP5.120
ESGEP5.121
ESGEP5.122
ESGEP5.123
ESGEP5.124
ESGEP5.125
ESGEP5.126
ESGEP5.127
ESGEP5.128
ESGEP5.129
ESGEP5.130
ESGEP5.131
ESGEP5.132
ESGEP5.133
ESGEP5.134
ESGEP5.135
ESGEP5.136
ESGEP5.137
ESGEP5.138
ESGEP5.139
ESGEP5.140
ESGEP5.141
ESGEP5.142
ESGEP5.143
ESGEP5.144
ESGEP5.145
ESGEP5.146
ESGEP5.147
ESGEP5.148
ESGEP5.149
ESGEP5.150
ESGEP5.151
ESGEP5.152
ESGEP5.153
ESGEP5.154
ESGEP5.155
ESGEP5.156
ESGEP5.157
ESGEP5.158
ESGEP5.159
ESGEP5.160
ESGEP5.161
ESGEP5.162
ESGEP5.163
ESGEP5.164
ESGEP5.165
ESGEP5.166
ESGEP5.167
ESGEP5.168
ESGEP5.169
ESGEP5.170
ESGEP5.171
ESGEP5.172
ESGEP5.173
ESGEP5.174
ESGEP5.175
ESGEP5.176
ESGEP5.177
ESGEP5.178
ESGEP5.179
ESGEP5.180
ESGEP5.181
ESGEP5.182
ESGEP5.183
ESGEP5.184
ESGEP5.185
ESGEP5.186
ESGEP5.187
ESGEP5.188
ESGEP5.189
ESGEP5.190
ESGEP5.191
ESGEP5.192
ESGEP5.193

```

```

SUBROUTINE ETSIF(1D,X,Y,PARACO,COPROP,IX,IY,SLV,C,AE,MIND,MUMEL,ETSIF-2
NEO,MAND)
ETSIF-3
C *****
ETSIF-4
C FORM ELASTIC TOTAL STIFFNESS MATRIX AE(MEO,MAND)
ETSIF-5
C *****
ETSIF-6
C *****
ETSIF-7
C *****
ETSIF-8
C *****
ETSIF-9
C *****
ETSIF-10
C *****
ETSIF-11
C *****
ETSIF-12
C *****
ETSIF-13
C *****
ETSIF-14
C *****
ETSIF-15
C *****
ETSIF-16
C *****
ETSIF-17
C *****
ETSIF-18
C *****
ETSIF-19
C *****
ETSIF-20
C *****
ETSIF-21
C *****
ETSIF-22
C *****
ETSIF-23
C *****
ETSIF-24
C *****
ETSIF-25
C *****
ETSIF-26
C *****
ETSIF-27
C *****
ETSIF-28
C *****
ETSIF-29
C *****
ETSIF-30
C *****
ETSIF-31
C *****
ETSIF-32
C *****
ETSIF-33
C *****
ETSIF-34
C *****
ETSIF-35
C *****
ETSIF-36
C *****
ETSIF-37
C *****
ETSIF-38
C *****
ETSIF-39
C *****
ETSIF-40
C *****
ETSIF-41
C *****
ETSIF-42
C *****
ETSIF-43
C *****
ETSIF-44
C *****
ETSIF-45
C *****
ETSIF-46
C *****
ETSIF-47
C *****
ETSIF-48
C *****
ETSIF-49
C *****
ETSIF-50
C *****
ETSIF-51
C *****
ETSIF-52
C *****
ETSIF-53
C *****
ETSIF-54
C *****
ETSIF-55
C *****
ETSIF-56
C *****
ETSIF-57
C *****
ETSIF-58
C *****
ETSIF-59
C *****
ETSIF-60
C *****
ETSIF-61
C *****
ETSIF-62
C *****
ETSIF-63
C *****
ETSIF-64
C *****
ETSIF-65
C *****
ETSIF-66
C *****
ETSIF-67
C *****
ETSIF-68
C *****
ETSIF-69
C *****
ETSIF-70
C *****
ETSIF-71
C *****
ETSIF-72
C *****
ETSIF-73
C *****
ETSIF-74
C *****
ETSIF-75
C *****
ETSIF-76
C *****
ETSIF-77
C *****
ETSIF-78
C *****

```

```

SUBROUTINE ETSIF(1D,X,Y,PARACO,COPROP,IX,IY,SLV,C,AE,MIND,MUMEL,ETSIF-2
NEO,MAND)
ETSIF-3
C *****
ETSIF-4
C FORM ELASTIC TOTAL STIFFNESS MATRIX AE(MEO,MAND)
ETSIF-5
C *****
ETSIF-6
C *****
ETSIF-7
C *****
ETSIF-8
C *****
ETSIF-9
C *****
ETSIF-10
C *****
ETSIF-11
C *****
ETSIF-12
C *****
ETSIF-13
C *****
ETSIF-14
C *****
ETSIF-15
C *****
ETSIF-16
C *****
ETSIF-17
C *****
ETSIF-18
C *****
ETSIF-19
C *****
ETSIF-20
C *****
ETSIF-21
C *****
ETSIF-22
C *****
ETSIF-23
C *****
ETSIF-24
C *****
ETSIF-25
C *****
ETSIF-26
C *****
ETSIF-27
C *****
ETSIF-28
C *****
ETSIF-29
C *****
ETSIF-30
C *****
ETSIF-31
C *****
ETSIF-32
C *****
ETSIF-33
C *****
ETSIF-34
C *****
ETSIF-35
C *****
ETSIF-36
C *****
ETSIF-37
C *****
ETSIF-38
C *****
ETSIF-39
C *****
ETSIF-40
C *****
ETSIF-41
C *****
ETSIF-42
C *****
ETSIF-43
C *****
ETSIF-44
C *****
ETSIF-45
C *****
ETSIF-46
C *****
ETSIF-47
C *****
ETSIF-48
C *****
ETSIF-49
C *****
ETSIF-50
C *****
ETSIF-51
C *****
ETSIF-52
C *****
ETSIF-53
C *****
ETSIF-54
C *****
ETSIF-55
C *****
ETSIF-56
C *****
ETSIF-57
C *****
ETSIF-58
C *****
ETSIF-59
C *****
ETSIF-60
C *****
ETSIF-61
C *****
ETSIF-62
C *****
ETSIF-63
C *****
ETSIF-64
C *****
ETSIF-65
C *****
ETSIF-66
C *****
ETSIF-67
C *****
ETSIF-68
C *****
ETSIF-69
C *****
ETSIF-70
C *****
ETSIF-71
C *****
ETSIF-72
C *****
ETSIF-73
C *****
ETSIF-74
C *****
ETSIF-75
C *****
ETSIF-76
C *****
ETSIF-77
C *****
ETSIF-78
C *****

```

[illegible]







```

306 KO=MD/ID
      IF(NHEAD .EQ. 1) GO TO 413
C
C      FIXED END FORCE AF(6) IN GLOBAL COORDINATE
DD 331 LA=1,4,3
LB=LA-1
DD 331 IL=1,3
I=IL+1
XA=0,0
DO 332 K=1,3
  332 XA=AF(I,IL)+SF(K*4,0)
  331 REFI=XA
413 CONTINUE
C
C      OBTAIN SA(6,6) RELATING ELEMENT END FORCES(LOCAL) TO
      JOINT DISPLACEMENT(GLOBAL)
DD 311 I=1,64
  311 SA(I)=0,0
  311 CONTINUE
      DO 312 LA=1,4,3
        LB=LA+2
        DO 312 MA=1,4,3
          MB=MA-1
          DO 312 I=LA,LB
            DO 312 JM=1,3
              312 XA=0,0
              DO 313 K=1,3
                313 XA=SA(I,K*4)+OT(K,JM)
                312 SA(I,J)=XA
              314 ASAT(I)=0,0
              DO 315 LA=1,4,3
                LB=LA-1
                DO 315 MA=1,4,3
                  MB=MA+2
                  DO 315 IL=1,3
                    I=IL+1
                    DO 315 J=MA,MB
                      XA=0,0
                      DO 316 K=1,3
                        316 XA=ASAT(I,K)+SA(K*4,0,J)
                        315 CONTINUE
                        315 IF(NHEAD .EQ. 1) GO TO 410
                        MD=6
                        WRITE(1) MD,MS,(LM(I),I=1,MD),((SL(I,J),I=1,MS),J=1,MD),
                          1 ((SA(I,J),I=1,MS),J=1,MD),
                          2 ((SF(I),I=1,MD))
                        GO TO 421
                      410 CONTINUE
                      WRITE NON-LINEAR INFORMATION ON TAPE 41
                      DO 310 I=1,6
                        DO 310 J=1,6
                          310 SA(I,J)=SA(I,J)-SA(I,J)
                      310 CONTINUE
                      WRITE(4) MD,MS,(LM(I),I=1,MD),((SL(I,J),I=1,MS),J=1,MD),
                        1 ((SA(I,J),I=1,MS),J=1,MD),
                        2 ((SF(I),I=1,MD))
                      421 RETURN
                    END
306 CONTINUE
307 SA(I,J)=XA
306 CONTINUE
CONCTS.135
CONCTS.136
CONCTS.137
CONCTS.138
CONCTS.139
CONCTS.140
CONCTS.141
CONCTS.142
CONCTS.143
CONCTS.144
CONCTS.145
CONCTS.146
CONCTS.147
CONCTS.148
CONCTS.149
CONCTS.150
CONCTS.151
CONCTS.152
CONCTS.153
CONCTS.154
CONCTS.155
CONCTS.156
CONCTS.157
CONCTS.158
CONCTS.159
CONCTS.160
CONCTS.161
CONCTS.162
CONCTS.163
CONCTS.164
CONCTS.165
CONCTS.166
CONCTS.167
CONCTS.168
CONCTS.169
CONCTS.170
CONCTS.171
CONCTS.172
CONCTS.173
CONCTS.174
CONCTS.175
CONCTS.176
CONCTS.177
CONCTS.178
CONCTS.179
CONCTS.180
CONCTS.181
CONCTS.182
CONCTS.183
CONCTS.184
CONCTS.185
CONCTS.186
CONCTS.187
CONCTS.188
CONCTS.189
CONCTS.190
CONCTS.191
CONCTS.192
CONCTS.193
CONCTS.194
CONCTS.195
CONCTS.196
CONCTS.197
CONCTS.198
CONCTS.199
SURROUTINE FRIC(SXX,VY,C)
C
C      *****
C      FDEM FRICTIONAL ELEMENT STIFFNESS MATRIX AND STORE ON TAPE 1
C      *****
C      DIMENSION XX(4),VY(4),C(5),S(0,0),SA(0,0),T(2,2)
COMMON/EN/LM(0),ASA(0,0)
COMMON/MD/L/READ
COMMON/TIME/JUMP,0,DT,NPRM,NTAPE,KPRINT
COMMON/ELASTC/SEA(0,0)
C
C      INITIALIZATION
DO 301 I=1,64
  301 S(I)=0,0
DO 301 J=1,64
  301 CONTINUE
C
C      FDEM ELEMENT STIFFNESS IN LOCAL COORDS--S(0,0)
S(1,1)=C(1)
S(1,3)=C(3)
S(2,2)=C(2)
S(2,4)=C(4)
S(3,3)=S(1,1)
S(4,4)=S(2,2)
S(1,3)=-S(1,3)
S(1,7)=-S(1,1)
S(2,6)=-S(2,4)
S(2,8)=-S(1,1)
S(3,7)=-S(1,3)
S(4,6)=-S(2,3)
S(4,8)=-S(2,4)
DO 303 J=1,4
  303 S(I*4,J*4)=S(I,J)
DO 304 I=2,8
  K=1-1
  DO 304 J=1,K
    S(I-J)=S(J,1)
  304 CONTINUE
C
C      FORM TRANSFORMATION MATRIX T(2,2)
DM=X(2)-X(1)
DM=X(2)-X(1)
CASE OF HORIZONTAL FRICTION ELEMENT
IF(DX.NE.0,0 .OR. DY.NE.0,0) GO TO 421
DY=VY(4)-VY(1)
421 CONTINUE
OL=SQRT(DM**2+DY**2)
C
C      STIFFNESS FOR TOTAL LENGTH L,K/INCH
DO 351 I=1,8
  DO 351 J=1,8
    S(I-J)=S(I,J)*OL*12,0
  351 CONTINUE
T(1,1)=OX/OL
T(1,2)=OY/OL
T(2,2)=T(1,1)
T(2,1)=-T(1,2)
C
C      FORM SA(0,0) RELATING ELEMENT END FORCES(LOCAL) TO
      JOINT DISPLACEMENT(GLOBAL)
DO 305 I=1,64
  305 SA(I)=0,0
DO 306 LA=1,2
  LB=LA+1
  DO 306 MA=1,7,2
    MB=MA-1
    DO 306 I=LA,LB
      DO 306 JM=1,2
        306 XA=0,0
        DO 307 K=1,2
          307 XA=SA(I,K*4)+OT(K,JM)
        306 CONTINUE

```

```
C      SUBROUTINE STATIC(SLV,AE,U,V,ACC,DU,OY,DA,NEQ,MHAND)
C      .....
C      .....
C      .....
C      SOLUTION OF STATIC CASE--DISPLACEMENT AT NODES
C      .....
C      .....
C      DIMENSION SLV(1),U(1),V(1),ACC(1),DU(1),OY(1),DA(1),AE(MEQ,1)
C      COMMON/TIME/JUMP,T,DT,NPRTN,MTEPE,KPRINT
C      .....
C      INITIALIZATION
C      DO 351 I=1,NEQ
C      V(I)=0.0
C      ACC(I)=0.0
C      DU(I)=0.0
C      DV(I)=0.0
C      DA(I)=0.0
C      351 CONTINUE
C      JUMP=0
C      NPRTN=0
C      KPRINT=0
C      T=0.0
C      REMIND 3 ((AE(I,J),I=1,NEQ),J=1,MHAND)
C      READ(3) 1,(AE(I,J),I=1,NEQ)
C      IF(CELL.IE.-O.) U(1)=SLV(1)
C      301 CONTINUE
C      CALL TOTAL(AE,MEO,MHAND)
C      CALL BACKS(AE,U,NEQ,MHAND)
C      DO 302 I=1,NEQ
C      DU(I)=U(I)
C      302 CONTINUE
C      RETURN
C      END
```

```

SUBROUTINE TRIA(A,NEG,IBAND)
C.....
C      TRIA-2
C      TRIA-3
C      TRIA-4
C      TRIA-5
C      TRIA-6
C      TRIA-7
C      TRIA-8
C      TRIA-9
C      TRIA-10
C      TRIA-11
C      TRIA-12
C      TRIA-13
C      TRIA-14
C      TRIA-15
C      TRIA-16
C      TRIA-17
C      TRIA-18
C      TRIA-19
C      TRIA-20
C      TRIA-21
C      TRIA-22
C      TRIA-23
C      TRIA-24
C      TRIA-25
C      TRIA-26
C      TRIA-27
C      TRIA-28
C      TRIA-29
C      TRIA-30
C      TRIA-31
C.....
C      TRIANGULIZE STIFFNESS MATRIX A OF AI=8
C.....
DIMENSION A(11)
NE=NEG-1
NM=IBAND-1
MM=NM-NEG
NN=NM-NEG
DO 301 I=1,NM
  DO 301 J=1,NE
    NT=N-NK
    IF (NT -GT-. 0) NM=NM-NEG
    IF (A(I) -EQ. 0.0) GO TO 301
    L=N
    IL=N+MEQ
    IH=N+NN
    DO 302 I=IL,IH,NEQ
      L=L+1
      C=A(I)/AIN
      CA=1/C
      ALJ=A(J)-CA*(K)
      J=J-NEQ
      A(I)=C
    302 CONTINUE
    301 RETURN
END
```











```

SUBROUTINE PRINTA(ID,IX,U,V,ACC,TEPS,PEPS,SIG,PSIG,MFX,YBAR,MFY,
1 MPASS,NIND,HSIG,MTH,MUMELE)
C
C *****
C PRINT THE CALCULATED RESULTS AND STORE ON TAPE 2 FOR PLOTTING
C *****
C
C COMMON/NATER/MUNATS,MUMATC,MUMATF,MUMATE,MUNATB,MUMGE,NINTCV,THICKPRINTA,9
1,NPLAN
C
C COMMON/ELPAR/MUNMP,MUNEI,NEQ,NBAND,KLIN
C
C COMMON/ABST/UGAT,UGYT,VGAT,VGYT,DACCX,DACCY
C
C DIMENSION ID(3,1),IX(6,1),U(1),V(1),ACC(1),TEPS(3,1),PEPS(3,1),
1 SIG(6,1),PSIG(6,1),MPASS(1),NIND(1),MFX(1),MFX(1),YBAR(1),
2 YBAR(1),MTH(1),MTH(1),MUM(1)
C
C COMMON/SPECIAL/ISTOP
C
C DIMENSION HSIG(9,MUMELE)
C
C
C DETERMINE TO BE PRINT OR NOT
C
C IF(JUMP .EQ. 1) KPRINT=NPRINT
C
C IF(JUMP .EQ. 1) GO TO 401
C
C IF(ISTOP .EQ. 1) GO TO 401
C
C IF(JUMP .NE. KPRINT) GO TO 411
C
C ISTOP=2
C
C KPRINT=NPRINT-NPRINT
C
C STATIC RESULT
C
C IF(JUMP .NE. 0) GO TO 401
C
C DO 391 I=1,MUMEL
C
C MPASS(I)=0
C
C 391 NIND(I)=0
C
C DO 392 I=1,MUMEL
C
C DO 393 I=1,9
C
C HSIG(I,M)=0.0
C
C 392 CONTINUE
C
C WRITE(6,501)
C
C GO TO 402
C
C 401 CONTINUE
C
C WRITE(6,502)
C
C 402 CONTINUE
C
C
C MODAL POINT DISPLACEMENT,VELOCITY,ACCELERATION
C
C WRITE(6,503)
C
C WRITE(6,101) JUMP,T
C
C
C GROUND DISPLACEMENT,VELOCITY,ACCELERATION
C
C IF(JUMP .EQ. 0) GO TO 405
C
C WRITE(6,104) UGAT,UGYT,VGAT,VGYT,DACCX,DACCY
C
C 405 CONTINUE
C
C DO 301 I=1,MUMMP
C
C DO 302 I=1,9
C
C DO 303 I=1,3
C
C M=ID(I,M)
C
C IF(M .EQ. 0) GO TO 303
C
C D(I)=U(I)
C
C D(I+3)=V(I)
C
C D(I+6)=ACC(I)
C
C 303 CONTINUE
C
C WRITE(6,102) N, ID(I),I-1,9)
C
C 301 CONTINUE
C
C
C STRESS-STRAIN AT CENTER OF SDIL ELEMENT
C
C WRITE(6,504)
C
C 411 CONTINUE
C
C DO 304 N=1,MUMEL
C
C NTYPE=IX(5,N)
C
C IF(NTYPE .NE. 1) GO TO 304
C
C DO 305 I=1,9
C
C D(I)=0.0
C
C DO 306 J=1,3
C
C HSIG(I,M)=SIG(I,M)
C
C O(I)=SIG(I,M)
C
C O(I+3)=TEPS(I,M)
C
C O(I+6)=PEPS(I,M)
C
C 306 CONTINUE
C
C HSIG(9,M)=FLOAT(MPASS(N))
C
C IF(ISTOP .EQ. 1 .OR. JUMP .EQ. 1) GO TO 416

```

```

WFORCE=00
WFORCE=01
WFORCE=02
WFORCE=03
WFORCE=04
WFORCE=05
WFORCE=06
WFORCE=07
WFORCE=08
WFORCE=09
WFORCE=10
WFORCE=11
WFORCE=12
WFORCE=13
WFORCE=14
WFORCE=15
WFORCE=16
WFORCE=17
WFORCE=18
WFORCE=19
WFORCE=20
WFORCE=21
WFORCE=22
WFORCE=23
WFORCE=24
WFORCE=25
WFORCE=26
WFORCE=27
WFORCE=28
WFORCE=29
WFORCE=30
WFORCE=31
WFORCE=32
WFORCE=33
WFORCE=34
WFORCE=35
WFORCE=36
WFORCE=37
WFORCE=38
WFORCE=39
WFORCE=40
WFORCE=41
WFORCE=42
WFORCE=43
WFORCE=44
WFORCE=45
WFORCE=46
WFORCE=47
WFORCE=48
WFORCE=49
WFORCE=50
WFORCE=51
WFORCE=52
WFORCE=53
WFORCE=54
WFORCE=55
WFORCE=56
WFORCE=57
WFORCE=58
WFORCE=59
WFORCE=60
WFORCE=61
WFORCE=62
WFORCE=63
WFORCE=64
WFORCE=65
WFORCE=66
WFORCE=67
WFORCE=68
WFORCE=69
WFORCE=70
WFORCE=71
WFORCE=72
WFORCE=73
WFORCE=74
WFORCE=75
WFORCE=76
WFORCE=77
WFORCE=78
WFORCE=79
WFORCE=80
WFORCE=81
WFORCE=82
WFORCE=83
WFORCE=84
WFORCE=85
WFORCE=86
WFORCE=87
WFORCE=88
WFORCE=89
WFORCE=90
WFORCE=91
WFORCE=92
WFORCE=93
WFORCE=94
WFORCE=95
WFORCE=96
WFORCE=97
WFORCE=98
WFORCE=99
WFORCE=100
WFORCE=101
WFORCE=102
WFORCE=103
WFORCE=104
WFORCE=105
WFORCE=106
WFORCE=107
WFORCE=108
WFORCE=109
WFORCE=110
WFORCE=111
WFORCE=112
WFORCE=113
WFORCE=114
WFORCE=115
WFORCE=116
WFORCE=117
WFORCE=118
WFORCE=119
WFORCE=120
WFORCE=121
WFORCE=122
WFORCE=123
WFORCE=124
WFORCE=125
WFORCE=126

```

```

IFLISTOP .NE. 2) GO TO 304
416 CONTINUE
WRITE(6,102) N,(O(1),I=1,9)
304 CONTINUE
IFLISTOP .EQ. 1 .OR. JUMP .EQ. 1) GO TO 417
IFLISTOP .NE. 2) GO TO 412
417 CONTINUE
WRITE(6,509)
DO 321 N=1,MUDEL
  NTYPE=IX(5,N)
  IF(NTYPE .NE. 1) GO TO 321
  WRITE(6,105) N,(PSIG(I),I=1,4),MPASS(N)
  CONTINUE
412 CONTINUE
IFNUMATC .EQ. 0) GO TO 406
IFLISTOP .EQ. 1 .OR. JUMP .EQ. 1) GO TO 418
IFLISTOP .NE. 2) GO TO 413
418 CONTINUE
C
C      END FORCES OF BEAM COLUMN
C      WRITE(6,505)
413 CONTINUE
DO 307 M=1,MUDEL
  NTYPE=IX(5,M)
  IF(NTYPE .NE. 2) GO TO 307
  DO 353 I=1,6
    HSG(I,M)=SIG(I,M)
  CONTINUE
353 CONTINUE
I=FLOAT(MIND(N))
DO 308 I=1,4
  O(1)=0
  O(11)=SIG(1,M)
  O(2)=SIG(2,M)
  O(3)=SIG(3,M)
  O(4)=SIG(4,M)
  IFLISTOP .EQ. 1 .OR. JUMP .EQ. 1) GO TO 419
  IFLISTOP .NE. 2) GO TO 307
419 CONTINUE
WRITE(6,102) N,(O(1),I=1,4),HSG(I,M)
307 CONTINUE
406 CONTINUE
IFNUMATF .EQ. 0 .AND. MUMATE .EQ. 0) GO TO 407
IFLISTOP .EQ. 1 .OR. JUMP .EQ. 1) GO TO 420
IFLISTOP .NE. 2) GO TO 414
420 CONTINUE
C
C      MODAL FORCE AT FRICTIONAL AND EXPANSION JOINT ELEMENT
C      CONTINUE
414 CONTINUE
DO 350 N=1,MUDEL
  NTYPE=IX(5,N)
  IF(NTYPE .NE. 3 .AND. NTYPE .NE. 4) GO TO 350
  N1=IX(1,N)
  N2=IX(2,N)
  N3=IX(3,N)
  M4=IX(4,N)
  DO 309 I=1,8
    O(1)=0
    DO 310 I=1,8
      HSG(I,M)=SIG(I,M)
    CONTINUE
310 O(11)=SIG(1,M)
HSG(9,M)=FLOAT(MIND(N))
IFLISTOP .EQ. 1 .OR. JUMP .EQ. 1) GO TO 421
IFLISTOP .NE. 2) GO TO 350
421 CONTINUE
WRITE(6,103) N,M1,M2,M3,M4,(O(1),I=1,8)
350 CONTINUE
407 CONTINUE
IFNUMATB .EQ. 0) GO TO 408
IFLISTOP .EQ. 1 .OR. JUMP .EQ. 1) GO TO 422
IFLISTOP .NE. 2) GO TO 415
422 CONTINUE
C
C      AXIAL FORCE AT BOUNDARY SPRING
C      WRITE(6,507)
415 CONTINUE
DO 311 N=1,MUDEL

```

```

PRINTR,80
PRINTR,81
PRINTR,82
PRINTR,83
PRINTR,84
PRINTR,85
PRINTR,86
PRINTR,87
PRINTR,88
PRINTR,89
PRINTR,90
PRINTR,91
PRINTR,92
PRINTR,93
PRINTR,94
PRINTR,95
PRINTR,96
PRINTR,97
PRINTR,98
PRINTR,99
PRINTR,100
PRINTR,101
PRINTR,102
PRINTR,103
PRINTR,104
PRINTR,105
PRINTR,106
PRINTR,107
PRINTR,108
PRINTR,109
PRINTR,110
PRINTR,111
PRINTR,112
PRINTR,113
PRINTR,114
PRINTR,115
PRINTR,116
PRINTR,117
PRINTR,118
PRINTR,119
PRINTR,120
PRINTR,121
PRINTR,122
PRINTR,123
PRINTR,124
PRINTR,125
PRINTR,126
PRINTR,127
PRINTR,128
PRINTR,129
PRINTR,130
PRINTR,131
PRINTR,132
PRINTR,133
PRINTR,134
PRINTR,135
PRINTR,136
PRINTR,137
PRINTR,138
PRINTR,139
PRINTR,140
PRINTR,141
PRINTR,142
PRINTR,143
PRINTR,144
PRINTR,145
PRINTR,146
PRINTR,147
PRINTR,148
PRINTR,149
PRINTR,150
PRINTR,151
PRINTR,152
PRINTR,153
PRINTR,154
PRINTR,155
PRINTR,156
PRINTR,157
PRINTR,158
PRINTR,159
PRINTR,160
PRINTR,161
PRINTR,162
PRINTR,163
PRINTR,164
PRINTR,165
PRINTR,166
PRINTR,167
PRINTR,168
PRINTR,169
PRINTR,170
PRINTR,171
PRINTR,172
PRINTR,173
PRINTR,174
PRINTR,175
PRINTR,176
PRINTR,177
PRINTR,178
PRINTR,179
PRINTR,180
PRINTR,181
PRINTR,182
PRINTR,183
PRINTR,184
PRINTR,185
PRINTR,186
PRINTR,187
PRINTR,188
PRINTR,189
PRINTR,190
PRINTR,191
PRINTR,192
PRINTR,193
PRINTR,194
PRINTR,195
PRINTR,196
PRINTR,197
PRINTR,198
PRINTR,199
PRINTR,200
PRINTR,201
PRINTR,202
PRINTR,203
PRINTR,204
PRINTR,205
PRINTR,206
PRINTR,207
PRINTR,208
PRINTR,209
PRINTR,210
PRINTR,211
PRINTR,212
PRINTR,213
PRINTR,214
PRINTR,215
PRINTR,216
PRINTR,217
PRINTR,218
PRINTR,219
PRINTR,220
PRINTR,221
PRINTR,222
PRINTR,223
PRINTR,224

```











```

SOILNE.79      ARZ=K25(2*1-1)
SOILNE.80      GO TO 410
SOILNE.81      AK2=(K25(2*1-1)+K25(2*1+1))/2.0
SOILNE.82      409 AK2=(K25(2*1-1)+K25(2*1+1))/2.0
SOILNE.83      410 CONTINUE
C
C
C      MODIFIED ELASTIC STIFFNESS IN KSI
C      GS=AK2*2.638*SIGNE
C      GS=G1-GS
C      MIND=2
C      RETURN
451 CONTINUE
      CALL PSOILLOSIG,SIG,PSIG,SY,GS,AMU,C,PHI,MIND)
      IF(MIND.EQ. 1) GO TO 406
      IF(MIND.EQ. 0) GO TO 406
      RETURN
406 CONTINUE
C
C      CHECK IF IT IS ACTIVE OR PASSIVE FAILURE,MPASS=1 ACTIVE FAILURE,
C      MPASS=2 PASSIVE FAILURE
C      MPASS=0 ELASTIC
C      IF(MIND.EQ. 0) RETURN
C      SIG=(SIG(1)+SIG(2))/2.0
C      SIGM=(SIG(1)+SIG(2))/2.0
C      IF(SIGN .GE. SIGSMIN) MPASS=1
C      IF(SIGN .LT. SIGSMIN) MPASS=2
C      RETURN
C      BILINEAR WITH COULOMB-HOHR NO HARDENING
C      *****
C      407 CONTINUE
C      CALL PSOILLOSIG,SIG,PSIG,SY,GS,AMU,C,PHI,MIND)
C      IF(MIND.EQ. 1) GO TO 411
C      IF(MIND.EQ. 0) GO TO 411
C      RETURN
411 CONTINUE
C      CHECK IF IT IS ACTIVE OR PASSIVE YIELD
C
C      SIGM=(SIG(1)+SIG(2))/2.0
C      IF(SIGN .GE. SIGSMIN) MPASS=1
C      IF(SIGN .LT. SIGSMIN) MPASS=2
C      RETURN
C      *****
C      C      SHEAR STRAIN CONTROL-SHEAR BEAM ONLY
C      *****
C      408 CONTINUE
C      GANMA=TEPS(3)
C      CALCULATE UPPER LIMIT AND LOWER LIMIT LINES
C      TAU=GANMA*(G1-G2)+G2*GANMAX
C      TAU=GANMA*(G2-G1)+G2*GANMAX
C      ELASTIC CASE
C      IF(SIG(3) .LT. TAU .AND. SIG(3) .GT. TAU) RETURN
C
C      CHECK LOADING OR UNLOADING WHEN YIELDING
C      PSSIG(3)=SIG(3)+DEPS(3)*G1
C      UNLOADING FROM YIELDING-ELASTIC CASE
C      IF(PSSIG(3) .LT. TAU .AND. PSSIG(3) .GT. TAU) RETURN
C
C      PLANE STRAIN FOR SHEAR BEAM ANALYSIS
C      IF(G2 .EQ. 0.0) G2=G1/100000000.0
C      GP=G1-G2
C      DO 452 I=1,6
C      SY(I)=2.0*(1.0-AMU)*GP/(1.0-2.0*AMU)
C      SY(1,21)=2.0*AMU*GP/(1.0-2.0*AMU)
C      SY(3,3)=GP
C      SY(2,21)=SY(1,1)
C      SY(2,11)=SY(1,2)
C      MIND=1
C      RETURN
C      END

```

```

SUBROUTINE PSOILLOSIG,SIG,PSIG,SY,GS,AMU,C,PHI,MIND)
*****
      FORN PLASTIC STRESS-STRAIN RELATIONSHIP-SY(LOCAL)
*****
PSOIL.2
PSOIL.3
*****
PSOIL.4
PSOIL.5
PSOIL.6
PSOIL.7
PSOIL.8
PSOIL.9
PSOIL.10
PSOIL.11
PSOIL.12
PSOIL.13
PSOIL.14
PSOIL.15
PSOIL.16
PSOIL.17
PSOIL.18
PSOIL.19
PSOIL.20
PSOIL.21
PSOIL.22
PSOIL.23
PSOIL.24
PSOIL.25
PSOIL.26
PSOIL.27
PSOIL.28
PSOIL.29
PSOIL.30
PSOIL.31
PSOIL.32
PSOIL.33
PSOIL.34
PSOIL.35
PSOIL.36
PSOIL.37
PSOIL.38
PSOIL.39
PSOIL.40
PSOIL.41
PSOIL.42
PSOIL.43
PSOIL.44
PSOIL.45
PSOIL.46
PSOIL.47
PSOIL.48
PSOIL.49
PSOIL.50

```



[illegible]



```

SUBROUTINE PFRCT(PARAFR,SA,DTU,P,C,NIND)
PRCTT-2
PRCTT-3
PRCTT-4
PRCTT-5
PRCTT-6
PRCTT-7
PRCTT-8
PRCTT-9
PRCTT-10
PRCTT-11
PRCTT-12
PRCTT-13
PRCTT-14
PRCTT-15
PRCTT-16
PRCTT-17
PRCTT-18
PRCTT-19
PRCTT-20
PRCTT-21
PRCTT-22
PRCTT-23
PRCTT-24
PRCTT-25
PRCTT-26
PRCTT-27
PRCTT-28
PRCTT-29
PRCTT-30
PRCTT-31
PRCTT-32
PRCTT-33
PRCTT-34
PRCTT-35
PRCTT-36
PRCTT-37
PRCTT-38
PRCTT-39
PRCTT-40
PRCTT-41
PRCTT-42
PRCTT-43
PRCTT-44
PRCTT-45
PRCTT-46

CHECK IF THE FRICTIONAL ELEMENT IS YIELD AND THEN FORM THE YIELD
STRESS-STRAIN CONSTANTS---CYI4(CI4)
.....

DIMENSION PARAFR(4),SAB(8),DTUIB(8),FI(8),CI4I,DFIBI
COMMON/TIME/JUMP,T-DT,MATN,MTAPE,PRINT

SET LINEAR INDICATOR---NIND
NIND=0
AKS=PARAFR(1)
AKM=PARAFR(2)

CALCULATE APPARENT ELASTIC INCREMENTAL END FORCES--DFIBI
DO 301 I=1,8
XA=0.-0
DO 302 J=1,8
XA=XAS+SAII,J*(DTUI/J)
302 CONTINUE
DFII(XA)
301 CONTINUE

AVERAGE APPARENT STRESS AT CENTER OF ELEMENT
SIGMNZ=0.,SOFI(1)=DFI(1)/COF(1)
SIGCS12=0.,SOFI(2)=DFI(2)/COF(2)
SIGCS13=0.,SOFI(3)=DFI(3)/COF(3)
SIGCS34=0.,SOFI(4)=DFI(4)/COF(4)
IF(SIGN12<.GT..0.0.AND.SIGN34<-.LT..0.0) GO TO 401

TENSION CASE
CI11(AKS/3./0.-AKM/1000000.,D
CI21(-AKN/3./0.-AKN/1000000.,D
CI31(AKS/6./0.-AKS/1000000.,D
CI41(-AKN/6./0.-AKN/1000000.,D
NIND=2
GO TO 402
401 CONTINUE

COMPRESSION,ELASTIC CASE
FU=PARAFR(3)
SHEAR=0.,S(IABS(SIGCS12)+ABS(SIGCS34))
STREG=FU*0.,S(IABS(SIGMNZ)+ABS(SIGNS34))
(IF$HEAR<-.LT..STREG) RETURN

```

-153-







-156-



```

7  * TIME INTERVAL FOR TAPE WRITING/DT *.11D//
8  * TIME OF FIRST PRINT OUT/DT *.11D//)
103 FORMAT(1, DAMPING RATIO 1ST MODE
1  *.F1D.6/
2  *.DAMPING RATIO 2ND MODE
3  *.F1D.6/
4  *.CONSTANT OR LINEAR ACCELERATION*.11D//)
104 FORMAT(1, INPUT EARTHQUAKE*(19F7.4))
105 FORMAT(1, TWO CONTROL FREQ FOR DAMP,OMEGA1,OMEGA2*(2E12.4))
END

SUBROUTINE MODES(INEQ,NBAND,NBLOCK,NF,NTOT,N1B)
MODES-2 .....
MODES-3 .....
MODES-4 .....
MODES-5 .....
MODES-6 .....
MODES-7 .....
MODES-8 .....
MODES-9 .....
MODES-10 .....
MODES-11 .....
MODES-12 .....
MODES-13 .....
MODES-14 .....
MODES-15 .....
MODES-16 .....
MODES-17 .....
MODES-18 .....
MODES-19 .....
MODES-20 .....
MODES-21 .....
MODES-22 .....
MODES-23 .....
MODES-24 .....
MODES-25 .....
MODES-26 .....
MODES-27 .....
MODES-28 .....
MODES-29 .....
MODES-30 .....
MODES-31 .....
MODES-32 .....
MODES-33 .....
MODES-34 .....
MODES-35 .....
MODES-36 .....
MODES-37 .....
MODES-38 .....
MODES-39 .....
MODES-40 .....
MODES-41 .....
MODES-42 .....
MODES-43 .....
MODES-44 .....
MODES-45 .....

COMMON A135500)
COMMON/DMEGA/OMEGA1,OMEGA2,NF1,NF2
COMMON/TAPES/NST1F,NMASS
NTOT=35500
NST1F=3
NMASS=4
NR1TE16,I,101) NEQ,NBAND,NF
N1M=3
NC=NF*(N1M
NNA=NEQ*NBAND
NN2=N18*NBAND
NN3=NN2*NEQ
NN4=NN3*NEQ
NN5=NN4*NEQ
NN6=NN5*NEQ
NN7=NN6*NEQ
NN8=NN7*NEQ
NN9=NN8*NEQ
NN10=NN9*NEQ
NN11=NN10*NEQ
NN12=NN11*NEQ
NN13=NN12*NEQ
IF (INTOT=NN13) 401,402,402
401 WR1TE(6,I,102) NN13
STOP
402 CONTINUE
CALL SECANTDIA(N1B),A(NM2),A(NM3),A(NM4),A(NM5),A(NM6),A(NM7),
1A(NM8),A(NM9),A(NM10),A(NM11),A(NM12),A(NM13),A(NM14),A(NM15),A(NM16),A(NM17),A(NM18),A(NM19),A(NM20),A(NM21),A(NM22),A(NM23),A(NM24),A(NM25),A(NM26),A(NM27),A(NM28),A(NM29),A(NM30),A(NM31),A(NM32),A(NM33),A(NM34),A(NM35),A(NM36),A(NM37),A(NM38),A(NM39),A(NM40),A(NM41),A(NM42),A(NM43),A(NM44),A(NM45),A(NM46),A(NM47),A(NM48),A(NM49),A(NM50),A(NM51),A(NM52),A(NM53),A(NM54),A(NM55),A(NM56),A(NM57),A(NM58),A(NM59),A(NM60),A(NM61),A(NM62),A(NM63),A(NM64),A(NM65),A(NM66),A(NM67),A(NM68),A(NM69),A(NM70),A(NM71),A(NM72),A(NM73),A(NM74),A(NM75),A(NM76),A(NM77),A(NM78),A(NM79),A(NM80),A(NM81),A(NM82),A(NM83),A(NM84),A(NM85),A(NM86),A(NM87),A(NM88),A(NM89),A(NM90),A(NM91),A(NM92),A(NM93),A(NM94),A(NM95),A(NM96),A(NM97),A(NM98),A(NM99),A(NM100),A(NM101),A(NM102),A(NM103),A(NM104),A(NM105),A(NM106),A(NM107),A(NM108),A(NM109),A(NM110),A(NM111),A(NM112),A(NM113),A(NM114),A(NM115),A(NM116),A(NM117),A(NM118),A(NM119),A(NM120),A(NM121),A(NM122),A(NM123),A(NM124),A(NM125),A(NM126),A(NM127),A(NM128),A(NM129),A(NM130),A(NM131),A(NM132),A(NM133),A(NM134),A(NM135),A(NM136),A(NM137),A(NM138),A(NM139),A(NM140),A(NM141),A(NM142),A(NM143),A(NM144),A(NM145),A(NM146),A(NM147),A(NM148),A(NM149),A(NM150),A(NM151),A(NM152),A(NM153),A(NM154),A(NM155),A(NM156),A(NM157),A(NM158),A(NM159),A(NM160),A(NM161),A(NM162),A(NM163),A(NM164),A(NM165),A(NM166),A(NM167),A(NM168),A(NM169),A(NM170),A(NM171),A(NM172),A(NM173),A(NM174),A(NM175),A(NM176),A(NM177),A(NM178),A(NM179),A(NM180),A(NM181),A(NM182),A(NM183),A(NM184),A(NM185),A(NM186),A(NM187),A(NM188),A(NM189),A(NM190),A(NM191),A(NM192),A(NM193),A(NM194),A(NM195),A(NM196),A(NM197),A(NM198),A(NM199),A(NM200),A(NM201),A(NM202),A(NM203),A(NM204),A(NM205),A(NM206),A(NM207),A(NM208),A(NM209),A(NM210),A(NM211),A(NM212),A(NM213),A(NM214),A(NM215),A(NM216),A(NM217),A(NM218),A(NM219),A(NM220),A(NM221),A(NM222),A(NM223),A(NM224),A(NM225),A(NM226),A(NM227),A(NM228),A(NM229),A(NM230),A(NM231),A(NM232),A(NM233),A(NM234),A(NM235),A(NM236),A(NM237),A(NM238),A(NM239),A(NM240),A(NM241),A(NM242),A(NM243),A(NM244),A(NM245),A(NM246),A(NM247),A(NM248),A(NM249),A(NM250),A(NM251),A(NM252),A(NM253),A(NM254),A(NM255),A(NM256),A(NM257),A(NM258),A(NM259),A(NM260),A(NM261),A(NM262),A(NM263),A(NM264),A(NM265),A(NM266),A(NM267),A(NM268),A(NM269),A(NM270),A(NM271),A(NM272),A(NM273),A(NM274),A(NM275),A(NM276),A(NM277),A(NM278),A(NM279),A(NM280),A(NM281),A(NM282),A(NM283),A(NM284),A(NM285),A(NM286),A(NM287),A(NM288),A(NM289),A(NM290),A(NM291),A(NM292),A(NM293),A(NM294),A(NM295),A(NM296),A(NM297),A(NM298),A(NM299),A(NM300),A(NM301),A(NM302),A(NM303),A(NM304),A(NM305),A(NM306),A(NM307),A(NM308),A(NM309),A(NM310),A(NM311),A(NM312),A(NM313),A(NM314),A(NM315),A(NM316),A(NM317),A(NM318),A(NM319),A(NM320),A(NM321),A(NM322),A(NM323),A(NM324),A(NM325),A(NM326),A(NM327),A(NM328),A(NM329),A(NM330),A(NM331),A(NM332),A(NM333),A(NM334),A(NM335),A(NM336),A(NM337),A(NM338),A(NM339),A(NM340),A(NM341),A(NM342),A(NM343),A(NM344),A(NM345),A(NM346),A(NM347),A(NM348),A(NM349),A(NM350),A(NM351),A(NM352),A(NM353),A(NM354),A(NM355),A(NM356),A(NM357),A(NM358),A(NM359),A(NM360),A(NM361),A(NM362),A(NM363),A(NM364),A(NM365),A(NM366),A(NM367),A(NM368),A(NM369),A(NM370),A(NM371),A(NM372),A(NM373),A(NM374),A(NM375),A(NM376),A(NM377),A(NM378),A(NM379),A(NM380),A(NM381),A(NM382),A(NM383),A(NM384),A(NM385),A(NM386),A(NM387),A(NM388),A(NM389),A(NM390),A(NM391),A(NM392),A(NM393),A(NM394),A(NM395),A(NM396),A(NM397),A(NM398),A(NM399),A(NM400),A(NM401),A(NM402),A(NM403),A(NM404),A(NM405),A(NM406),A(NM407),A(NM408),A(NM409),A(NM410),A(NM411),A(NM412),A(NM413),A(NM414),A(NM415),A(NM416),A(NM417),A(NM418),A(NM419),A(NM420),A(NM421),A(NM422),A(NM423),A(NM424),A(NM425),A(NM426),A(NM427),A(NM428),A(NM429),A(NM430),A(NM431),A(NM432),A(NM433),A(NM434),A(NM435),A(NM436),A(NM437),A(NM438),A(NM439),A(NM440),A(NM441),A(NM442),A(NM443),A(NM444),A(NM445),A(NM446),A(NM447),A(NM448),A(NM449),A(NM450),A(NM451),A(NM452),A(NM453),A(NM454),A(NM455),A(NM456),A(NM457),A(NM458),A(NM459),A(NM460),A(NM461),A(NM462),A(NM463),A(NM464),A(NM465),A(NM466),A(NM467),A(NM468),A(NM469),A(NM470),A(NM471),A(NM472),A(NM473),A(NM474),A(NM475),A(NM476),A(NM477),A(NM478),A(NM479),A(NM480),A(NM481),A(NM482),A(NM483),A(NM484),A(NM485),A(NM486),A(NM487),A(NM488),A(NM489),A(NM490),A(NM491),A(NM492),A(NM4
```

```

MODES-123
MODES-124
MODES-125
MODES-126
MODES-127
MODES-128
MODES-129
MODES-130
MODES-131
MODES-132
MODES-133
MODES-134
MODES-135
MODES-136
MODES-137
MODES-138
MODES-139
MODES-140
MODES-141
MODES-142
MODES-143
MODES-144
MODES-145
MODES-146
MODES-147
MODES-148
MODES-149
MODES-150
MODES-151
MODES-152
MODES-153
MODES-154
MODES-155
MODES-156
MODES-157
MODES-158
MODES-159
MODES-160
MODES-161
MODES-162
MODES-163
MODES-164
MODES-165
MODES-166
MODES-167
MODES-168
MODES-169
MODES-170
MODES-171
MODES-172
MODES-173
MODES-174
MODES-175
MODES-176
MODES-177
MODES-178
MODES-179
MODES-180
MODES-181
MODES-182
MODES-183
MODES-184
MODES-185
MODES-186
MODES-187
MODES-188
MODES-189
MODES-190
MODES-191
MODES-192
MODES-193
MODES-194
MODES-195
MODES-196
MODES-197
MODES-198
MODES-199
MODES-200

JS=IS+1
IF (JS.LE.MTF) GO TO 240
WRITE (6,1030)
STOP
240 RB=RB/(NSCH+1)
GO TO 230
C
C
C ITERATION FOR INDIVIDUAL ROOT
300 WRITE (6,1040)
NITE(JR)=1
WRITE (6,1050) JR,NITE(JR),RA,ETA,FA,ETA,ISC
NITE(JR)=2
WRITE (6,1050) JR,NITE(JR),RB,ETA,FB,ETA,ISC
C
C STOP WHEN REQUIRED NO. OF ROOTS SMALLER THAN RC AND NOV=0 FOUND
310 IF (NSCH-GE.MROOT) GO TO 900
C
C OJF=FB-FA
IF (OJF.NE.O.O) GO TO 320
WRITE (6,1060)
GO TO 900
320 OEL=FB*(RB-RA)/OJF
RC=RB-ETA*DEL
TCL=RCBTOLE*RC
IF (ABSIRC-RB).GT.TOL) GO TO 330
WRITE (6,1070)
ROOT(JR)=RB
GO TO 400
C
330 CALL BANDET JA,B,V,MAYA,M,MMA,RC,MSCH,DETC,ISC,1)
FC=DETC
NITE(JR)=NITE(JR)+1
IF (JR.EQ.1) GO TO 340
JJ=JR-1
GO 350 K=1,JJ
350 FC=FC/(RC-ROOT(K))
340 WRITE (6,1080) JR,NITE(JR),RC,DETC,FC,ETA,ISC-
C
C START INVERSE ITERATIONS
MESS=O
IF (JR.EQ.1) GO TO 380
DO 360 I=1,JJ
IF (ROOT(I).LT.RC) MES=MES+1
360 NOV=MSCH-MES
380 IF (NOV.EQ.O) GO TO 370
WRITE (6,1080) NOV
ROOT(JR)=RC
IF (NOV.GT.1) MSK=1
C
GO TO 400
370 RR=RA
FR=FA
OETA=ETA
RA=RB
FB=FB
DETO=ETB
RB=RC
FR=FC
OETB=DETC
C
C RESET ETA IF NECESSARY
C
C
C TOL=RB*ACTOL
IF (ABS(RA-RB).LT.TOL) ETA=ETA*2
IF (NITE(JR).LE.MITEM) GO TO 310
WRITE (6,1015) NITE(JR),JR
GO TO 900
C
C CHECK FOR STORAGE
C
400 IF (JR.LE.MC) GO TO 405
WRITE (6,1090)
GO TO 900
C
405 NOR=JR-1

```

```

CALL SECOND (TINS)
WRITE (6,1100) NOR
FC=LR.EQ.1) GO TO 410
DO 420 I=1,N
V(I)=1.O
KX=2
420 DO 430 J=1,M
430 W(I)=B(I)*V(J)
JS=O
RTA=O.O
GO TO 510
C
C INVERSE ITERATION
440 NITE(JR)=NITE(JR)+1
DO 450 I=1,M
V(I)=W(I)
450 CALL BANDET JA,B,V,MAYA,M,MMA,RC,MSCH,DETC,ISC,KK)
IF (JS.EQ.1) GO TO 460
RT=O.O
ROT=O.O
DO 470 I=1,M
470 ROT=ROT+W(I)*V(I)
DO 475 I=1,M
W(I)=B(I)*V(I)
475 ROT=O.O
DO 480 I=1,M
480 RQ=ROT+RQ
RQ=ROT/RQB
RT=ROOT(JR)+RQ
WRITE (6,1110) JR,NITE(JR),RT,RQ
TOL=RT-ROOTL
IF (ABS(IRT-RTA).GT.TOL) GO TO 510
IS=1
GO TO 440
C
510 RTA=RT
RS=SOBT(RQB)
DO 490 I=1,M
490 W(I)=W(I)/RS
IF (NOR.EQ.O) GO TO 550
DO 520 K=1,NOR
AL=O.O
DO 530 I=1,M
AL=AL+V(I)*W(I)
530 DO 540 I=1,M
W(I)=W(I)-AL*W(I,K)
540 CONTINUE
C
550 IF (NITE(JR).LE.MITEM) GO TO 440
WRITE (6,1015) NITE(JR),JR
GO TO 900
C
460 ROT=O.O
ERR=ROB
DO 570 I=1,M
570 ROT=ROT+W(I)*V(I)
DO 560 I=1,M
W(I)=B(I)*V(I)
560 ROT=O.O
DO 580 I=1,M
RQB=ROB+V(I)*W(I)
580
C
C OBTAIN A RATHER LARGE ERROR BOUND
C
RQ=ROT/RQB
ROOT(JR)=ROOT(JR)+RQ
ERR=SOBT(RQB)
ERRV(JR)=ROOT(JR)-ERR

```

```

MODES-347
MODES-348
MODES-349
MODES-350
MODES-351
MODES-352
MODES-353
MODES-354
MODES-355
MODES-356
MODES-357
MODES-358
MODES-359
MODES-360
MODES-361
MODES-362
MODES-363
MODES-364
MODES-365
MODES-366
MODES-367
MODES-368
MODES-369
MODES-370
MODES-371
MODES-372
MODES-373
MODES-374
MODES-375
MODES-376
MODES-377
MODES-378
MODES-379
MODES-380
MODES-381
MODES-382
MODES-383
MODES-384
MODES-385
MODES-386
MODES-387
MODES-388
MODES-389
MODES-390
MODES-391
MODES-392
MODES-393
MODES-394
MODES-395
MODES-396
MODES-397
MODES-398
MODES-399
MODES-400
MODES-401
MODES-402
MODES-403
MODES-404
MODES-405
MODES-406
MODES-407
MODES-408
MODES-409
MODES-410
MODES-411
MODES-412
MODES-413
MODES-414
MODES-415
MODES-416
MODES-417
MODES-418
MODES-419
MODES-420
MODES-421
MODES-422
MODES-423

MODES-270
MODES-271
MODES-272
MODES-273
MODES-274
MODES-275
MODES-276
MODES-277
MODES-278
MODES-279
MODES-280
MODES-281
MODES-282
MODES-283
MODES-284
MODES-285
MODES-286
MODES-287
MODES-288
MODES-289
MODES-290
MODES-291
MODES-292
MODES-293
MODES-294
MODES-295
MODES-296
MODES-297
MODES-298
MODES-299
MODES-300
MODES-301
MODES-302
MODES-303
MODES-304
MODES-305
MODES-306
MODES-307
MODES-308
MODES-309
MODES-310
MODES-311
MODES-312
MODES-313
MODES-314
MODES-315
MODES-316
MODES-317
MODES-318
MODES-319
MODES-320
MODES-321
MODES-322
MODES-323
MODES-324
MODES-325
MODES-326
MODES-327
MODES-328
MODES-329
MODES-330
MODES-331
MODES-332
MODES-333
MODES-334
MODES-335
MODES-336
MODES-337
MODES-338
MODES-339
MODES-340
MODES-341
MODES-342
MODES-343
MODES-344
MODES-345
MODES-346

ERRV(JR)=ROOT(JR)*ERR
C
BS=SQRT(RB)
DO 590 I=1,M
  M(I)=M(I)/BS
  V(I)=V(I)/BS
DO 600 I=1,M
  W(I,JR)=M(I)
  W(I,JR)=V(I)
C
CALL SECOND (TIM2)
TIM2=TIM2-TIM3
WRITE (11,120) TIM3
TIM1=TIM2
TIM2=TIM3
C
DECIDE STRATEGY FOR ITERATION TOWARD NEXT ROOT
IF (NOV-GT-O) GO TO 700
IF (ABS(ROOT(JR)-RB)-GT-TOL) GO TO 710
IF (RA-GT-O) GO TO 720
CALL BANOET (A,B,V,MAXA,M,MWA,RA,MSCH,DETA,ISC,I)
RA=RB/2.
FA=DETA
RB=RA
DETA=DETA
RA=RB
DETA=DETA
GO TO 710
C
IF (ROOT(JR)-GT-RC) MSR=1
IF (MSK-EQ-1) GO TO 730
IF (ABS(RC-ROOT(JR))-LT-TOL) GO TO 740
IF (ABS(ROOT(JR)-RB)-LT-TOL) GO TO 750
FA=RB
RA=RB
DETA=DETA
GO TO 710
C
OETA=OETB
RB=RC
FB=FC
OETB=OETC
GO TO 710
C
IF (ABS(ROOT(JR)-RB)-GT-70L) GO TO 710
IF (RA-GT-O) GO TO 760
CALL BANOET (A,B,V,MAXA,M,MWA,RA,MSCH,DETA,ISC,I)
FA=OETA
RB=RA
FB=FA
OETB=OETA
RA=RB
FA=FB
DETA=OETB
FB=FB/(RB-ROOT(JR))
FB=FB/(RB-ROOT(JR))
JN=JN+1
ETA=2.0
GO TO 500
C
IF (RA-GT-O) GO TO 780
RA=RB/2.
CALL BANOET (A,B,V,MAXA,M,MWA,RA,MSCH,DETA,ISC,I)
FA=OETA
RB=RA
FB=FA
OETB=OETA
RA=RB
FA=FB
DETA=OETB
FB=FB/(RB-ROOT(JR))
FB=FB/(RB-ROOT(JR))
JN=JN+1
IF (ROOT(JR)-LE-RC) NOV=NOV-1
JN=JN+1

```







-161-

```

IF(IJJ,LE,MEQ) GO TO 403
404 CONTINUE 502) NP,11
WRITE(16,502) NP,11
GO TO 304
403 IF(IJJ,LE,0) GO TO 404
L=L+1
KO(1,L)=NP
KO(2,L)=11
KO(3,L)=JJ
KO(4,L)=0
JOISJJ=1
IFIL,LT,8) GO TO 304
WRITE(10) KO,L
K=K+1
L=0
304 CONTINUE
GO TO 1000
C
C READ AND INPUT STRESS OUTPUT SPECIFICATION
402 CONTINUE
MS=K
WRITE(16,503) KK1
L=0
READ I,KK2
READ I,MYTYPE,MEL,IS
A BLANK CARD FOR ENDING
IF(MEL,GT,0) GO TO 405
IFIL,EQ,0) GO TO 406
WRITE(20) KO,L
K=K+1
GO TO 406
405 CONTINUE
IFIL,EQ,0,AND,L,EQ,0) WRITE(16,504)
WRITE(10) MYTYPE,MEL,IS
DO 305 I=1,9
I=IS(I)
IF(I) (LE,0) GO TO 305
JA=99)MEL-L)I+11
L=L+1
KO(1,L)=MYTYPE
KO(2,L)=MEL
KO(3,L)=11
KO(4,L)=JJ
ISTR(11,MEL)=1
IFIL,LT,8) GO TO 305
WRITE(20) KO,L
K=K+1
305 CONTINUE
GO TO 2000
406 CONTINUE
MS=K
C
C READ AND PRINT WALL FORCE OUTPUT SPECIFICATION
L=0
READ I,KK3
READ I,MW,1W
IF(MW,GT,0) GO TO 407
IFIL,EQ,0) GO TO 408
WRITE(10) KO,L
K=K+1
407 CONTINUE
IF(K,EQ,0,AND,L,EQ,0) WRITE(16,505)

```

```

OUTPUT-149
OUTPUT-150
OUTPUT-151
OUTPUT-152
OUTPUT-153
OUTPUT-154
OUTPUT-155
OUTPUT-156
OUTPUT-157
OUTPUT-158
OUTPUT-159
OUTPUT-160
OUTPUT-161
OUTPUT-162
OUTPUT-163
OUTPUT-164
OUTPUT-165
OUTPUT-166
OUTPUT-167
OUTPUT-168
OUTPUT-169
OUTPUT-170
OUTPUT-171
OUTPUT-172
OUTPUT-173
OUTPUT-174
OUTPUT-175
OUTPUT-176
OUTPUT-177
OUTPUT-178
OUTPUT-179
OUTPUT-180
OUTPUT-181
OUTPUT-182
OUTPUT-183
OUTPUT-184
OUTPUT-185
OUTPUT-186
OUTPUT-187
OUTPUT-188
OUTPUT-189
OUTPUT-190
OUTPUT-191
OUTPUT-192
OUTPUT-193
OUTPUT-194
OUTPUT-195
OUTPUT-196
OUTPUT-197
OUTPUT-198
OUTPUT-199
OUTPUT-200
OUTPUT-201
OUTPUT-202
OUTPUT-203
OUTPUT-204
OUTPUT-205
OUTPUT-206
OUTPUT-207
OUTPUT-208
OUTPUT-209
OUTPUT-210
OUTPUT-211
OUTPUT-212
OUTPUT-213
OUTPUT-214
OUTPUT-215
OUTPUT-216
OUTPUT-217

```

```

WRITE(16,104) MW,1W
DO 306 J=1,3
J=1W(1)
IF(J,EQ,0) GO TO 306
JJ=30)MW-1)
JWALL(11,MW)=1
K=K+1
KO(1,L)=MW
KO(2,L)=11
KO(3,L)=JJ
KO(4,L)=0
IFIL,LT,6) GO TO 306
WRITE(10) KO,L
K=K+1
L=0
306 CONTINUE
GO TO 3000
408 CONTINUE
MS=K
C CALCULATE LOCATION IN BUFFER FOR DISPLACEMENT(ACCELERATION),
C STRESS,WALL FORCE
MOIS=0
MSTR=0
MVAL=0
DO 307 I=1,MEO
IF(I)IS(11,EQ,0) GO TO 307
MOIS=MOIS+1
IOIS(11)=MOIS
307 CONTINUE
C
DO 308 N=1,MUREL
DO 308 I=1,9
IF(I)ISTR(11,N,EQ,0) GO TO 308
MSTR=MSTR+1
ISTR(11,N)=MSTR
308 CONTINUE
DO 309 I=1,3
IF(I)WALL(11,N,EQ,0) GO TO 309
MVAL=MVAL+1
WALL(11,N)=MVAL
309 CONTINUE
1) FORMAT(15)
101) FORMAT(15,AX,3141
103) FORMAT(1214,58,12131
104) FORMAT(AX,14,48,3141
501) FORMAT(10)DISPLACEMENT AND ACCELERATION COMPONENTS FOR%
1) WHICH OUTPUT TIME HISTORY IS REQUIRED //
2) MODE DISPLACEMENT(ACCELERATION) COMPONENTS//
302) FORMAT(15,AX,14,AX,4)FIXED DOF...NO OUTPUT%
503) FORMAT(10) OUTPUT TYPE=1 PRINT,=2 PRINT + PLOT%,.....,12/1
504) FORMAT(10) ELEMENT STRESS COMPONENTS FOR WHICH%
1) OUTPUT TIME HISTORY IS REQUIRED //
2) ELEMENT STRESS COMPONENTS//
3) TYPE NO.//
505) FORMAT(10) WALL FORCES FOR WHICH OUTPUT%
1) TIME HISTORY IS REQUIRED //
2) WALL NO. COMPONENTS(1-FR,2-YBAR,3-FV)10/1
END

```

-163-



```

411 CONTINUE
JJ=K013,I)
II=I015(I,J)
XX=UH(I,I,J)
GO TO 415
412 CONTINUE
JJ=K013,I)
II=I015(I,J)
XX=UH(I,I,J)
GO TO 415
413 CONTINUE
LL=K012,I)
II=K013,I)
II=I015(I,J)
XX=UH(I,I,J)
GO TO 415
414 CONTINUE
LL=K011,I)
II=K012,I)
II=I015(I,J)
XX=UH(I,I,J)
ABSOLUTE MAX
415 CONTINUE
AX=ABS(XX)
IF(AX-XM(1)) 416,416,417
417 CONTINUE
XM(1)=AX
TM(1)=TT
418 CONTINUE
X11,M)=XX
TAIM)=TT
305 CONTINUE
304 CONTINUE
303 CONTINUE
C
GO TO (410,419) KKI
410 CONTINUE
O3=O3+1,MOS
WRITE(6,104) TAIM),(X11,M)=1,L)
306 CONTINUE
WRITE(6,105) (XM(1),I=1,L)
WRITE(6,106) (TM(1),I=1,L)
GO TO 420
419 CONTINUE
IF(KKI.EQ.2) WRITE(INT) IFF,KKK,L,KD,XM,X
GO TO 410
420 CONTINUE
301 CONTINUE
RETURN
101 FORMATION TIME=2X,0110,IM-,12,X))
102 FORMATION TIME=2X,0114,2M-,13,IM-,12))
103 FORMATION TIME=2X,0118,IM-,12,X))
104 FORMATION TIME=2X,0122,X,2,0E12,ABSOLUTE VALUES,0 MAXIMUM 0.0E12-4)
105 FORMATION TIME=2X,0126,X,2,0E12,ABSOLUTE VALUES,0 MAXIMUM 0.0E12-4)
106 FORMATION TIME=2X,0130,X,2,0E12,ABSOLUTE VALUES,0 MAXIMUM 0.0E12-4)
501 FORMATION TIME HISTORY FOR SELECTED DISPLACEMENT COMPONENTS*,
1 5N,....13-3TX,0FILE NO.0.13//
2 20X,MODE NUMBERS AND DISPLACEMENT COMPONENTS*)
502 FORMATION TIME HISTORY FOR SELECTED ACCELERATION COMPONENTS*,
1 5N,....13-3TX,0FILE NO.0.13//
2 20X,MODE NUMBERS AND ACCELERATION COMPONENTS*)
503 FORMATION TIME HISTORY FOR SELECTED STRESS COMPONENTS*,
1 5N,....13-41X,0FILE NO.0.13//
2 20X,ELEMENT TYPE-ELEMENT NO.-STRESS(1,0),YIELD(9)0//)
504 FORMATION TIME HISTORY FOR SELECTED WALL FORCE*,
1 5N,....13-4TX,0FILE NO.0.13//
2 20X,WALL NO.-COMPONENTS,1=X,2=Y,0,3=V,0//
END

```

```

OUTPUT-427
OUTPUT-428
OUTPUT-429
OUTPUT-430
OUTPUT-431
OUTPUT-432
OUTPUT-433
OUTPUT-434
OUTPUT-435
OUTPUT-436
OUTPUT-437
OUTPUT-438
OUTPUT-439
OUTPUT-440
OUTPUT-441
OUTPUT-442
OUTPUT-443
OUTPUT-444
OUTPUT-445
OUTPUT-446
OUTPUT-447
OUTPUT-448
OUTPUT-449
OUTPUT-450
OUTPUT-451
OUTPUT-452
OUTPUT-453
OUTPUT-454
OUTPUT-455
OUTPUT-456
OUTPUT-457
OUTPUT-458
OUTPUT-459
OUTPUT-460
OUTPUT-461
OUTPUT-462
OUTPUT-463
OUTPUT-464
OUTPUT-465
OUTPUT-466
OUTPUT-467
OUTPUT-468
OUTPUT-469
OUTPUT-470
OUTPUT-471
OUTPUT-472
OUTPUT-473
OUTPUT-474
OUTPUT-475
OUTPUT-476
OUTPUT-477
OUTPUT-478
OUTPUT-479
OUTPUT-480
OUTPUT-481
OUTPUT-482
OUTPUT-483
OUTPUT-484
OUTPUT-485
OUTPUT-486
OUTPUT-487
OUTPUT-488
OUTPUT-489
OUTPUT-490
OUTPUT-491
OUTPUT-492
OUTPUT-493
OUTPUT-494

```



TE  
662 .A3 no. FHW  
RD-75-10

BORROWER

26.10.80


Form DOT F 172  
FORMERLY FORM DC

DOT LIBRARY



00054614

